ENHANCED PETROLEUM HYDROCARBON REMEDIATION BY BIOSTIMULATION: EFFECTS ON GROUNDWATER MICROBIAL COMMUNITIES, GEOCHEMISTRY, AND MINERALOGY

A Thesis Submitted to the College of
Graduate and Postdoctoral Studies
In Partial Fulfillment of the Requirements
For the Degree of Master of Science
In the Department of Geological Sciences
University of Saskatchewan
Saskatoon

By

SCOTT DONALD COLVILLE

PERMISSION TO USE

In presenting this thesis in partial fulfillment of the requirements for a Postgraduate degree from the University of Saskatchewan, I agree that the Libraries of this University may make it freely available for inspection. I further agree that permission for copying of this thesis/dissertation in any manner, in whole or in part, for scholarly purposes may be granted by the professor or professors who supervised my thesis/dissertation work or, in their absence, by the Head of the Department in which my thesis work was done. It is understood that any copying or publication or use of this thesis or parts thereof for financial gain shall not be allowed without my written permission. It is also understood that due recognition shall be given to me and to the University of Saskatchewan in any scholarly use which may be made of any material in my thesis.

Requests for permission to copy or to make other uses of materials in this thesis in whole or part should be addressed to:

Head of the Department of Geological Sciences
University of Saskatchewan
114 Science Place
Saskatoon, Saskatchewan S7N 5E2 Canada
OR
Dean
College of Graduate and Postdoctoral Studies
University of Saskatchewan
116 Thorvaldson Building, 110 Science Place
Saskatoon, Saskatchewan S7N 5C9 Canada

ABSTRACT

Groundwater at a petroleum hydrocarbon (PHC) contaminated site in Saskatoon, SK was amended with a solution of nitrate as nitric acid, sodium tripolyphosphate, and ferric-ammonium-citrate to enhance PHC remediation. Groundwater was collected for geochemical and microbiological analyses before, during, and after biostimulation amendments. Sediment samples were also collected to characterize mineralogy before and after biostimulation. I hypothesized that the biostimulation solution would enrich taxa that couple Fe(III) reduction to PHC oxidation, increase levels of dissolved and mineralized Fe(III) reduction products, and enhance PHC remediation. I performed high-throughput amplicon sequencing of the 16S rRNA gene of genomic DNA extracted from filtered groundwater samples and performed a microbial community analysis on the data. Groundwater samples were also analyzed for general chemistry (e.g., pH, alkalinity, cations, and anions), PHCs (e.g., BTEX), and metabolites of PHC biodegradation. Sediment mineralogy was characterized using synchrotron techniques (e.g., Fe XANES). This was a novel approach provided unique insights into the biogeochemistry of PHC biodegradation.

Metabolite results provided strong evidence that the biodegradation is occurring at this site and multiple lines of evidence suggest that Fe(III) and sulfate reduction were the key biogeochemical processes occurring at the site. Relatives of Fe(III) reducers (*Geobacter* and unclassified *Comamonadaceae*) and sulfate reducers (*Desulfosporosinus*) dominated the microbial community profiles of the contaminated monitoring wells. During biostimulation, proportions of unclassified *Comamonadaceae* increased relative to other bacteria in some monitoring wells because of the availability of fixed nitrogen (e.g., ammonia). In other areas of the site this did not occur; in these cases, PHC concentrations decreased less. Multiple lines of evidence also suggest that nitrate in the biostimulation solution caused FeS oxidation. This nitrate-dependent FeS oxidation possibly decreased PHC biodegradation potential either by decreasing nutrient availability and/or shifting the microbial community profile. Overall, these results suggest that the biostimulation solution stimulated Fe(III) reduction.

ACKNOWLEDGEMENTS

Firstly, I need to acknowledge my supervisor Dr. Joyce McBeth. The work I completed in this thesis would not have been possible without your support and guidance throughout my program. Further thanks and acknowledgements to my committee members Drs. Matt Lindsay and Sam Butler for their support and feedback on my work. I am also grateful to Dr. Mehdi Nemati for acting as the external examiner during my thesis defense.

This project would not have been possible without funding provided by FCL, NSERC, and the Department of Geological Sciences Devolved Scholarship. I also need to acknowledge Kris Bradshaw and Jay Grosskleg of FCL for supporting us throughout the project. Thank you to the team at Stantec (Marshall Pachal, Chris Mathies, Wen Hui Xiong, Becky Weir, and Sam Rokeby) for collecting field samples and providing analytical geochemistry data. Further thanks to Dr. Lisa Gieg and her student Gabrielle Scheffer at the University of Calgary for preforming metabolite analyses. I'd also like to thank and acknowledge beam line staff and scientists at the Canadian Light Source for providing support and guidance during beam time (Michel Fodje and Shaun Labiuk at CMCF; Yongfeng Hu and Qunfeng Xiao at SXRMB; Emilio Heredia and Viorica (Ibi) Bondici at BioXAS).

Thanks to former and current members of the McBeth Research Group (Nicki Harris, Jonathan Vyskocil, Ibi Bondici, Kate Crawford, and Sarah Rudderham) and fellow geology graduate students all your support and friendship. A special thanks to Katrina Dorosh for all your help in the lab. Finally, thank you to my parents and family for your constant support through my long journey in academia and in life. Thank you.

To my grandparents.

TABLE OF CONTENTS

LIST OF TABLES

LIST OF FIGURES

LIST OF ABBREVIATIONS

PHC	petroleum hydrocarbon
UST	underground storage tank
CCME	Canadian Council of Ministers of the Environment
MPE	multi-phase extraction
BTEX	benzene, toluene, ethylbenzene, and xylenes
F1 PHCs	C6 to C10 petroleum hydrocarbons
F2 PHCs	C11 to C16 petroleum hydrocarbons
F1 – BTEX	F1 PHCs excluding BTEX
ISCO	*in situ* chemical oxidation
TPP	tripolyphosphate
CMC	critical micelle concentration
$\delta^{13}C$	$^{13}C/^{12}C$
$\delta^{18}O$	$^{18}O/^{16}O$
mBGL	meters below ground level
ORP	oxidation reduction potential
EC	electrical conductivity
GC/MS	gas chromatography/mass spectrometry
ICP	inductively coupled plasma
IC	ion chromatography
PHREEQC	pH-redox-equilibrium
SI	saturation index
PXRD	powder x-ray diffraction
XAS	x-ray adsorption spectroscopy
XRF	x-ray fluorescence
LaB_6	lanthanum hexaboride
PCA	principal component analysis

ESRF	European Synchrotron Research Facility
LCF	linear combination fitting
DNA	deoxyribonucleic acid
rRNA	ribosomal ribonucleic acid
OTU	operational taxonomic unit
CBE	charge balance error
BzSucc	benzylsuccinate
MeBzSucc	methylbenzylsuccinate
NMDS	non-metric multidimensional scaling
SDS	sodium dodecyl sulfate

CHAPTER 1 INTRODUCTION

Petroleum hydrocarbon (PHC) contamination from leaking underground storage tanks (USTs) is a ubiquitous problem at fuel stations that can create a legacy of environmental and economic liabilities for site owners and managers as well as create health hazards. The Canadian Council of Ministers of the Environment (CCME) estimates that there are tens of thousands of PHC-contaminated sites within Canada, and that these sites have an estimated economic and environmental liabilities of $10 billion (CCME 2008). Engineered remediation systems (e.g., pump and treat) can be ineffective at remediating PHCs and excavation of contaminated soil (i.e. dig-and-dump) is an unsustainable practice because the site does not remain in productive use while it is being remediated. Therefore, there is a growing interest in enhancing *in situ* PHC remediation by stimulating indigenous PHC-degrading microbial communities. Contaminated groundwater and sediments can be amended with nutrients (e.g., nitrogen and phosphorus), electron acceptors (e.g., ferric iron), and organic acids (e.g., citric acid) to enhance PHC biodegradation. However, studies are needed to understand how these biostimulation solutions affect site microbiology and geochemistry and to improve *in situ* remediation strategies.

1.1 Objectives and Hypotheses

A PHC plume associated with a gas station site in Saskatoon, SK was previously remediated using a multi-phase extraction (MPE) system. However, diminishing returns prompted the site managers to change their approach and switch to biostimulation to enhance PHC remediation and remove recalcitrant PHCs. The site groundwater was amended with a solution of nitrate (NO_3^-) added as nitric acid, sodium tripolyphosphate ($Na_5P_3O_{10}$), and ferric ammonium citrate ($(NH_4)_5[Fe(C_6H_4O_7)_2]$) to enhance PHC remediation. The objectives of this study are to:

1) examine the effects of the biostimulation solution on site microbiology and geochemistry over time, and
2) develop a conceptual model of the microbiological and geochemical effects of biostimulation at the site.

The hypotheses of this study are that the biostimulation solution would:

1) enrich taxa of bacteria capable of coupling Fe(III) reduction to PHC oxidation,
2) increase levels of dissolved and mineralized Fe(III) reduction products, and
3) enhance PHC remediation at the site.

CHAPTER 2 LITERATURE REVIEW

2.1 Health Hazards from Petroleum Hydrocarbon Contamination

Due to the pervasiveness of petroleum products in modern society, there are many different exposure sources of PHCs in the environment. When contamination occurs from leaking USTs the most likely routes of exposure are drinking water from a contaminated groundwater well or inhaling vapour from the contaminated soil (ATSDR 1999). A mixture of linear (e.g., hexane) and ringed hydrocarbons (e.g., benzene and other polyaromatic hydrocarbons) can exist at PHC-contaminated sites. This mixture of PHCs can cause a variety of human health risks that affect the central nervous system, blood, immune system, liver, spleen, kidney, fetus development, and lungs (ATSDR 1999). Furthermore, certain PHCs (e.g., benzene) are known carcinogens (CCME 2008). In Canada, PHCs are classified and reported based on the number of carbon atoms they contain (CCME 2008). For example, F1 PHCs contain 6 to 10 carbon atoms and F2 PHCs have 11 to 16. Due to historic reasons and their carcinogenic nature; benzene, toluene, ethylbenzene, and xylenes (BTEX) are often reported separately from the F1 PHCs (F1 – BTEX). In Saskatchewan, soil and water quality guidelines (Table 2.1) are created and modified using a tiered approach. Tier one is the most stringent and assumes the worst case scenario; however, these quality guidelines can be modified (tier two) dependent on the site location (e.g., commercial site versus residential site) and possible exposure pathways (e.g., nearby drinking water source) at the site (Government of Saskatchewan 2016).

Table 2.1. Saskatchewan groundwater and soil tier one quality guidelines for PHCs at commercial and residential sites. Reproduced from Government of Saskatchewan (2016).

Petroleum Hydrocarbon	Potable Groundwater (µg/L)	Soil (mg/kg)	
		Fine Grained	Course Grained
F1 PHCs	2,200	170	30
F2 PHCs	1,100	230	150
Benzene	5	0.046	0.078
Toluene	60	0.52	0.12
Ethylbenzene	140	0.073	0.14
Xylenes	90	0.99	1.9

2.2 Methods of Petroleum Hydrocarbon Remediation

Physical, chemical and/or biological methods can be used to remediate PHC-contaminated sites. These remediation methods can either be *ex situ* or *in situ*. *Ex situ* treatments remove the soil or groundwater for off-site treatment and *in situ* strategies treat contaminated soil or groundwater in place. Remedial strategies might also use a combination of remediation methods to reach clean-up objectives.

2.2.1 Physical Remediation Methods

Ex situ treatments such as excavation and disposal (i.e. dig-and-dump) and soil washing are used to remediate contaminated sites when soil needs to be removed from the contaminated site (e.g., redeveloping land that requires soil excavation). Dig-and-dump is the most straightforward method of remediating a contaminated site. Contaminated soils are identified, excavated, and disposed of at regulated landfills (Suthersan et al. 2017). Soil washing is the separation of contaminated sediment (e.g., clay) from clean sediments (Russell 2012). It can be enhanced by the addition of surfactants and detergents that promote the removal of sorbed PHCs (Deshpande et al. 1999).

Soil vapour extraction, air sparging, and pump-and-treat are all examples of *in situ* physical remediation (Suthersan et al. 2017). Soil vapour extraction can be used to remove volatile PHCs by applying a vacuum pressure to the soil vadose zone through an extraction well (Shan et al. 1992). This remediation method can be enhanced by injecting air into the groundwater to promote the volatilization of dissolved PHCs (Marley et al. 1992). Pump-and-treat was one of the first *in situ* remediation technologies used in the 1980s and is still commonly used today (Suthersan et al. 2017). It is an effective strategy because it can easily be combined with either other methods by amending the extracted groundwater to promote either chemical or biological remediation.

2.2.2 Chemical Remediation Methods

Chemical reaction mechanisms such as precipitation, oxidation, reduction, and nucleophilic substitution can be used to remediate a variety contaminants in the environment (Suthersan et al. 2017). Chemical remediation is typical done *in situ* and one of the most common methods is *in situ* chemical oxidation (ISCO) by the application of oxidizing agents containing permanganate (MnO_4^-) or hydrogen peroxide (Krembs et al. 2010) These chemical

methods are an attractive method of remediation because rapid reaction rates allow site owners to reach remediation objectives sooner (Suthersan et al. 2017). However, the potential of ISCO could be limited if oxidants destroy microbial communities that can further degrade contaminants (Chen et al. 2016).

2.2.3 Biological Remediation Methods

Bioremediation uses metabolic processes to immobilize or degrade contaminants (Suthersan et al. 2017). Bioremediation can either be done *in situ* or *ex situ*. Land farming is an example of *ex situ* bioremediation for PHC-contaminated soil. This is done by spreading the contaminated soil over an impermeable surface to control runoff of contaminated water, adding nutrient (nitrogen and phosphorus) fertilizers and periodically tilling the soil to promote aerobic biodegradation (Russell 2012). *In situ* bioremediation can be accomplished through either biostimulation or bioaugmentation (Suthersan et al. 2017). Biostimulation assumes that given the right geochemical conditions (e.g., nutrient availability) the indigenous microbial communities present at a contaminated site have the potential to degrade contaminants (Suthersan et al. 2017). In contrast, bioaugmentation is used to increase the population of specific, desirable microbial communities by injecting commercially grown microbes into the contaminated subsurface in the hopes that they will overcome the indigenous microbial communities (Suthersan et al. 2017). Bioaugmentation can have limited success compared to biostimulation because commercially grown microbes can struggle to outcompete indigenous microbial communities that have become acclimatized to the contaminated environment (Tyagi et al. 2011).

2.3 Microbiology and Remediation

2.3.1 Microbial Communities at Petroleum Hydrocarbon Contaminated Sites

Bioremediation primarily targets microbes belonging to the bacterial and archaeal domains (Suthersan et al. 2017). These microbes can derive energy from organic compounds (chemoorganotrophs), inorganic compounds (chemolithotrophs), or from light (phototrophs) (Madigan et al. 2014). Microbes that use organic compounds as a source of carbon are heterotrophs and autotrophs use CO_2 as a source of carbon (Madigan et al. 2014). These microbes can again be classified by their respiration method (Madigan et al. 2014). Aerobes use O_2 as an electron acceptor and anaerobes can use other chemicals under anoxic conditions (Madigan et al. 2014).

Soil can contain over 4,000 unique microbial genomes and have high phenotypic diversity (Torsvik et al. 1990b, 1990a). Janssen (2006) conducted a review of taxa present in clone libraries of 16S rRNA genes from soil (Table 2.2). He found that approximately 52 % of clones could be classified into well-known subphyla (class or subclass). Furthermore, he found that nearly 39 % of clones were in phylum *Proteobacteria*.

Table 2.2. Well characterized subphyla of uncontaminated soil bacteria. Proportion of 3,398 clones. Reproduced from Janssen (2006).

Subphylum	Proportion (%)	Number of genera in group
Actinobacteridae	4.3	158
Flavobacteria	0.50	25
Sphingobacteria	4.3	28
Bacilli	1.9	79
Clostridia	0.59	135
α-proteobacteria	16	160
β-proteobacteria	11	93
δ-proteobacteria	2.8	70
γ-proteobacteria	7.8	194
Total	52	942

Saul et al. (2005) studied the changes in bacterial diversity of PHC-contaminated soil in Antarctica. They found that PHC-contaminated samples were enriched with bacteria belonging to phylum *Proteobacteria* compared to uncontaminated samples. Specifically, relatives of *Pseudomonas, Sphingomonas* and *Variovorax* were enriched in their contaminated samples. Some of these relatives and other bacteria in phylum *Proteobacteria* can degrade PHCs (Saul et al. 2005). For example, *Geobacter* can couple benzene oxidation to Fe(III) reduction and is a member of the *δ-proteobacteria* subphylum (Zhang et al. 2012).

2.3.2 Microbial Nutrient Requirements and Biostimulation

Microbes require carbon, nitrogen, macronutrients, and micronutrients for growth (Madigan et al. 2014). By reviewing relevant literature, Cleveland and Liptzin (2007) found that soil biomass and soil have typical C:N:P ratios of 60:7:1 and 186:13:1 respectively. At PHC-contaminated sites nitrogen and phosphorus are often limiting factors for microbial communities. To address these nutrient limitations, PHC-contaminated sites are amended with nitrogen and phosphorus solutions to promote microbial growth for PHC biodegradation (e.g., Xiong et al. 2012 and Ponsin et al. 2014). The microbial resource-ratio theory can then be applied to predict

the influence of nutrients on PHC biodegradation rates (Smith et al. 1998). Smith et al. (1998) report that the resource-ratio theory predicts:

1) changes in supply ratios of nitrogen and phosphorous alter PHC biodegradation rates by shifting the microbial community structure; and
2) changes in total supply levels of nitrogen and phosphorus levels alter PHC biodegradation rates by increasing the total biomass of PHC-degraders.

Furthermore, Siciliano et al. (2016) found that the speciation of phosphorus-bearing minerals influenced the composition of indigenous microbial communities while the total amount of bioavailable phosphorus (i.e., adsorbed phosphorus) influenced the rate of PHC biodegradation. They also found that phosphate bioavailability was decreased when it precipitated to form minerals with Ca and Mg (e.g., brushite and newberyite). Hamilton et al. (2018) further studied the speciation and fate of tripolyphosphate (TPP) amended to a PHC-contaminated site. They found that the TPP rapidly sorbed to the soil matrix and persisted in the environment for over a year. Therefore, they concluded that TPP is an effective phosphorus amendment for enhancing PHC biodegradation in calcareous soils.

Low-molecular weight organic acids (e.g., citric acid) can also be added to PHC-contaminated sites to enhance PHC biodegradation. These organic acids can enhance microbial activity in three different ways. They can enhance phosphorus bioavailability, increase PHC availability through desorption processes, or stimulate initial microbial activity by acting as a carbon source for bacteria (Chen et al. 2017). Chen et al. (2017) studied the effects of citrate and nutrient amendments as a biostimulation solution at a former gas station site in Saskatoon, SK. They found that citrate enhanced PHC biodegradation by increasing the amount of bioavailable phosphorus. Citrate may increase the availability of phosphorus through competitive ligand, mineral dissolution, and/or organic phosphorus dissolution (Wei et al. 2010, Chen et al. 2017). Furthermore, Chen et al. (2017) found that biostimulation solution enhanced Fe(III)-reducing activity at the site. They speculated citrate may have either enhanced Fe(III) reduction by acting as a carbon source or by increasing phosphorus availability. Another possibility is that citrate increased Fe(III) solubility through chelation.

While carbon is not usually limited at PHC-contaminated sites, surfactants can be used to increase the solubility of non-aqueous phase liquids (NAPLs) and to promote the desorption of

PHCs to increase carbon bioavailability (Mulligan et al. 2001, Christofi and Ivshina 2002). Surfactants can be classified as either synthetic surfactants or biosurfactants. Biosurfactants are produced through microbial processes or derived from plant materials (Makkar and Rockne 2003). The surfactant molecular structure consists of a hydrophilic polar head and a hydrophobic non-polar tail (Christofi and Ivshina 2002). Due to its non-polar nature and hydrophobicity, the surfactant tail cannot form intermolecular hydrogen bonds with the surrounding water molecules (Christofi and Ivshina 2002). This increases the free energy of the system and Christofi and Ivshina (2002) summarized the different pathways the surfactant molecule can take to decrease the free energy of the system. They report that the surfactant molecule could:

1) adsorb to the surfaces of sediment particles,
2) absorb to the organic matrix of the soil, or
3) form an intermolecular bond between the hydrophobic tail and a hydrophobic compound such as a NAPL or sorbed contaminant.

The formation of micelles is how surfactants increase the solubility of hydrophobic contaminants. When enough surfactant molecules form an intermolecular bond between the hydrophobic tail and a contaminant, the contaminant is solubilized into a micelle (Christofi and Ivshina 2002). The concentration at which micelles form is known as the critical micelle concentration (CMC). Micelle formation is used to increase the solubility of contaminants for pump and treat remediation systems but increasing PHC solubility also increases the availability of PHCs for biodegradation, and; therefore, the surfactant can act as a biostimulation solution. However, this is not always true and the availability of PHCs for biodegradation can actually decrease if the contaminant becomes strongly encapsulated within the micelle (Mulligan et al. 2001).

2.3.3 Microbial Effects on Groundwater Geochemistry

Microbes conserve energy through redox reactions by passing electrons from electron donors through their cell membrane to a terminal electron acceptor (Madigan et al. 2014). This produces an electrochemical gradient across the cell membrane called the proton motive force (Madigan et al. 2014). The proton motive force is then used in the production of energy rich compounds (e.g., ATP) which are used for cell growth (Madigan et al. 2014). The electron acceptors that are mostly commonly used in microbial metabolism in the environment are

oxygen, nitrate, iron, manganese and sulfate. These electron acceptors are generally consumed in a preferential order dependent on the thermodynamically available energy (Bethke et al. 2011). This creates a sequence of redox reactions (Table 2.3) known as the thermodynamic ladder in geomicrobiology (Bethke et al. 2011).

Table 2.3. Common redox half-reactions that occur in anoxic groundwater. Reproduced from Bethke et al. (2011).

Electron donating half-reactions		ΔG (kJ/mol)
Acetotrophy	$CH_3COO^- + 4H_2O \rightarrow 2HCO_3^- + 9H^+ + 8e^-$	-216
Hydrogenotrophy	$4H_2 \rightarrow 8H^+$	-185
Electron accepting half-reactions		**ΔG (kJ/mol)**
Denitrification	$8e^- + \frac{8}{5} NO_3^- + \frac{48}{5} H^+ \rightarrow \frac{4}{5} N_2 + \frac{24}{5} H_2O$	-550
Mn(IV) reduction	$8e^- + 4MnO_2 + 16H^+ \rightarrow 4Mn^{2+} + 8H_2O$	-417 to -383
Mn(III) reduction	$8e^- + 8MnOOH + 24H^+ \rightarrow 8Mn^{2+} + 16H_2O$	-347 to -333
Fe(III) reduction	$8e^- + 4Fe(OH)_3 + 24H^+ \rightarrow 8Fe^{2+} + 24H_2O$	-4 to 96
Sulfate reduction	$8e^- + SO_4^{2-} + 9H^+ \rightarrow HS^- + 4H_2O$	150
Methanogenesis	$8e^- + HCO_3^- + 9H^+ \rightarrow CH_4 + 3H_2O$	184

Microbes will consume more energetically favorable electron acceptors first, but this sequence of redox reactions can be altered depending on the form and availability of electron acceptors and the structure of microbial communities. For example, Fe(III) reduction is typically more energetically favourable than sulfate reduction at circumneutral pH. However, as pH increases, sulfate reduction can become more energetically favourable (Kirk et al. 2016).Furthermore, syntrophic relationships between Fe(III) reducers and sulfate reducers can lead to co-occurrence of Fe(III)- and sulfate reduction (Flynn et al. 2014). This zonation of redox reactions in groundwater is important because the rate and extent of PHC biodegradation can depend on the redox potential of the groundwater. At a crude oil contaminated aquifer near Bemidji, MN, USA, the development of methanogenic zones has led to the transport of hydrocarbon compounds that would have normally degraded under aerobic or Fe(III)-reducing conditions (Bekins et al. 2001).

2.4 Iron Biogeochemistry

2.4.1 Iron (III) and Iron Reduction

Iron is the fourth most abundant element on Earth and makes up as much as 5 % of the Earth's crust by mass and 3 % of soil mass (Fischer 1988). The major iron-bearing materials include silicates, clay minerals, sulfides, carbonates, and iron oxides (Fischer 1988). The most common bioavailable form of iron in aquifers are iron oxides which commonly occur as poorly crystalline material (e.g., ferrihydrite) or in more crystalline phases such as goethite and hematite (Roden 2003). Goethite, hematite, and ferrihydrite are the most common forms of iron oxides in soils, but other forms such as lepidocrocite and maghemite are also found in aquifers (Fischer 1988). These sources of iron can be critical to microbial life and are used by microbes as terminal electron acceptors to conserve energy in dissimilatory Fe(III) reduction (Lovley 1993). Iron can also be incorporated into essential biological systems (e.g., iron-sulfur proteins) within the cell (Madigan et al. 2014). This process of incorporating iron into biological systems is referred to as assimilatory Fe(III) reduction (Lovley 1993). While assimilatory Fe(III) reduction is important to microbial life, it is generally considered less important in PHC biodegradation because most microorganisms only require trace amounts of iron to grow and function (Madigan et al. 2014). However, the availability of Fe(II) can affect the extent of Fe(III) reduction if microbes (e.g., *Geobacter*) have high Fe(II) assimilation needs (e.g., for iron-sulfur proteins) (O'Neil et al. 2008). In comparison, dissimilatory Fe(III) reduction process is critically important in bioremediation because of the influences it has on aquifer biogeochemistry and because of the potential to degrade and detoxify contaminants (Lovley 1993).

Fe(III)-bearing aquifer materials have varying physical properties that can affect the rate and extent of microbial reduction. Physical properties (e.g., degree of crystallinity, particle size, surface area, and solubility) and potential sinks of the reduced Fe(II) can affect the rate and extent of microbial Fe(III) reduction in soil systems (Munch and Ottow 1980, Fischer 1988, Roden 2003, Bonneville et al. 2004). Properties of the microorganism, such as cell type and density, can affect the rate and extent of Fe(III) reduction (Fischer 1988, McLean et al. 2002, Bonneville et al. 2004).

2.4.2 Secondary Iron (II) Minerals

The formation of secondary Fe(II)-bearing minerals (e.g., magnetite and pyrite) is important because the rate and extent of iron oxide reduction can be impeded by precipitation, sorption, and complexation of the reduced Fe onto the surfaces of microbes or the iron oxide surfaces (Hansel et al. 2004). Fe(III)-reducing bacteria that couple PHC oxidation with Fe(III) reduction can lead to the formation of siderite, ferroan calcite, vivianite, and magnetite (Bell et al. 1987, Fredrickson et al. 1998, Tuccillo et al. 1999, Zachara et al. 2004). Local pH-eH conditions often control secondary Fe(II) mineral formation.

Hansel et al. (2004) studied microbial acetate oxidation coupled with iron oxide oxidation in flow columns and found that the major Fe(II)-bearing material that formed was magnetite. They found that magnetite accounted for up to 50 % of the Fe(II)-bearing minerals and that the percentage of magnetite formed increased along the flow path. Magnetite is an interesting Fe(II)-bearing mineral because it is magnetic and this property could be used as a proxy to quickly identify regions of Fe(III) reduction at PHC-contaminated sites (Atekwana et al. 2014). Atekwana et al. (2014) conducted magnetic susceptibility surveys along groundwater flow paths at the Bemidji research site. They confirmed that, despite only making up a small percentage of the Fe(II)-bearing materials, magnetite created a strong magnetic susceptibility response in zones of where PHC biodegradation was coupled with and Fe(III) reduction. Bell et al. (1987) also studied the formation of secondary Fe(II)-bearing minerals under Fe(III)-reducing conditions. They found that at high pH (approximately pH 8.5) and low Eh (approximately -200 mV), magnetite was the dominant secondary Fe(II) mineral. However, as pH decreased, siderite became more favourable. They determined that this relationship between magnetite and siderite formation was driven by local pH-Eh conditions.

Atekwana et al. (2014) and Hansel et al. (2004) both reported that magnetite was an important sink for the reduced Fe(II). However, the percentage of the Fe(II)-bearing material that was magnetite differed between the two studies. Hansel et al. (2004) reported that magnetite was the major Fe(II)-bearing material while Atekwana et al. (2014) reported that magnetite was a minor but important component of Fe(II)-bearing material. This difference in the two studies could have occurred because of the flow columns used by Hansel et al. (2004). The columns used by Hansel et al. (2004) were constructed with a mixture of sand and iron oxides. In contrast, Atekwana et al. (2014) studied an aquifer with more complex geochemistry. Therefore, it can be

concluded that the formation of Fe(II)-bearing materials is strongly influenced by local groundwater geochemistry. For example, if sulfate reduction and Fe(III) reduction are concurrent, iron sulfides may be an important sink of reduced Fe. Furthermore, dissolved Fe concentrations and pH are local groundwater geochemistry parameters that can influence the formation of secondary Fe(II) minerals.

The formation and fate of iron sulfides (e.g., pyrite) also strongly influences the cycling of sulfur, iron, and carbon in the environment (Burton et al. 2009). At a PHC-contaminated site in Western Australia, Prommer et al. (1999) found pyrite in the majority of their contaminated sediment samples but none in the clean background samples. However, they concluded that Fe(III) reduction was not a significant remediation process at their site, since dissolved Fe concentrations were high in the background monitoring well and sediments were likely reduced prior to PHC-contamination. Dissolved Fe still played an important role at the site; however; because it removed toxic sulfide from the groundwater through iron sulfide precipitation (Prommer et al. 1999). Beller et al. (1992) came to a similar conclusion in their study of toluene degradation by a sulfate-reducing enrichment. They saw concurrent sulfate and Fe(III) reduction, but by comparing experimental stoichiometry to the theoretical they concluded that most of the toluene was oxidized by sulfate and sulfate reducers. A portion of Fe(III) was used to oxidize toluene but was mostly used as an electron acceptor for biogenic hydrogen sulfide oxidation (Beller et al. 1992). Syntrophic relationships between sulfate reducers and Fe(III) reducers can be an important biogeochemical reaction that can occur with iron-bearing minerals in aquifers (Flynn et al. 2014). Therefore, it is important to consider the effects sulfur and sulfate reducers on Fe(III) reduction and PHC oxidation.

2.4.3 Nitrogen Influences on Iron-cycling

Depending on the form (e.g., nitrate versus ammonia) nitrogen can influence iron-cycling as either a nutrient or through microbially-driven, nitrate-dependent Fe(II) oxidation. Fe(III) reducers that cannot fix nitrogen can increase in abundance when fixed nitrogen is readily available. For example, Mouser et al. (2009) studied the influence of ammonium availability on the composition of Fe(III)-reducing communities at a uranium-contaminated site in Colorado, USA. They found that *Rhodoferax* (a member of the *Comamonadaceae* family) dominated over *Geobacter* when ammonium was readily available. The key difference between *Geobacter* and *Rhodoferax*, they concluded, was the ability of *Geobacter* species to fix nitrogen. *Rhodoferax*, in

contrast, cannot fix nitrogen but will outcompete other Fe(III) reducers in environments where fixed nitrogen is present in abundance (Mouser et al. 2009). Therefore, the availability of fixed nitrogen (e.g., ammonium) heavily influences the relationship between *Geobacter* and *Rhodoferax* (Mouser et al. 2009).

Microbially-driven, nitrate-dependent oxidation of Fe(II) by microbes is possible under circumneutral pH conditions, but becomes less energetically favourable in acidic groundwater (Hedrich et al. 2011). Postma et al. (1991) studied the reduction of a nitrate plume from agricultural activities in a sandy unconfined aquifer. They concluded, based on electron balances, that pyrite was the main electron donor during nitrate reduction. Conversely, Schippers and Jørgensen (2002) suggested that microbial pyrite oxidation does not occur because pyrite is resistant to proton dissolution. Fe(II) monosulfide (FeS) is susceptible to proton dissolution and they were able to enrich FeS-oxidizing communities with nitrate as the electron acceptor. Schippers and Jørgensen (2002) suggested that microbial-driven FeS oxidation by nitrate occurs first by the dissolution of FeS by proton attack. The dissolved Fe(II) can then be oxidized to form a Fe(III) (oxy)hydroxide and the dissolved sulfide can be oxidized to intermediate sulfur products (e.g., elemental sulfur) and eventually sulfate (Schippers and Jørgensen 2002). Both Postma et al. (1991) and Schippers and Jørgensen (2002) concluded that the main denitrification product must be gaseous due to a lack of nitrite or ammonia. Postma et al. (1991) also noted that the reaction rate must be fast compared to the groundwater flow rate due to a sharp redox boundary. Torrentó et al. (2011) also studied the removal of nitrate contamination by denitrification enhanced through pyrite addition. They found that nitrate removal was enhanced by pyrite and concluded that bacteria belonging to the *Xanthomonadaceae* family (e.g., *Pseudoxanthomonas*) were responsible for the chemoautotrophic nitrate reduction. However, these results contradicted Schippers and Jørgensen (2002) findings where FeS (but not pyrite) could be oxidized by nitrate, but more recent research by Bosch et al. (2012) shows that anaerobic pyrite oxidation by nitrate is possible. In their study the pyrite oxidation was microbially mediated by *Thiobacillus denitrificans*. Clearly, there is some disagreement on nitrate-dependent Fe(II) oxidation in the literature. Under circumneutral pH conditions the reaction is energetically possible but is highly dependent on microbial communities and the Fe(II) mineralogy.

2.5 Monitoring Bioremediation

2.5.1 Soil Vapour Chemistry and Isotopes

The composition of soil vapour can provide some evidence of biodegradation and the biogeochemical reactions occurring. Respiration products (e.g., CO_2 and nitrogen gases) and oxygen are specifically useful. CO_2 is produced during heterotrophic microbial respiration and an enrichment of CO_2 in the soil vadose zone could indicate enhanced microbial respiration (Madigan et al. 2014). CO_2 is also an end-product of PHC biodegradation (often referred to as CO_2 mineralization). Reardon et al. (1979) found the average CO_2 concentration of uncontaminated, sandy calcareous soil was 0.2 % with seasonal fluctuations. In comparison, the well-studied PHC-plume at Bemidji, MN, USA saw an enrichment of CO_2, consistent with higher levels of organic carbon degradation (Molins et al. 2010). Molins et al. (2010) reported that the concentration of CO_2 was approximately 1 % at the plume fringe and it increased to 10 % in the plume core (the central region of the contaminated area). Nitrogen gases (N_2 and N_2O) could also indicate denitrifying conditions (Blicher-Mathiesen et al. 1998). Molins et al. (2010) also found an enrichment of N_2 relative to atmospheric pressures (>83 %) at the Bemidji research site (Table 2.4). Aerobic biodegradation also decreases the amount of oxygen in the subsurface. Molins et al. (2010) found that the concentration of oxygen decreased from approximately 20 % at the plume fringe to less than 2 % at the plumes core.

Table 2.4. Soil vapour composition found at Bemidji plume (Molins et al. 2010).

Vapour Component	Plume Fringe	Plume Core
N_2	79 %	>83 %
O_2	20 %	2.0 %
CO_2	1.0 %	10 %

In addition to soil vapour composition, remediation and biodegradation is often monitored through the use of compound specific isotope analysis (Hunkeler et al. 2009). This done by comparing the isotopic signature of a sample to a reference standard. The result is then expressed in per mille (‰) (Equation 2.1) using the isotopic ratio (R) of the sample (x) and the standard (std).

$$\delta(‰) = \left(\frac{R_x}{R_{std}} - 1\right) x\, 1000 \qquad (2.1)$$

For PHC remediation, carbon and oxygen isotope analyses of the CO_2 vapour produced during biodegradation can be useful in tracking bioremediation. Specifically, the fractionations $^{13}C/^{12}C$ ($\delta^{13}C$) and $^{18}O/^{16}O$ ($\delta^{18}O$) are sampled for and compared to a background and source value to determine the extent of remediation (Hunkeler et al. 2009). The extent of remediation increases as $\delta^{13}C$ (Table 2.5) approaches the background values. Aerobic biodegradation of PHCs can deplete ^{13}C by 3.6 to 6.2 ‰ compared to the original $\delta^{13}C$ (Hunkeler et al. 2001). This corresponded to an enrichment of ^{13}C in the biomass by 3.8 ‰ (Hunkeler et al. 2001). Yeh and Epstein (1981) studied the carbon and hydrogen isotopic fractionation of crude oils. They found that non-marine oil had a $\delta^{13}C$ ranging from -29.9 to -31.5 ‰, and that crude oil from Saskatchewan had $\delta^{13}C$ ranging from -29.7 to -31.1 ‰. These values; however, were not consistent with $\delta^{13}C$ found by Kelley et al. (1997) who studied the isotope fractionation of BTEX (benzene, toluene, ethylbenzene, and xylenes). They found that the $\delta^{13}C$ varied slightly between the BTEX compounds. $\delta^{13}C$ ranged from -23.8 to -26.6 ‰ for benzene, -22.9 to -25.2 ‰ for toluene, and from -22.4 to -25.3 ‰ for the xylene isomers (Kelley et al. 1997). The difference between the two studies can likely be attributed to a difference between crude and refined petroleum products. A typical background value for $\delta^{13}C$ is approximately -20.0 ‰, but this can vary by regional climate and by dominate plant type (Parada et al. 1983). CO_2 produced from carbonates may have a significantly different $\delta^{13}C$. Values of +0.28 to +2.18 ‰ and +0.12 to +4.50 ‰ have been reported for dolomite and calcite found in unconsolidated continental sediments (Degens and Epstein 1964).

Table 2.5. Typical $\delta^{13}C$ values for background and petroleum hydrocarbons.

	$\delta^{13}C$ (‰)	Reference
Background Soil	-20.0 ‰ (typical)	Parada et al. 1983
Saskatchewan Crude Oil	-29.7 to -31.1	Yeh and Epstein 1981
Benzene	-23.8 to -26.6	Kelley et al. 1997
Toluene	-22.9 to -25.2	
Xylene	-22.4 to -25.3	
Dolomite	+0.28 to +2.18	Degens and Epstein 1964
Calcite	+0.12 to +4.50	

The isotopic signature of the oxygen in CO_2 may also useful for monitoring the extent and pathways of bioremediation. The oxygen isotope in CO_2 is governed by the equilibrium between air and water (Hoefs 2009). Bottinga and Craig (1968) found that the $\delta^{18}O$ (Table 2.6)

of atmospheric CO_2 was in equilibrium with ocean water and was approximately +41 ‰ at 25 °C. Aggarwal et al. (1997) used stable carbon and oxygen isotope analysis of CO_2 produced during PHC biodegradation in an inoculated mineral media solution. They found that the $\delta^{18}O$ of CO_2 did not vary much once it reached equilibrium during their 43-day experiment. They found a $\delta^{18}O$ of CO_2 of approximately +35 ‰. Their mineral media; however, did not contain carbonates that could be a source of CO_2 in soils when dissolved (Appelo and Postma 2005). Degens and Epstein (1964) studied the stable carbon and oxygen isotopes of calcite and dolomite in a variety of geological materials. In unconsolidated continental sediments they found $\delta^{18}O$ values of -3.89 to -5.77 ‰ and -4.04 to -7.27 ‰ for dolomite and calcite respectively.

Table 2.6. Typical values of $\delta^{18}O$ of CO_2.

	$\delta^{18}O$ (‰)	Reference
Atmosphere	+41	Bottinga and Craig 1968
Media headspace	+35	Aggarwal et al. 1997
Dolomite	-3.89 to -5.77	Degens and Epstein 1964
Calcite	-4.04 to -7.27	

2.5.2 Metabolites

Low-molecular weight organic acids accumulate in PHC-contaminated aquifers undergoing biodegradation (Cozzarelli et al. 1994, Van Stempvoort et al. 2009). These by-products of heterotrophic microbial respiration, called metabolites (Table 2.7), can provide unequivocal evidence that PHCs are being removed by biodegradation and not physical or chemical process (e.g., dilution or abiotic oxidation). Beller et al. (1995) first proposed using metabolites to monitor PHC bioremediation. They proposed that to be useful indicators of PHC biodegradation, metabolites must have:

1) a clear biochemical link to specific PHCs,
2) no commercial or industrial use, and
3) biological and chemical stability.

For example, benzylsuccinate and isomers of methylbenzylsuccinate are metabolite end-products produced during the anaerobic biodegradation of toluene and xylene isomers (Beller et al. 1995). Benzoate and phenol are possible metabolite products of benzene biodegradation (Beller 2000). However, benzoate and phenol are not ideal metabolites because they can occur

naturally in groundwater. In addition, benzoate can also form from toluene biodegradation (Ulrich et al. 2005). Benzylsuccinate and methylbenzylsuccinate are superior metabolites compared to others (e.g., benzoate and phenol) because they are more specific to anaerobic biodegradation of their respective PHC-parent compounds (toluene and xylenes).

Table 2.7. Metabolites and PHC-parent compounds. Summarized from Beller (2000).

Metabolite	PHC-parent compounds	Condition
Benzoate	Numerous (e.g., benzene, toluene, ethylbenzene)	Aerobic or Anaerobic
Phenol	Benzene	Aerobic or Anaerobic
Benzylsuccinate	Toluene	Anaerobic
Methylbenzylsuccinate	Xylenes	Anaerobic
Cresols	Not definitive	Aerobic or Anaerobic
Toluates	Xylenes	Aerobic or Anaerobic

These microbial produced low-molecular weight organic acids can enhance mineral weathering in PHC-contaminated aquifers and increase the electrical conductivity of groundwater (Atekwana et al. 2005). Atekwana et al. (2005) used this relationship between metabolites and enhanced mineral weathering to infer that zones of high electrical conductivity were also zones of active PHC biodegradation. This relationship between electrical conductivity and PHC biodegradation could be used to create informed groundwater sampling and monitoring plans for PHC-contaminated sites (Atekwana et al. 2005). Metabolites have a clear use in monitoring bioremediation and providing evidence of PHC biodegradation. However, it should be noted that these metabolites can have toxic effects similar to their parent compounds (Melbye et al. 2009, Mao et al. 2009).

CHAPTER 3 METHODS

3.1 Site Description

The study site (Figure 3.1) is a PHC-contaminated site in Saskatoon, SK. A Saskatoon Co-op Association gas station has existed on the site since approximately the 1960s, and recent site assessments revealed subsurface contamination extending south beneath the roadway and nearby apartment building. Previous remediation work conducted between 2013 and 2015 includes MPE to remove the bulk of the PHC-contamination and air sparging to promote aerobic biodegradation of the PHCs. Despite these remediation efforts, PHC-contamination exists that is recalcitrant to physical removal by the MPE system. These diminishing returns from the MPE system prompted a switch to biostimulation to enhance anaerobic biodegradation starting in 2016. Briefly, the biostimulation solution (detailed in Section 3.2) was delivered to the contaminated region of the site by extracting, amending, and re-injecting the contaminated groundwater using an array of vertical injection and recovery wells in front of the apartment.

For this study, 6 boreholes (S15-01, S15-02, S15-03, S15-04, S15-05, and S15-06) were drilled and constructed into groundwater monitoring wells in October 2015 by Stantec Consulting on behalf of FCL. These monitoring wells were screened over a 6 m interval. Well S15-01 is screened from 2 to 8 meters below ground level (mBGL) and the remaining wells are screened from 1.5 to 7.5 mBGL. Well S15-01 is located outside of the contaminated region on the western portion of the site and serves as a control and background monitoring well for the study. The monitoring wells sampled during this study (Figure 3.1) also include older wells previously installed at the site, and are distributed on the north side of the apartment building with one monitoring well (11-10) on the south side of the building.

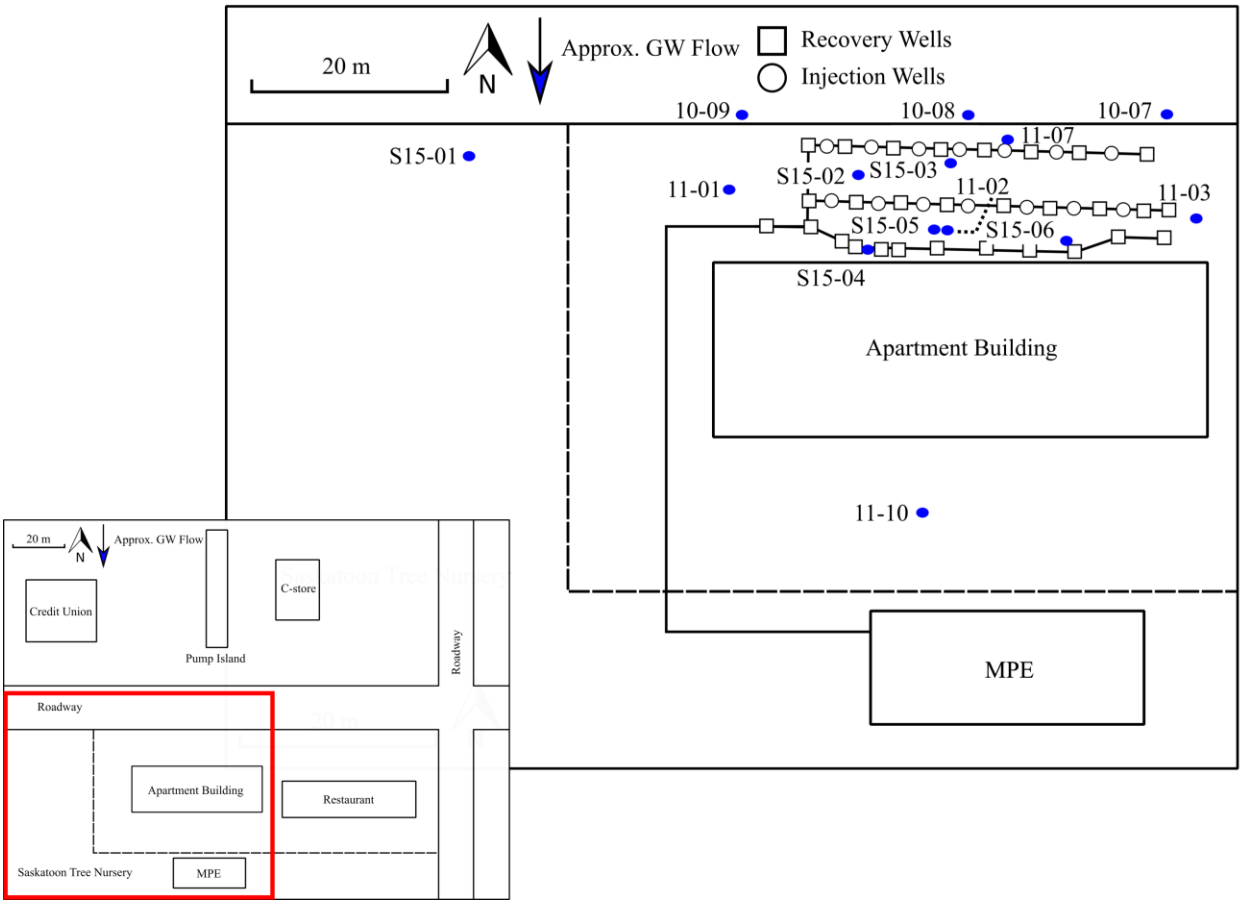

Figure 3.1. The study site showing monitoring and remediation well locations. Inset figure details the location of the gas station, apartment building, and MPE remediation system.

The surficial geology of the region is primarily unconsolidated glaciolacustrine deposits up to 100 m thick (Christiansen 1992). These deposits are calcareous (primarily dolomite) and the clay mineralogy is composed of montmorillonite, illite, kaolinite, and chlorite (Christiansen 1968). In general, the borehole stratigraphy at the site consists of top soil overlaying sand or silt from the surface to approximately 4 mBGL with interlayers of clay or clay till from approximately 4 mBGL to 9 mBGL. The water table is located between 3 to 5 mBGL and the groundwater flows approximately south.

3.2 Remediation System and Biostimulation Solution

The MPE system located at the site is operated by Stantec on behalf of FCL and consists of a series of vertical injection and recovery wells, soil vapour extraction wells, two above ground storage tanks, a pump-house with exhaust for the MPE system, a silt knock out, and a granulated activated carbon filter. Soil vapour extraction wells near the apartment building serve to create a vapour barrier to further protect residents of the apartment building from PHC vapour intrusion. The exhaust of the MPE system is monitored for O_2, CO_2, hexane equivalents, and isobutylene equivalents by an RKI Eagle2 gas monitor (RKI Instruments, Union City, CA, USA) equipped with a catalytic sensor and photoionization detector.

The array of injection and recovery wells (open squares and circles in Figure 3.1) are distributed on the north side of the apartment building. The recovery wells have a diameter of 51 mm and are screened over a 2 m interval (generally from 4.5 to 6.5 mBGL). The injection wells have a dimeter of 38 mm and are screened over a 1.5 m interval (generally from 4 to 5.5 mBGL). The manifold of the injection and recovery wells can be controlled such that the biostimulation solution delivery can be targeted to specific regions of the site. Approximately 60,000 L of groundwater amended with nitrate added as nitric acid (1.5 L and 0.8 mM), sodium tripolyphosphate (1.3 kg and 0.07 mM), and ferric-ammonium-citrate (6.1 kg and 0.5 mM) was circulated at the site approximately every two weeks during biostimulation solution delivery periods. Amended groundwater was gravity fed into the aquifer via the injection well array. Recovered groundwater was filtered through an activated carbon filter to remove any PHCs and re-amended with the biostimulation solution prior to injection into the subsurface.

3.3 Field Sampling

3.3.1 Sediment Sampling

Sediment samples were collected from S15 boreholes prior to biostimulation (October 2015) and from S17 boreholes (located near existing wells) after one field season of biostimulation (July 2017). These sediment samples were used to assess the effects of biostimulation on sediment mineralogy by synchrotron techniques and XRF (Table 3.1). The boreholes were advanced by a direct push method by Intercore Environmental Services (Maidstone, SK). Sediment cores were subsampled either in the field (S15 boreholes) or at the university (S17 boreholes). Core sections were transported to the university on the same day as

collection and stored at 10 °C prior to sampling. Subsampling was conducted within one to three days of core collection. Sediment samples were collected from borehole cores at approximately 50 cm or 100 cm intervals using aseptic procedures and stored at -20 °C in 50 mL conical tubes.

Table 3.1. Summary of methods used on sediment samples.

Method	Sample Date	
	October 2015	July 2017
PXRD	✓	✓
XRF		✓
Fe XANES	✓	✓
Sulfur XANES	✓	✓

3.3.2 Groundwater Sampling

Groundwater samples were collected prior to biostimulation (October 2015 and June 2016), during biostimulation (August 2016 and October 2016), and after one field season of biostimulation (June 2017 and November 2017). Groundwater samples were collected for geochemical and microbiological analyses (Table 3.2) by Stantec field technicians. When possible, samples for geochemistry were collected after geochemical field parameters had stabilized. However, low groundwater levels or slow recharge rates prevented this for some sampling points. Geochemical samples were collected and stored in coolers. For microbiology samples, groundwater (approximately 1 L) was collected into sterile glass bottles and transported to the university on the same day as collection and processed immediately. Groundwater (300 mL) was vacuum-filtered through a sterile 0.2 µm filter (Pall Life Sciences, New York, NY, USA and Sartorius Stedim Biotech, Goettingen, DE) to create triplicate filter samples for microbiological analyses. Less groundwater may have been filtered in cases where the groundwater filtered slowly or where insufficient groundwater was recovered to create 300 mL triplicate samples. The replicate groundwater filters were then aseptically transferred into sterile 15 mL conical tubes and stored at -20 °C. The filtered groundwater was transferred to amber glass jars, preserved by acidifying to pH 2 with 6 M hydrochloric acid (HCl) (ThermoFisher Scientific, Waltham, MA, USA). These filtered groundwater samples were sent for metabolite analysis at Dr. Lisa Gieg's lab (University of Calgary). To prepare a technical replicate for the

microbiological analyses, groundwater (2 L) collected from S15-01 in August 2016 was filtered through a single filter.

Table 3.2. Summary of methods used on groundwater samples.

Method	Sample Date					
	October 2015	June 2016	August 2016	October 2016	June 2017	November 2017
Geochemical	✓	✓	✓	✓	✓	✓
Metabolites		✓	✓		✓	✓
DNA Extractions	✓	✓	✓	✓	✓	✓
16S rRNA gene sequencing		✓	✓	✓	✓	

3.3.3 Soil Vapour Chemistry and Isotopes

Vapour samples (Table 3.3) from select monitoring wells (S15-01, S15-02, S15-04, and S15-05) were collected prior to biostimulation (June 2016) and after one field season of biostimulation (November 2016). Soil gas samples were collected by Stantec field technicians. Soil gas samples were collected by first purging the monitoring well headspace using a hand pump, connecting the provided sample bag to the monitoring well port by a luer-lock, and filling the sample bag with a hand pump till it is approximately two-thirds full (10-15 squeezes and approximately 300 mL volume). These vapour samples were analyzed for composition by gas chromatography (GC) and CO_2 isotopes ($\delta^{13}C$ and $\delta^{18}O$) at Isotech Laboratories Inc. (Champaign, IL, USA).

Table 3.3. Summary of methods used on vapour samples.

Method	Sample Dates	
	June 2016	November 2016
Composition (GC)	✓	✓
CO_2 isotopes ($\delta^{13}C$ and $\delta^{18}O$)	S15-01, S15-04, S15-05	S15-01

3.4 Geochemical Methods

3.4.1 Groundwater Geochemistry

Groundwater samples collected by Stantec field technicians were analyzed for field parameters and general chemistry (temperature, pH, dissolved oxygen, oxidation reduction potential (ORP), electrical conductivity (EC), alkalinity), PHCs (BTEX, CCME F1 − BTEX and F2), major cations (Ca, Fe_T, Mg, Mn_T, K, Na), major anions (Cl, SO_4, ΣH_2S), and nutrients (NO_3-N, NO_2-N, NH_3-N, P_T). Samples collected for metals (e.g., Fe_T) were filtered (0.45 µm) and preserved with HNO_3, nutrient samples were preserved with H_2SO_4, and PHC samples were preserved with $NaHSO_4$. All sample bottles came with acid pre-aliquoted. All samples were stored on ice and delivered for analysis on the same day as collection. Field parameters (temperature, pH, dissolved oxygen, ORP, and EC) were measured by Stantec using a YSI 556 multi-parameter sonde (YSI Inc., Yellow Springs, OH, USA) and analytical procedures (Table 3.4) were completed by Maxxam Analytics (Saskatoon, SK).

Table 3.4. Summary of geochemical analytical methods used. Geochemical analyses were performed at Maxxam Analytical.

Analyte	Analytical Method	Reference Method
Alkalinity	Titration	SM-22-2320
BTEX, CCME F1 − BTEX and CCME F2	GC/MS	CCME-CWS/ EPA 8260c
NH_3-N, Cl, SO_4, ΣH_2S, P_T	Colourimetry	EPA 350.1/SM 22-4500
Ca, Fe_T, Mg, Mn_T, K, Na	ICP	EPA 200.7
NO_3-N, NO_2-N	IC	SM 22 4110 B m

3.4.2 Metabolites

Groundwater samples (1 L) were collected, filtered (0.2 µm filter), acidified to pH 2 with 6 M HCl acid, and stored (4°C) in amber glass jars immediately after field sampling. Analysis for metabolite products was performed by Dr. Lisa Gieg's laboratory (University of Calgary). These analyses were performed as outlined in Gieg and Suflita (2002). Briefly, samples were: 1) extracted by mixing with ethyl acetate and drying over anhydrous sodium sulfate, 2) concentrated by rotary evaporation under N_2 stream, 3) derivatized to a trimethylsilyl ester product, and 4) analyzed by GC/MS for metabolite products and quantified using metabolite

standards. Calibration curves of representative standards (e.g., 3-methylbenzylsuccinic acid is representative of all methylbenzylsuccinic acid isomers) were used to quantify metabolite concentrations. The detection limit of this method is 10 nM and metabolite concentrations can be trusted within an order of magnitude (Toth and Gieg 2018).

3.4.3 Groundwater Geochemical Modeling

Geochemical results were modelled using PHREEQC (pH-redox-equilibrium modeling software, Version 3.3.7) and the wateq4f database to calculate saturation indices (SI) of various minerals (Ball and Nordstrom 1991, Parkhurst and Appelo 1999). The SI (Equation 3.1) provides evidence of the likelihood of mineral formation or dissolution based on ion activity and is calculated using the ion activity product (IAP) and the solubility product (K_{sp}) (Appelo and Postma 2005).

$$SI = \log\left(\frac{IAP}{K_{sp}}\right) \quad (3.1)$$

A positive SI indicates that the groundwater is supersaturated with respect to that mineral and the mineral has the potential to precipitate or that dissolution is unlikely (Appelo and Postma 2005). A positive SI without mineral precipitation could be caused by kinetic limitations in the field setting or by possible analytical errors in the data (Appelo and Postma 2005). Conversely, a negative SI indicates that the groundwater is undersaturated with respect to that mineral and precipitation is unlikely or that dissolution is possible (Appelo and Postma 2005). A sensitivity analysis of PHREEQC models was performed by repeating the simulations using a calculated redox potential (calculated pe from the first model) for select monitoring wells (S15-01, S15-04, and S15-05) and comparing the results (SI for calcite, dolomite, and gypsum). This analysis was completed to determine if the PHREEQC model was sensitive to the measured redox potential of the groundwater.

3.5 Mineralogical Methods

3.5.1 Sample Collection and Preparation

A selection of sediment samples were sub-sampled for mineralogical characterization by powder x-ray diffraction (PXRD), bulk x-ray adsorption spectroscopy (XAS), and x-ray fluorescence (XRF) analyses. Sediment sub-samples were collected into 15 mL conical tubes and

freeze dried for 24 hours, finely ground, and homogenized with a mortar and pestle. The mortar and pestle were cleaned with Ottawa sand (Sigma-Aldrich, St. Louis, MO, USA) and rinsed with ethanol between each sample.

3.5.2 Powder X-ray Diffraction

PXRD data was collected on the Canadian Macromolecular Crystallography Facility beam line (08ID-1) at the Canadian Light Source. Homogenous, finely ground sediment sub-samples were transferred to polyimide capillary tubes (Cole-Parmer, Vermont Hills, Il, USA) and sealed with glue (Loctite 454) to mount the sample into the beam spot. The beam radiation was monochromated with a Si(111) double crystal monochromator with a maximum energy of 18 keV (0.69 Å). Data was collected at the maximum energy with the area detector set 250 mm from the sample holder. Each sample was scanned in triplicate for 10 or 20 seconds to ensure a scan with adequate data quality was collected. GSAS-II was used to calibrate the collected two dimensional diffraction images and integrate them to one dimensional diffraction peak profiles (Toby and Von Dreele 2013). A lanthanum hexaboride (LaB_6) standard was used for beam calibration and the 2D diffraction images were integrated from 5° to 40° (2θ) between the 90° and 270° azimuths. Mineral phase identification was performed using X'pert Highscore Plus (Version 3.0, PANalytical, Almelo, Netherlands).

3.5.3 X-ray Fluorescence

Elemental composition of sediment samples collected in June 2017 was determined by XRF. Homogenous, finely ground sub-samples (approximately 4 – 6 g) were loaded into plastic sample holders and sealed with x-ray film. The XRF was performed on an ARL Optim'X X-ray Analyzer (ThermoFisher Scientific, Waltham, MA, USA) in the Peak Lab (Department of Soil Science, University of Saskatchewan). The XRF data was analyzed using OptiQUANT software (ThermoFisher Scientific, Waltham, MA, USA).

3.5.4 Sulfur X-ray Adsorption Spectroscopy

Bulk sulfur XAS was performed on the Soft X-ray Micro-characterization beamline (06B-1) at the Canadian Light Source. Homogenous, finely ground sediment sub-samples were lightly dusted onto carbon tape adhered to a copper sample plate and mounted in the solid-state end station under vacuum. The beam radiation was monochromated with a Si(111) double crystal

monochromator and the incident energy was scanned from -31 eV to +55 eV relative to the theoretical K-edge energy of sulfur (2472 eV). The pre-edge region was scanned from -31 eV to -7 eV at 2 eV increments, the edge region was scanned from -7 eV to +15 eV at 0.15 eV increments, and the post-edge region was scanned from +15 eV to +55 eV at 0.75 eV increments. The dwell time of each scan was adjusted to account for varying levels in the sulfur content of each sub-sample (more time for samples with lower sulfur content). Spectra of samples and standards were collected in duplicate by measuring total electron yield and fluorescence yield simultaneously.

Data reduction was performed using the ATHENA software package (Ravel and Newville 2005). Duplicate spectra were imported, aligned, merged, and calibrated to the sulfur K-edge for a gypsum standard (2481.7 eV). The pre-edge and post-edge region of the merged spectra were normalized to create a unity edge jump. Principal component analysis (PCA) was performed using SIXPack (version 1.40) to determine the minimum number of components needed to mathematically reproduce the sample spectra (Webb 2005). A variety of organic and inorganic sulfur reference compounds from the European Synchrotron Research Facility (ESRF) ID21 Sulfur XANES spectra database were used in ATHENA for linear combination fitting (LCF) (ESRF 2018). The LCF fit range was limited to -10 eV to +40 eV relative to the edge. Component weights in the model were neither forced to fall between 0 and 1 nor forced to sum to 1. Goodness of fit was determined by χ^2 value and residual plot. Fits were generally rejected if weighted components were not between 0 or 1, the residual plot was large, or the sum of the component weights was greater than 1.1. Since the sum of the components was not forced to sum to 1, the resultant component weights were normalized to sum to one.

3.5.5 Iron X-ray Adsorption Spectroscopy

Bulk Fe XAS was performed in fluorescence mode on the BioXAS side beamline (07ID-2S) at the Canadian Light Source with a 32-element Ge detector. Homogenous, finely ground sediment sub-samples were packed into XAS slotted sample holders. The beam radiation was monochromated with a Si(220) double crystal monochromator and the incident energy was scanned from -50 eV to +400 eV relative to the theoretical K-edge energy of Fe (7112 eV). The pre-edge region was scanned from -50 eV to -20 eV at 2 eV increments, the edge region was scanned from -20 eV to +30 eV at 0.5 eV increments, and the post-edge region was scanned from +30 eV to +100 eV at 2 eV increments and from +100 eV to +400 eV at 5 eV increments.

The dwell time of each scan was either 0.5 s or 3 s, dependent on the Fe content of each sub-sample. An in-line Fe foil standard was scanned concurrently with samples and reference standards at the beam line to calibrate the collected spectra. If a sample or standard was too thick or concentrated to allow for transmission, the Fe foil was scanned before and after the sample. Spectra of samples and standards were collected in triplicate by measuring transmission yield and fluorescence yield simultaneously. The data reduction procedure for Fe XAS data was similar to the data reduction for sulfur XAS data reduction, but spectra for Fe reference standards were collected at the beamline and confirmed by PXRD (as outlined previously). The LCF fit range was limited to -40 eV to +60 eV relative to the edge.

3.6 Microbiological Methods

3.6.1 DNA Extraction

Deoxyribonucleic acid (DNA) was extracted from groundwater filters using a FastDNA SPIN Kit for Soil (MP Biomedicals, Santa Ana, CA, USA) and a modified procedure to improve DNA yields. The modifications to the manufacturer's procedure for the groundwater filters include:

1) aseptically cutting the filters on sterile petri dishes before being transferred into the lysing matrix tubes provided in the kit,
2) shaking the lysing matrix tubes for 15 minutes on a vortex at max speed after adding the kit buffers,
3) an extra ethanol washing step to remove impurities (e.g., organic acids and PHCs)
4) eluting twice with 50 µL of DNase-free water, and
5) incubating eluted DNA at 55 °C for 5 minutes between the eluting steps.

The DNA extracts were quantified using a Qubit 2.0 Fluorometer (Invitrogen, Carlsbad, CA, USA) and quality checked using an Epoch Microplate Spectrophotometer (BioTek, Winooski, VT, USA) according to the manufacturer's protocol. High quality DNA has a A_{260}/A_{280} between 1.8 to 2.0 and a A_{260}/A_{230} greater than 2.0 (Mahmoudi et al. 2011). An A_{260}/A_{230} less than 2.0 can indicate contamination from organics that can inhibit gene amplification (Tsai and Olson 1992). DNA extracts were stored at -20 °C prior to analyses.

3.6.2 Microbial Community Analysis

DNA extracts were sequenced using high-throughput amplicon sequencing (MiSeq platform, Illumina, San Diego, CA, USA) and a universal primer set (515F/806R) that targets the V4 region of the 16S rRNA gene for both Bacteria and Archaea at Research & Testing Laboratories (Lubbock, TX, USA). Typically, 20 µL of DNA extract was sent for sequencing, but up to 60 µL was sent if the DNA concentrations were low. A DNA sample from S15-01 groundwater (August 2016) was sent with each sequence batch to serve as a technical replicate. The sequencing data was processed using the mothur software package and following the Miseq standard operating procedure (Schloss et al. 2009). Briefly, sequence contigs were assembled from paired reads, screened to remove sequences with ambiguous bases, aligned, screened to remove sequences that did not align or had homopolymers greater than or equal to 8 bases, screened for chimeras that were then removed, and classified. Sample data was compared to ensure replicate samples (generally in triplicate) had consistent patterns in read abundance at the phylum and genus level, then replicate data was pooled. Reads were clustered into operational taxonomic units (OTUs) using the opticlust algorithm and classified using the RDP classifier trainset (v.9.0). The sample datasets ranged between 34,308 and 198,866 reads per set. Prior to further analyses the reads were subsampled to 34,308 reads per sample set. Good's coverage, number of OTUs, Inverse Simpson index (diversity estimator), Shannon index (diversity), Chao estimator (richness estimator), and Ace estimator (estimate of total OTUs) were calculated. NMDS (non-metric multidimensional scaling) distance matrices, stress and R^2 values were calculated using both Yue and Clayton and Jaccard distance calculators and plotted using OriginPro 2016 (version 9.3.2.303, academic license). The correlation of the relative abundance of each OTU with the two axes in the NMDS dataset was calculated using the corr.axes command and Spearman calculation method and select contributors were plotted over the respective NMDS plots as biplots.

3.6.3 Microcosm Experiments

A bench-scale microcosm experiment was completed to test the effects of malate (replacing citrate) and the possible addition of a surfactant to the biostimulation solution. The objective of this experiment was to confirm the potential of Fe(III) reduction in batch experiments and to see if surfactants and malate stimulated Fe(III)-reducing microbial activity.

The experiment consisted of three surfactant treatments (sodium dodecyl sulfate, refined biosurfactant, and unrefined biosurfactant), a malate treatment, a malate and refined biosurfactant treatment, an untreated control, and a sterile control. The biosurfactant used in the experiment was a plant derived surfactant acquired from Canadian Carnation Biproducts (Saskatoon, SK). The unrefined biosurfactant product contained more plant materials (e.g., carbohydrates and proteins) compared to the refined biosurfactant. All treatments and controls were completed in triplicate.

The CMC of the surfactant was approximated by measuring the EC of distilled water at increasing surfactant concentrations. The CMC is roughly approximated by the concentration at which a change in EC trend is observed (Pérez-Rodríguez et al. 1998). Surfactant treatments were added at concentrations above the CMC determined by this method to account for experimental error and surfactant sorption to sediments.

Sediment (35 g) from the contaminated region of the site and groundwater (50 mL) collected from S15-01 was placed in a sterile 100 mL serum bottles to create the replicates for the experiment. The replicate microcosms were then crimp sealed and incubated in the dark at 10 °C for 6 weeks. The microcosms were sampled weekly to assess the changes in Fe(II)/Fe(III) and pH. The concentrations of Fe(II) and Fe(III) were determined by ferrozine (Stookey 1970, Viollier et al. 2000). Filters were also collected for DNA extraction to determine the effects of treatments on microbial communities in the groundwater. Sediment samples were also collected for DNA extraction and mineralogical characterization. These analyses; however, were not completed.

3.7 Statistical Methods

The quality of the groundwater geochemistry was evaluated using the charge balance error (CBE). The CBE was calculated in PHREEQC (Equation 3.2).

$$\text{CBE (\%)} = \frac{\sum \text{cations} + \sum \text{anions}}{\sum \text{cations} - \sum \text{anions}} \text{x}100 \qquad (3.2)$$

A CBE less than 5 % indicates good data quality, but less than 10 % is acceptable for environmental samples. The mean and standard error of sample data were calculated from data collected between June 2016 and June 2017. Results below detection limits were assumed to be

equal to zero. The standard error (Equation 3.3) was calculated using the standard deviation (σ) and the number of samples (n).

$$\sigma_{\bar{x}} = \frac{\sigma}{\sqrt{n}} \tag{3.3}$$

Correlation between select geochemical parameters was assessed using the Pearson's r value (Equation 3.4) calculated by linear regression fitting in OriginPro 2016 (version 9.3.2.303, academic license) using the covariance between the two variables (cov(x, y)) and their respective standard deviations (σ_x and σ_y).

$$r_{x,y} = \frac{\mathrm{cov}(x, y)}{\sigma_x \sigma_y} \tag{3.4}$$

A positive correlation between the two variables exists when r is greater than 0.6, and a negative correlation exists when r is less than -0.6. No correlation exists when r is between -0.6 and 0.6.

CHAPTER 4 RESULTS

4.1 Biostimulation Solution Delivery

The MPE system used for remediation and biostimulation solution delivery operated during the 2016 and 2017 field seasons. In total, there were eight biostimulation batch injections during 2016 (July 4, July 12, July 22, July 29, August 22, September 16, October 11, and October 26) and three batch injections in 2017 (July 7, October 5, and October 11). Each batch consisted of approximately 60,000 L of amended groundwater gravity fed over approximately 24-hours per batch. Biofouling in 2017 delayed further batch injections and the last two batch injections in 2017 (October 5 and October 11) used municipal potable water to reduce the risk of further biofouling (personal communication, Stantec Consulting). The two rows of injections wells nearest to the apartment building were used throughout the solution delivery, but the row nearest to road way was only used for the initial batch injection; thus, most of the amended groundwater was delivered to the western side of the site near S15-02, S15-03, S15-04, and S15-05. Based on observed flow rates in the injection system, the solution delivery was highest in the proximity of S15-04 and S15-05 (unpublished data, Stantec Report, 2018).

Groundwater height contour maps for June 2016 and June 2017 (Figure 4.1, Table A.1 in Appendix A) show a slight increase in groundwater height over this period of time near the remediation wells, but the groundwater continued to flow in a general southwardly direction.

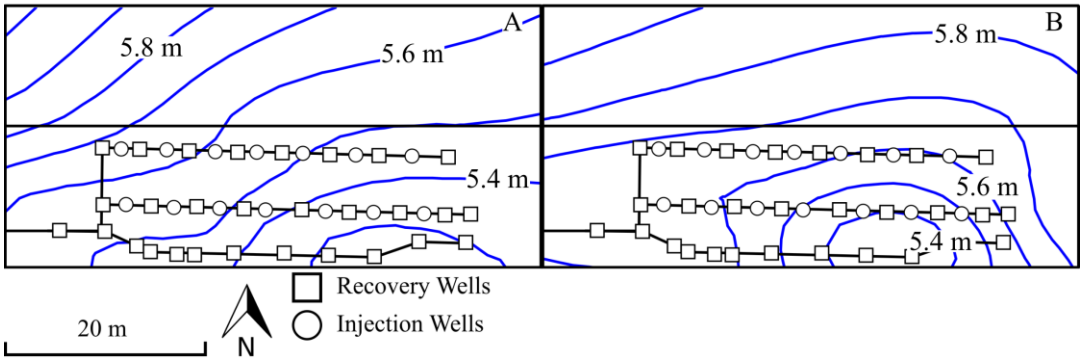

Figure 4.1. Groundwater table contour map during the study. Relative to a datum 9 mBGL (the typical depth of a borehole at the site). The groundwater is typically 3 – 5 mBGL Sub-figures: A) June 2016. B) June 2017.

Based on measurements of the MPE exhaust (hexane and isobutylene equivalents) it is estimated that the MPE system removed 54 kg of vapour phase PHCs and 0.055 kg of dissolved phase PHCs during the 2016 field season (unpublished data, Stantec Report, 2018). Furthermore, over the same time-period, measurements of the CO_2 content of the MPE exhaust were used to estimate that approximately 290 kg of PHCs were removed by biodegradation. Based on O_2 consumption it was estimated that 198 kg of PHCs were removed by biodegradation (unpublished data, Stantec Report, 2018).

4.2 Groundwater Geochemistry

4.2.1 Petroleum Hydrocarbons and Metabolites

Metabolites and respective PHC parent compound concentrations (Table A.2, Table A.3, and Table A.4) were plotted as a combined bubble and scatter plot to observe the effect of the biostimulation solution on PHC biodegradation for select monitoring wells (S15-02, S15-03, S15-04, and S15-05). Monitoring wells were plotted based on the likelihood that they were biostimulated and are representative of a range of geochemical conditions at the study site.

A comparison the concentration of benzene to benzoate and phenol (Figure 4.2 and Figure 4.3, respectively) shows a general decrease in the concentration of benzene over time with a corresponding elevation of benzoate concentrations (red circles, Figure 4.2) compared to the concentration of benzoate in the background monitoring well (open circles, Figure 4.2 and Figure 4.3). Furthermore, the concentration of benzoate was slightly elevated in S15-02 and S15-04 but near background concentrations in S15-03 and S15-05. The concentrations of benzene and phenol (blue circles, Figure 4.3) followed a similar trend to benzene. However, in comparison to benzoate, phenol concentrations were one to two orders of magnitude higher compared to the background concentrations of phenol. Benzene concentrations are still on average 1000x higher than the tier one potable groundwater quality guideline for benzene (Table 2.1).

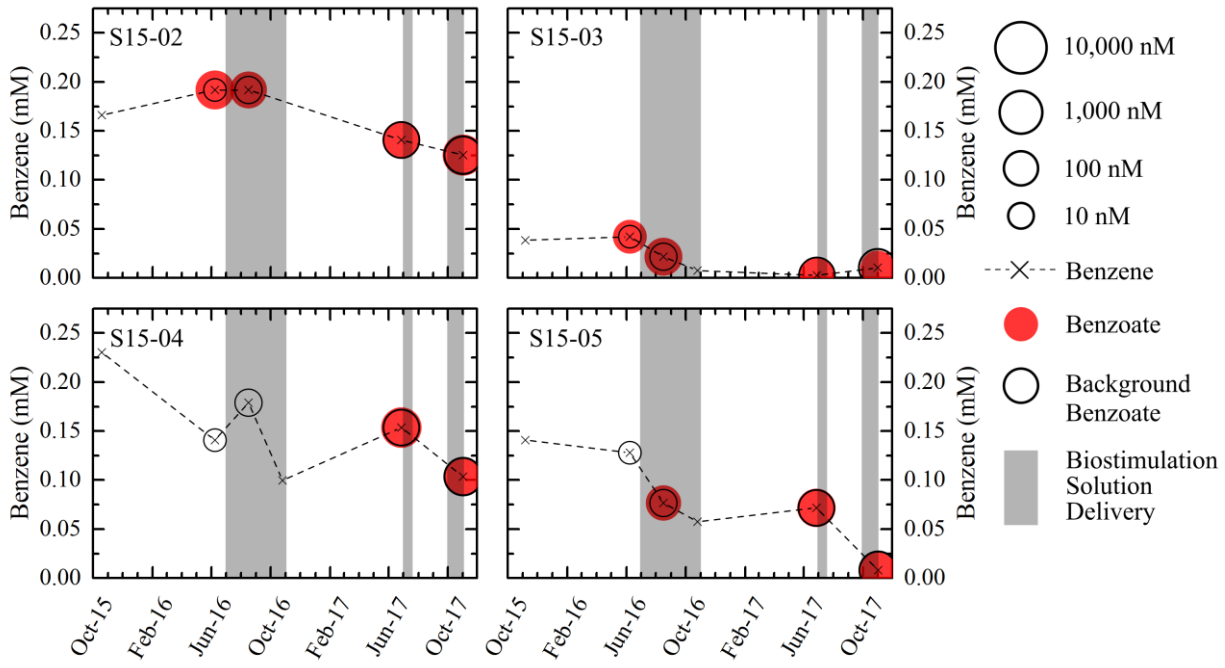

Figure 4.2. Concentrations of benzene (x) and benzoate (red circles) for select monitoring wells and background monitoring well (black open circle) over the study period. Benzoate concentrations correspond to the size of the circle (log scale). Grey bands indicate periods of biostimulation solution delivery.

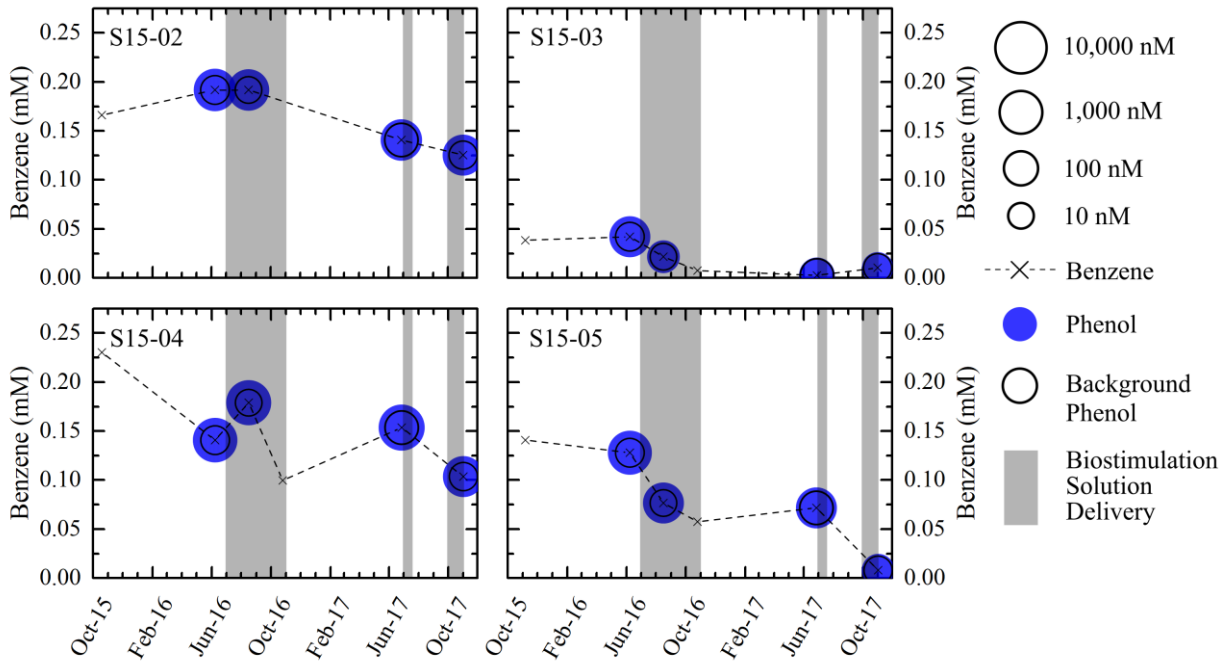

Figure 4.3. Concentrations of benzene (x) and phenol (blue circles) for select monitoring wells and background monitoring well (black open circle) over the study period. Phenol concentrations correspond to the size of the circle (log scale). Grey bands indicate periods of biostimulation solution delivery.

A comparison of the concentrations of toluene and benzylsuccinate (teal circles, Figure 4.4) for select monitoring wells over the study period shows a dramatic decrease in toluene concentrations in wells S15-02, S15-04, and S15-05. These results contrasted with benzene results which saw a less drastic decrease. Data from these monitoring wells show different trends with respect to benzylsuccinate. In S15-04, benzylsuccinate was initially present in 2016 but was then undetectable in 2017 despite the presence of measurable toluene. In S15-05, the reverse is true and benzylsuccinate was low or undetectable in 2016 and increased in 2017. In S15-02, benzylsuccinate was present throughout the study and increased slightly in 2017. The concentration of toluene in S15-03 was already very low prior to biostimulation and benzylsuccinate was not detected during the study period. Toluene concentrations are still on average almost 60x higher than the tier one potable groundwater quality guideline (Table 2.1).

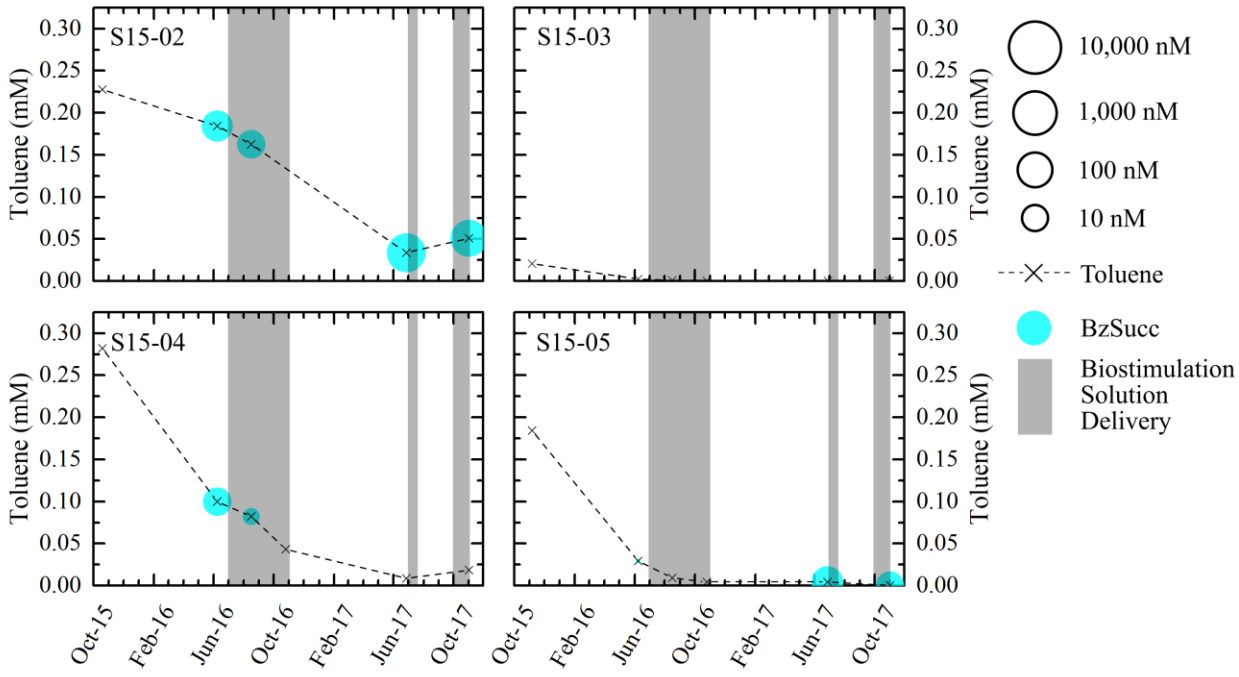

Figure 4.4. Concentrations of toluene (x) and benzylsuccinate (teal circles) for select monitoring wells over the study period. Benzylsuccinate concentrations correspond to the size of the circle (log scale). Grey bands indicate periods of biostimulation solution delivery. Note: benzylsuccinate was not detected in the background monitoring well or S15-03.

Ethylbenzene concentrations (Figure 4.5) generally decreased for select monitoring wells over the study period. No conclusive metabolite exists for ethylbenzene; however, benzoate is a possible metabolite of both benzene and ethylbenzene. Furthermore, ethylbenzene concentrations showed a similar trend as benzene concentrations. Ethylbenzene concentrations decrease in all monitoring wells noted but decreased more in S15-05 than S15-04. Ethylbenzene concentrations are still on average approximately 6x higher than the tier one potable groundwater quality guideline (Table 2.1).

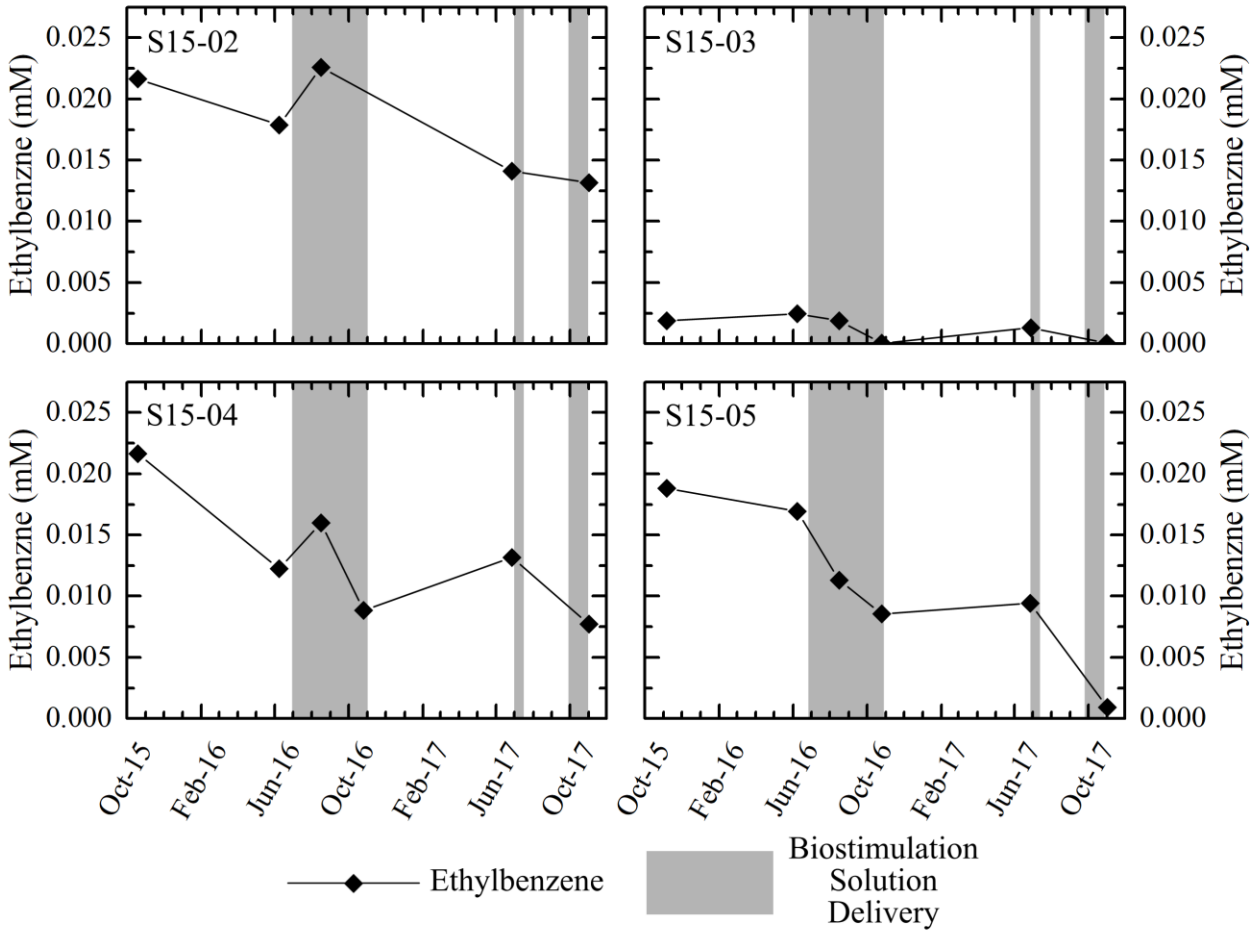

Figure 4.5. Concentration of ethylbenzene for select monitoring wells over time. Grey bands indicate periods of biostimulation solution delivery.

A comparison of the concentrations of xylenes and methylbenzylsuccinate (purple circles, Figure 4.6) shows the concentration of xylenes decreased but methylbenzylsuccinate was not detected until 2017. The concentration of methylbenzylsuccinate was highest in S15-02 which also corresponded to the highest concentration of xylenes at the end of the sampling period (October 2017). Xylene concentrations are still on average almost 40x higher than the tier one potable groundwater quality guideline (Table 2.1).

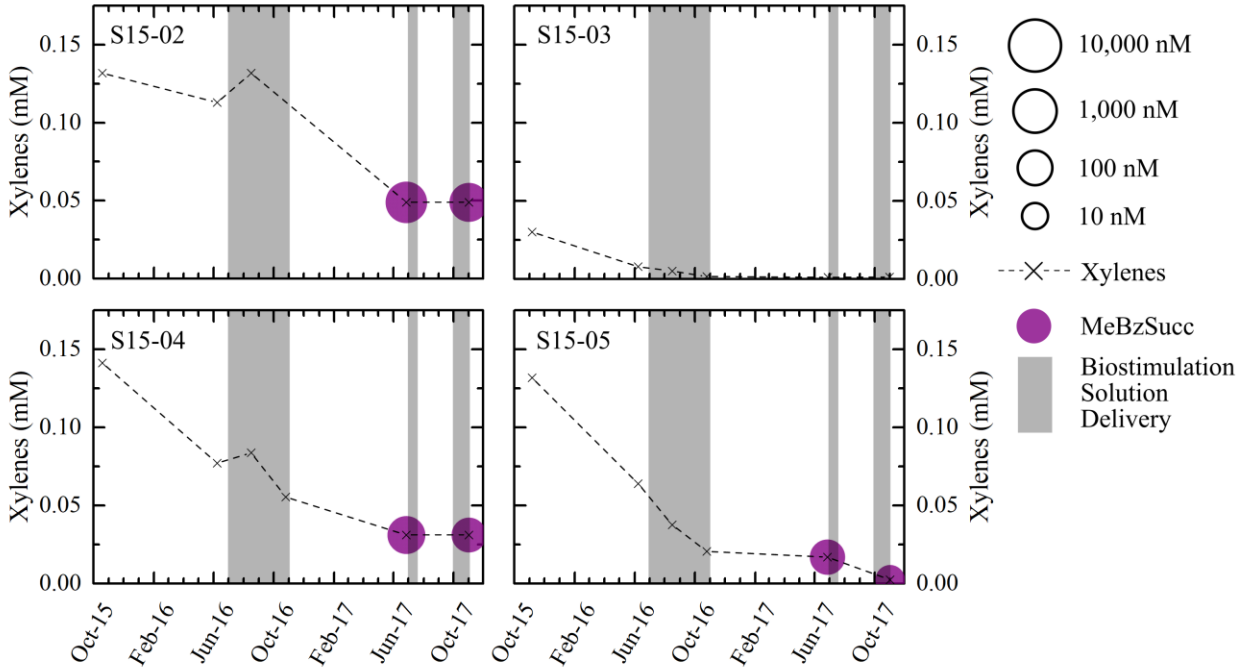

Figure 4.6. Concentrations of xylenes (x) and methylbenzylsuccinate (purple circles) for select monitoring over the study period. Methylbenzylsuccinate concentrations correspond to the size of the circle (log scale). Grey bands indicate periods of biostimulation solution delivery. Note: methylbenzylsuccinate was not detected in the background monitoring well or S15-03.

The trend of the CCME F2 PHCs (Figure 4.7) for select monitoring wells over the study period shows a decrease in concentration of F2 PHCs at the study site during biostimulation. However, it should be noted that concentrations were initially low and most the PHC-contamination exists from BTEX. Like benzene, the decrease in F2 PHCs appears to be slower in S15-04 compared to S15-05. Concentrations of F1 − BTEX (Table A.3) and F2 PHCs were low compared to BTEX concentrations. Therefore, the discussion of this thesis focuses on results concerned with BTEX remediation.

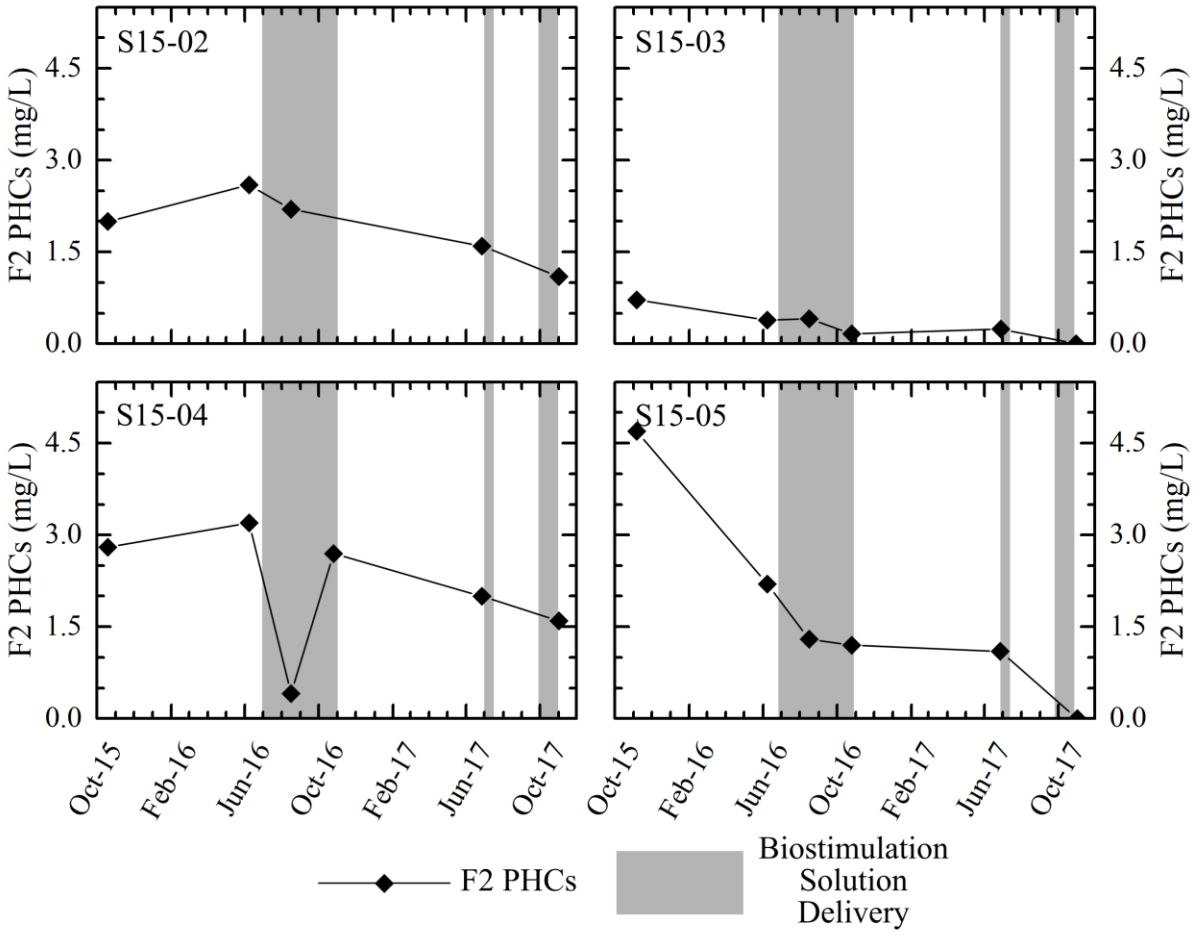

Figure 4.7. Concentration of CCME F2 PHCs for select monitoring wells over time. Grey bands indicate periods of biostimulation solution delivery.

4.2.2 Field and General Groundwater Geochemistry

Throughout the biostimulation period groundwater temperature was approximately 9.9 ± 0.3 °C (n = 27), dissolved oxygen at the site was low (1.6 ± 0.1 mg/L; n = 27), and contaminated groundwater conditions were more reducing compared to the background conditions (-83 ± 14 mV; n = 23 compared to +86 ± 4 mV; n = 4). Groundwater pH (Figure 4.8) remained circumneutral (pH 6.7 ± 0.1; n = 27) throughout the study but decreased slightly in some monitoring wells (S15-02, S15-04, and S15-05). The groundwater pH increased slightly in S15-03 during biostimulation.

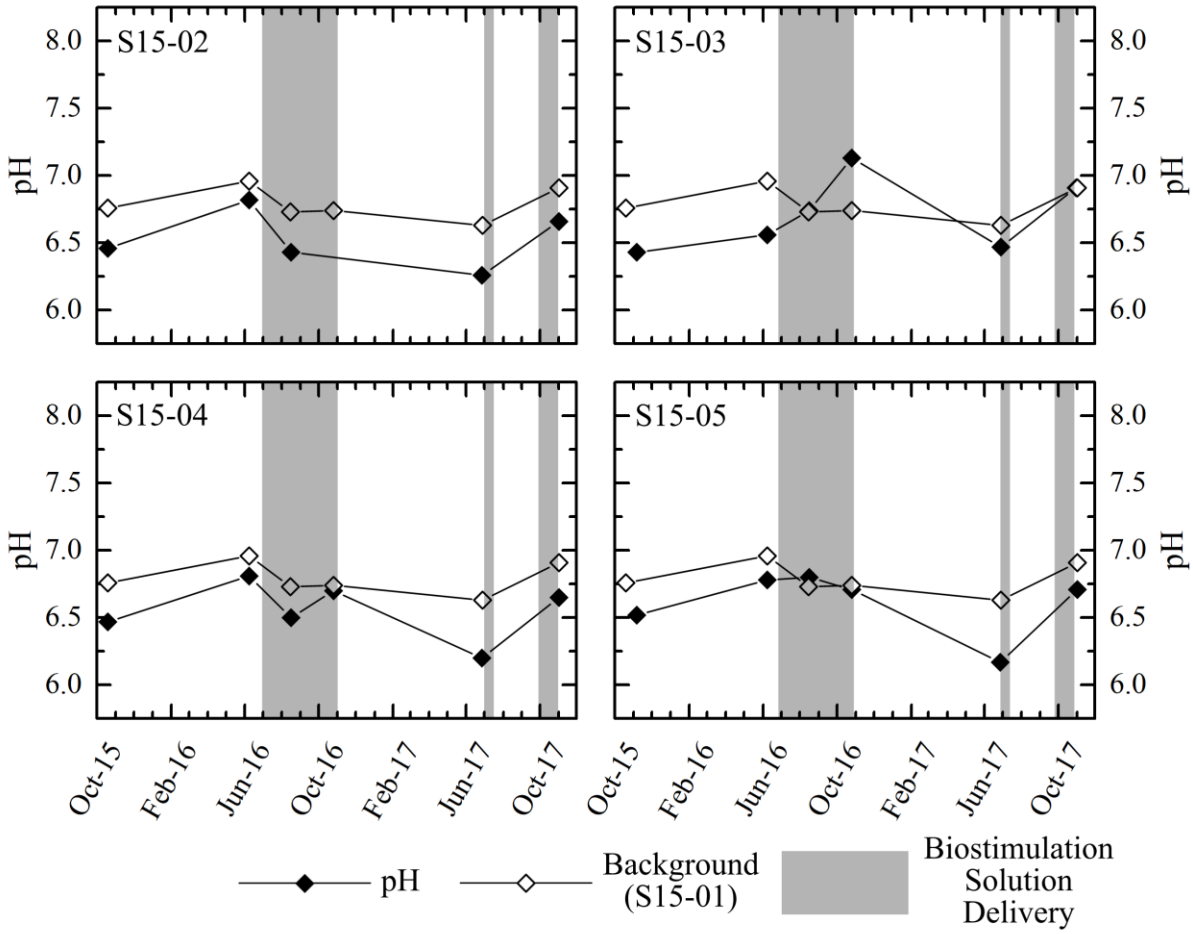

Figure 4.8. Groundwater pH during biostimulation. Grey bands indicate periods of biostimulation solution delivery.

Compared to background alkalinity (523 ± 19 mg/L $CaCO_3$; n = 4), the alkalinity of the contaminated groundwater was elevated (688 ± 23 mg/L $CaCO_3$; n = 23). The trend of alkalinity (Figure 4.9) during biostimulation for select monitoring wells shows that, during biostimulation, alkalinity appears to increase in some monitoring wells (S15-03) and decrease in others (S15-04 and S15-05). This could possibly be caused by a difference in location relative to the injection wells. Well S15-04 saw a sharp increase in alkalinity initially in 2017 (June 2017) followed by a sharp decrease (October 2017). Well S15-05 also had a slight increase in alkalinity in 2017 (June 2017) followed by a sharp decrease (October 2017).

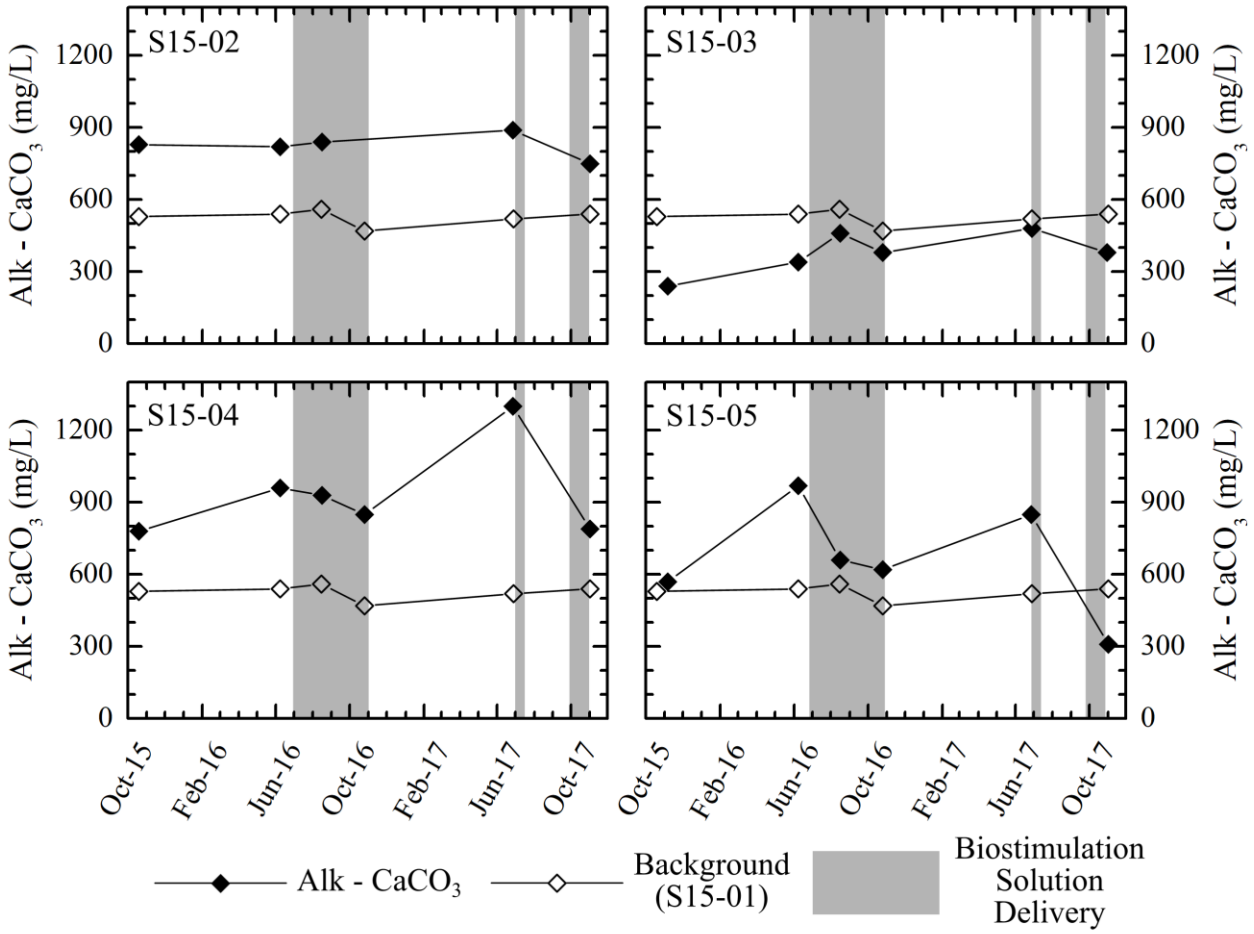

Figure 4.9. Groundwater alkalinity expressed as $CaCO_3$ during biostimulation. Grey bands indicate periods of biostimulation solution delivery.

Alkalinity relationships with Ca and Mg + Ca differed across the sampled monitoring wells (Table 4.1). Alkalinity was negatively correlated with Ca in both S15-04 and S15-05 but positively correlated with Ca in the background monitoring well. With respect to Mg + Ca, alkalinity was negatively correlated with in S15-05 but did not have a strong correlation in the other monitoring wells.

Table 4.1. Pearson's r values for Alkalinity & Ca and Alkalinity & Mg + Ca.

Well ID	Alkalinity ($CaCO_3$) Ca	Alkalinity ($CaCO_3$) Mg + Ca
S15-01 (n = 4)	0.648	0.435
S15-02 (n = 3)	-0.467	-0.573
S15-03 (n = 4)	0.448	0.460
S15-04 (n = 4)	-0.617	-0.438
S15-05 (n = 4)	-0.862	-0.842

The EC (Figure 4.10) of the contaminated groundwater (2.6 ± 0.1 mS/cm; n = 23) was higher than background (1.6 ± 0.1 mS/cm; n = 4) and increased during the delivery of the biostimulation solution delivery. In some monitoring wells (S15-03, S15-04, and S15-05) the EC increase was approximately two-fold during biostimulation. In contrast, the EC of S15-02 only increased slightly compared to the other monitoring wells.

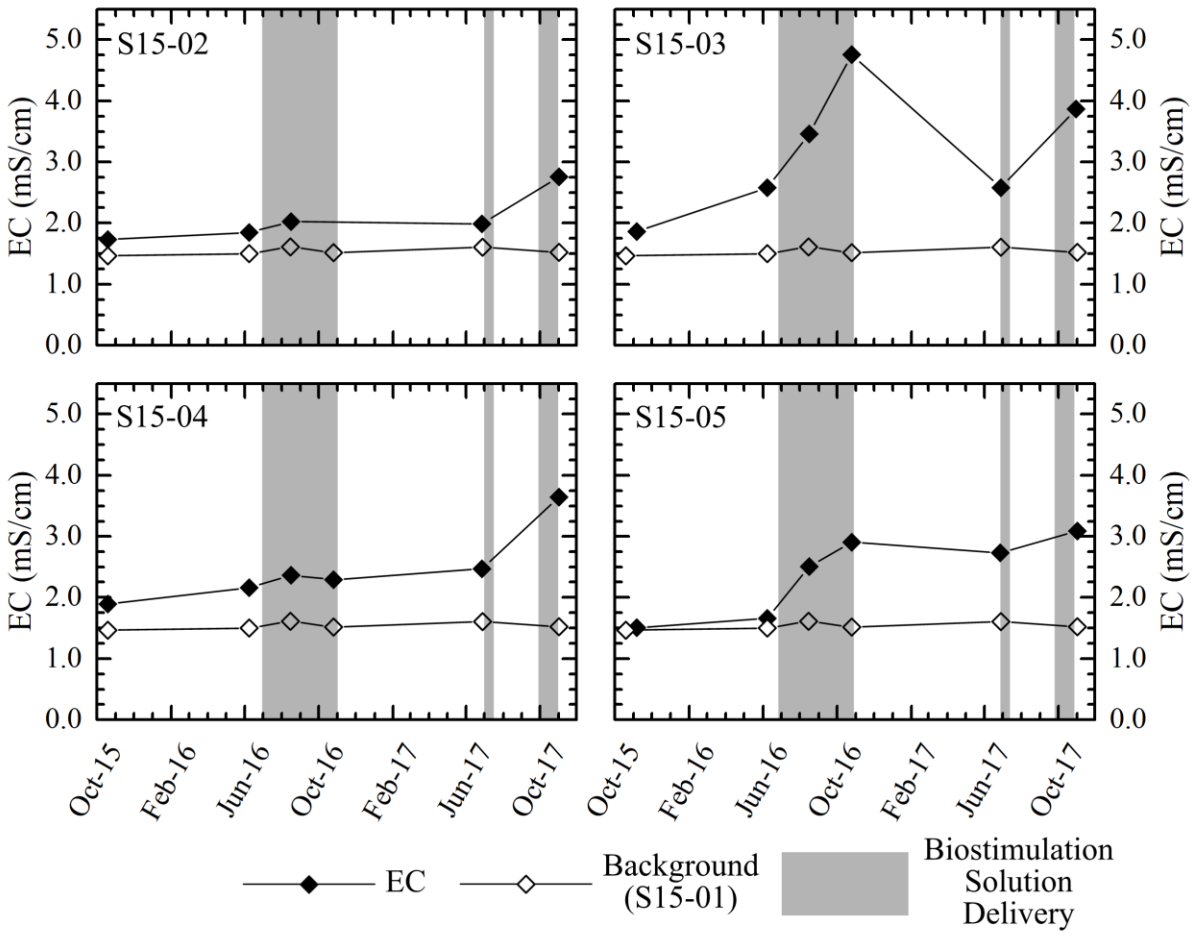

Figure 4.10. Groundwater electrical conductivity during biostimulation. Grey bands indicate periods of biostimulation solution delivery.

4.2.3 Major Cations

Average concentrations of major cations over the study period are presented in. All major cation concentrations (Table 4.2) are elevated in the contaminated groundwater compared to background to some degree. In particular, Mg (two-fold), Na (ten-fold), dissolved Mn (ten-fold), and dissolved Fe (ten-fold) were the most elevated in the contaminated groundwater compared to the background monitoring well.

Table 4.2. Concentrations of major cations in background & contaminated groundwater.

Major Cations	Background Groundwater n = 4 (mg/L)	Contaminated Groundwater n = 23 (mg/L)
Ca	340 ± 10	383 ± 21
Mg	108 ± 3	206 ± 13
K	7.3 ± 0.2	8.4 ± 0.3
Na	16 ± 1	137 ± 7
Mn_T	0.20 ± 0.03	4.4 ± 0.3
Fe_T	0.16 ± 0.01	7.4 ± 1.5

Between October 2015 and June 2016, the dissolved Fe (Figure 4.11) concentrations increased substantially in select monitoring wells. During biostimulation the trend of dissolved Fe was not consistent throughout the monitoring wells. In 2016 dissolved Fe increased in some monitoring wells (S15-02 and S15-04), decreased (S15-05), and remains constant in others (S15-03). All monitoring wells saw an increase in dissolved Fe concentrations from November 2016 to June 2017 followed by a decrease after the 2017 batch injections.

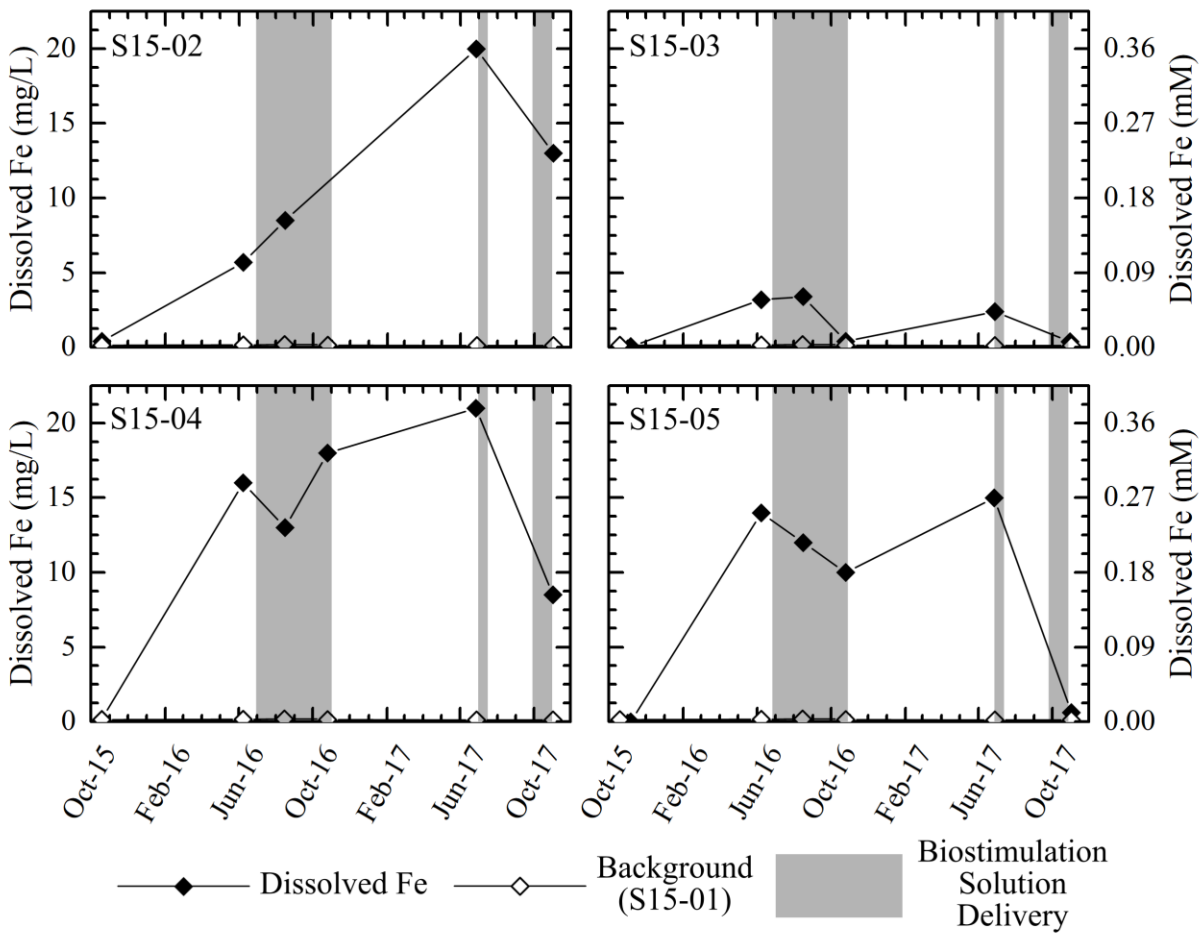

Figure 4.11. Dissolved Fe_T concentration during biostimulation. Grey bands indicate periods of biostimulation solution delivery.

Ca (Figure 4.12) and Mg (Figure 4.13) concentrations exhibit similar trends. Concentrations increased substantially in some monitoring wells (S15-03 and S15-05) but not others (S15-02 and S15-04). Both Ca and Mg decreased in concentration from November 2016 to June 2017 followed by an increase once biostimulation resumed.

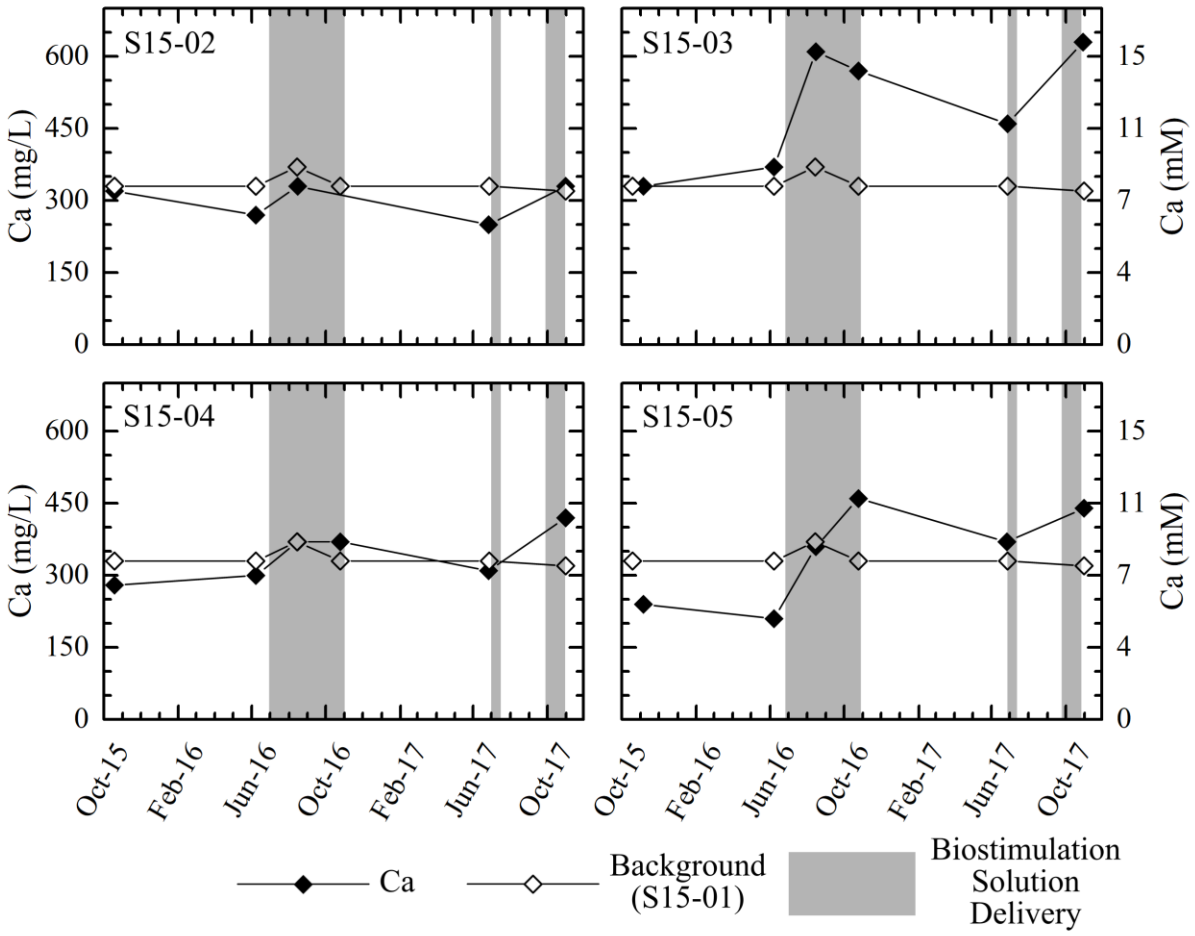

Figure 4.12. Groundwater calcium concentration during biostimulation. Grey bands indicate periods of biostimulation solution delivery.

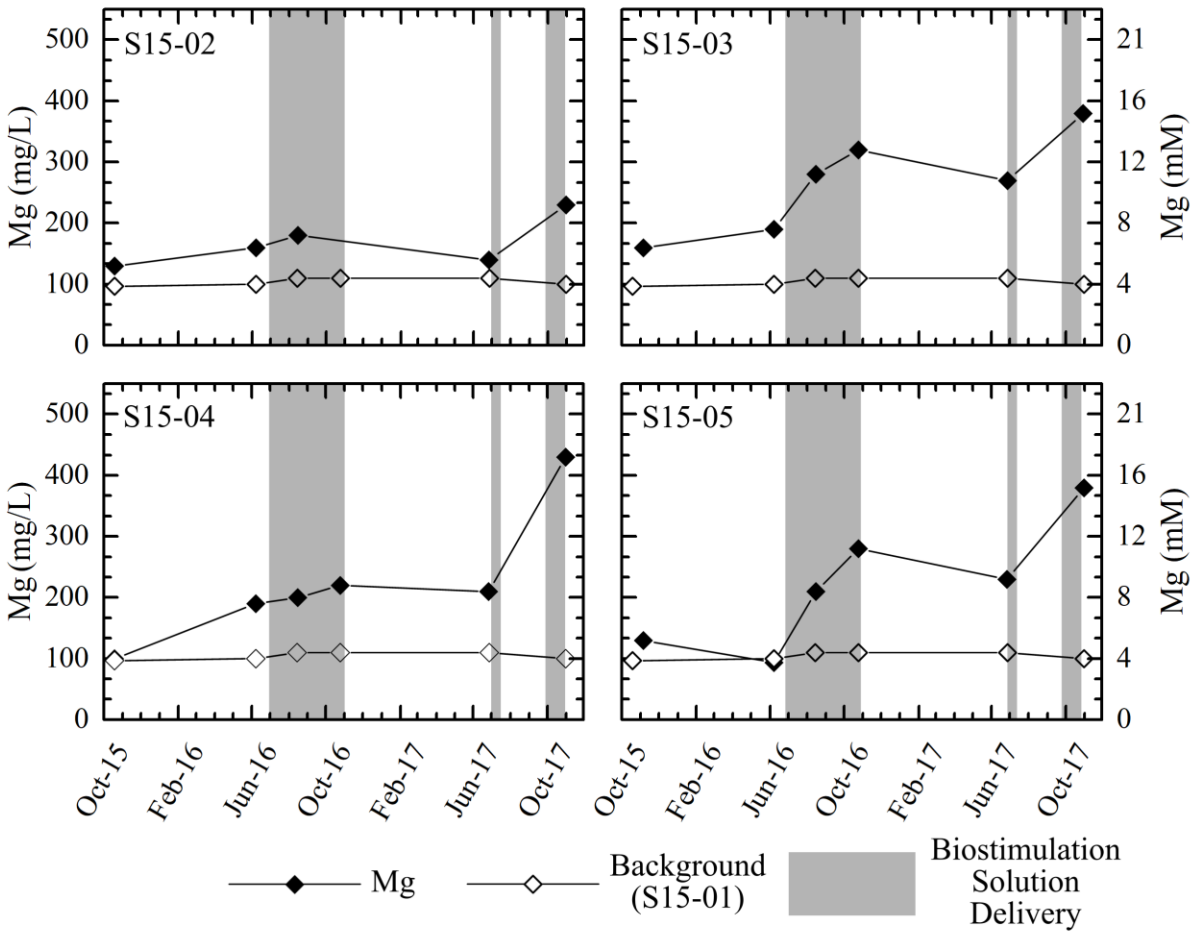

Figure 4.13. Groundwater magnesium concentration during biostimulation. Grey bands indicate periods of biostimulation solution delivery.

The Pearson r values for Mg, Ca, and Na (Table 4.3) shows both strong and weak positive correlations between major cations.

Table 4.3. Pearson's r values for Mg & Ca, Na & Ca, and Na & Mg.

Well ID	Mg Ca	Na Ca	Na Mg
S15-01 (n = 4)	0.333	0.683	0.878
S15-02 (n = 3)	0.961	0.402	0.132
S15-03 (n = 4)	0.847	0.834	0.871
S15-04 (n = 4)	0.513	0.280	0.947
S15-05 (n = 4)	0.995	0.799	0.819

4.2.5 Major Anions

The major anions (Table 4.4) at the study site are chloride, sulfide, and sulfate. Sulfide was not detected in the background monitoring well and sulfate concentrations were lower compared to the contaminated monitoring wells. Chloride concentrations were also lower in contaminated groundwater compared to the background.

Table 4.4. Concentrations of major anions in background & contaminated groundwater. ND = not detected.

Major Anions	Background Groundwater n = 4 (mg/L)	Contaminated Groundwater n = 23 (mg/L)
Cl	195 ± 17	166 ± 18
ΣH_2S	ND	0.4 ± 0.1
SO_4	430 ± 12	1141 ± 129

Sulfate concentrations (Figure 4.14) increased dramatically in S15-03 and S15-05 during 2016 biostimulation. The concentration of sulfate also increased in S15-04 to a smaller degree during this time. Sulfate levels in S15-02 were consistently low and comparable to background in 2016; in contrast, sulfide concentrations in S15-02 were the highest of the sampled monitoring wells.

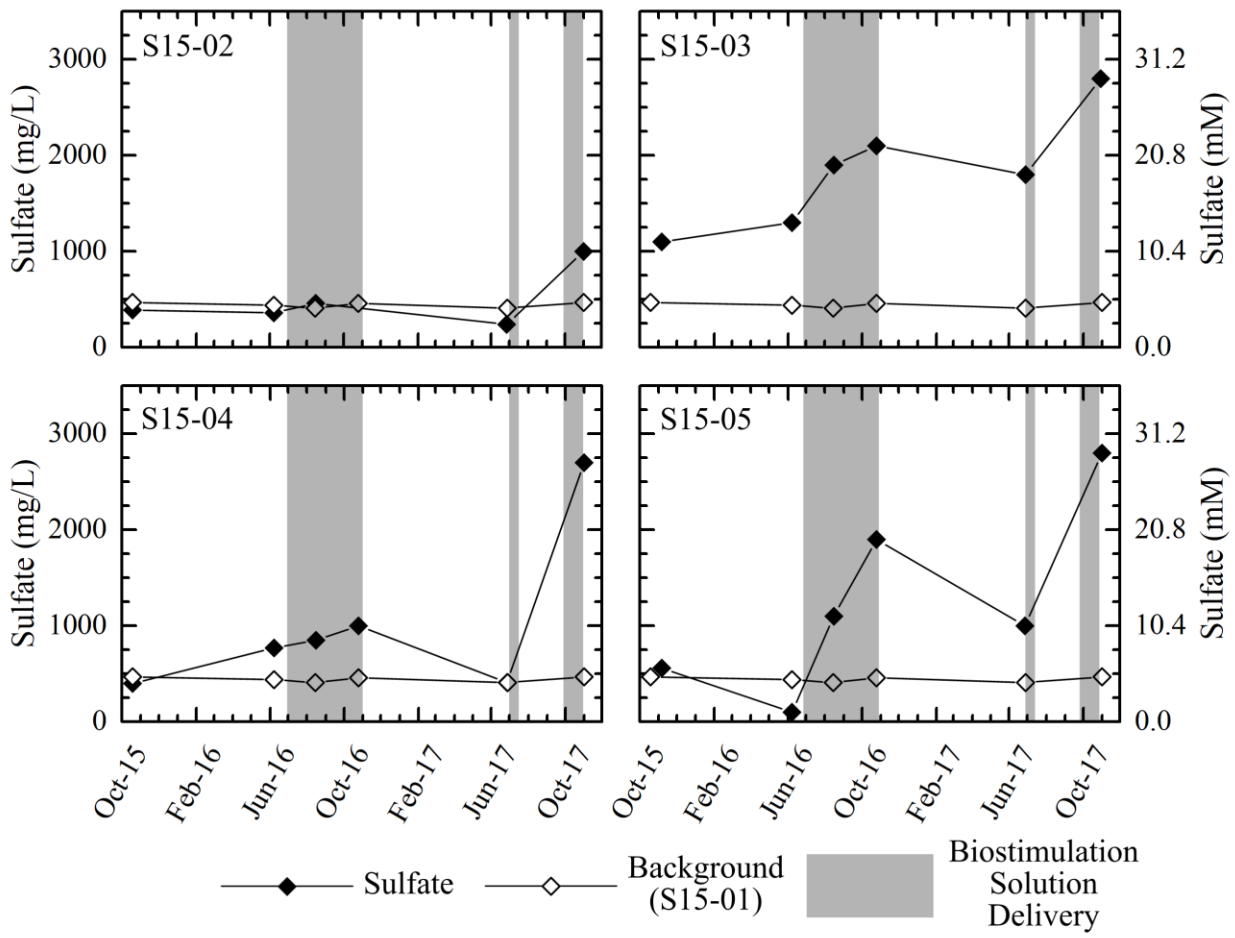

Figure 4.14. Groundwater sulfate concentrations during biostimulation. Grey bands indicate periods of biostimulation solution delivery.

Sulfide concentrations (Figure 4.15) initially increased in both S15-02 and S15-04 after the initial biostimulation. In S15-02 the concentration continued to increase as the study proceeded but in S15-04 the concentration decreased after the initial increase. In S15-05, sulfide concentrations decreased after the initial biostimulation and throughout the study. Sulfide concentrations were low or non-detectable throughout the study in S15-03.

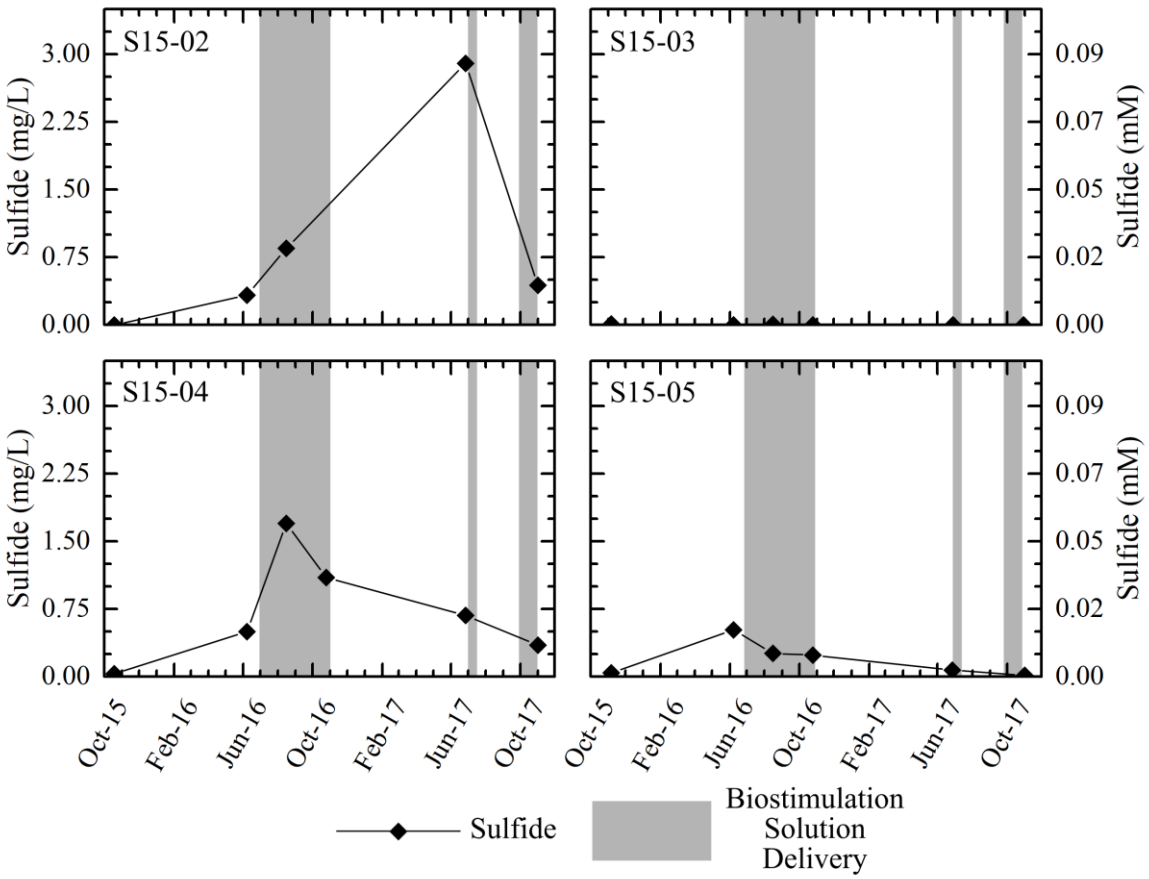

Figure 4.15. Groundwater sulfide concentrations during biostimulation. Grey bands indicate periods of biostimulation solution delivery. Note: sulfide was not detected in the background monitoring well.

In addition to these observed trends, sulfate also showed interesting correlations to Ca (Table 4.5). Sulfate and Ca were positively correlated in S15-02, S15-03, S15-04, and S15-05. However, compared to the other contaminated monitoring wells, the correlation between sulfate and Ca was weaker in S15-04. Sulfate and Ca were not correlated in the background monitoring well.

Table 4.5. Pearson's r values for sulfate and Ca.

Well ID	Sulfate Ca
S15-01 (n = 4)	-0.544
S15-02 (n = 3)	0.945
S15-03 (n = 4)	0.876
S15-04 (n = 4)	0.704
S15-05 (n = 4)	0.987

4.2.6 Nutrients

Average concentrations of nutrients in background and contaminated groundwater during biostimulation are presented in Table 4.6. Average dissolved phosphorus concentrations in the contaminated groundwater were higher than background values, but the contaminated groundwater remained depleted in nitrate and nitrite compared to background throughout the study. Nitrate and nitrite concentrations were often below detection throughout the study. The average concentration of ammonia was approximately equal in the background and contaminated groundwater but was more variable in the background.

Table 4.6. Concentrations of nutrients in background and contaminated groundwater.

Nutrients	Background Groundwater n = 4 (mg/L)	Contaminated Groundwater n = 23 (mg/L)
NH_3-N	0.19 ± 0.10	0.19 ± 0.02
NO_2-N	0.013 ± 0.008	0.006 ± 0.002
NO_3-N	0.68 ± 0.02	0.17 ± 0.09
P_T	0.010 ± 0.002	0.033 ± 0.008

Figure 4.16 shows the trend of ammonia concentrations of select monitoring wells during biostimulation. In 2016, ammonia concentrations were elevated in S15-03 and S15-05 compared to S15-02 and S15-04. However, ammonia increased in all monitoring wells over the study period.

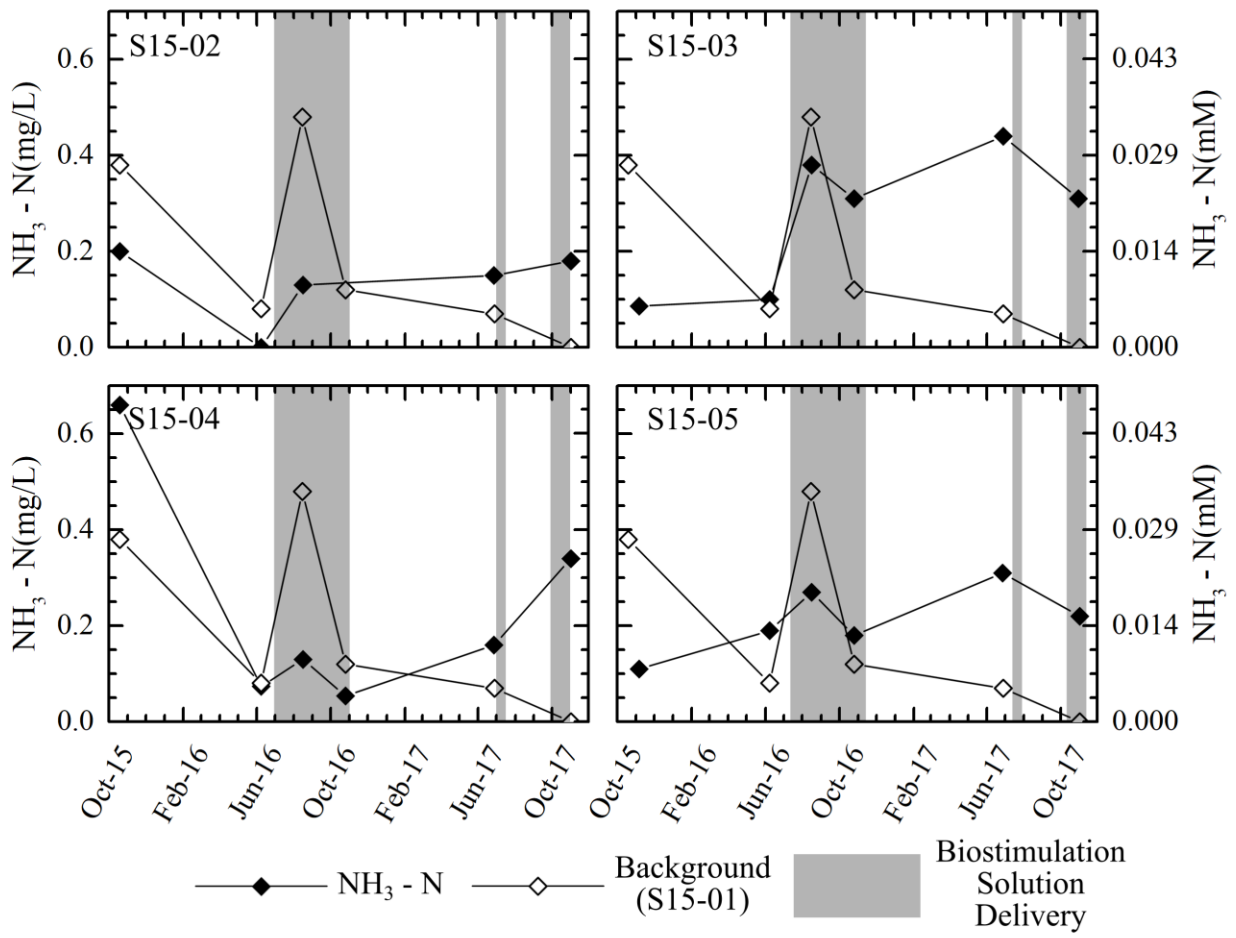

Figure 4.16. Groundwater ammonia concentration expressed as N during biostimulation. Grey bands indicate periods of biostimulation solution delivery.

4.2.7 Geochemical Modeling

The CBE of the collected groundwater geochemical data shows that the data quality is typical good (CBE < 5 %) or at least acceptable (CBE < 10 %). Calculated SI data (Table 4.7, Table A.9 and A.10) shows that the contaminated groundwater was supersaturated with respect to magnetite and pyrite and undersaturated with respect to vivianite. Calcite, dolomite, siderite, gypsum, and amorphous FeS were all near saturation in the contaminated groundwater. Calcite, dolomite, and gypsum showed observable trends towards under saturation or supersaturation during over the sampling period. The PHREEQC models were determined not to be sensitive to the redox potential (pe) of the groundwater through the completed sensitivity analysis (Table A.11).

Table 4.7. Average saturation indices in background and contaminated groundwater. n.d = no data.

	Background Well	Contaminated Wells
Magnetite	6.1 ± 1.5 (n = 4)	3.4 ± 0.8 (n = 22)
Pyrite	n.d	10.6 ± 0.7; (n = 16)
Amorphous FeS	n.d	-0.06 ± -0.01 (n = 16)
Siderite	-1.1 ± 0.1 (n = 4)	-0.09 ± 0.2 (n = 22)
Vivianite	-8.0 ± 0.5 (n = 4)	-4.6 ± 0.5; (n = 18)
Calcite	0.15 ± 0.08 (n = 4)	0.11 ± 0.05; (n = 23)
Dolomite	-0.12 ± 0.16 (n = 4)	0.07 ± 0.10; (n = 23)
Gypsum	-0.64 ± 0.01 (n = 4)	-0.42 ± 0.07; (n = 23)

Calcite (Figure 4.17) was consistently near saturation in S15-02, S15-04, and S15-05 during the study period with a slight trend toward undersaturation in S15-02 and S15-05. The background monitoring well also showed a similar trend toward with respect to calcite saturation. In contrast, groundwater in S15-03 became supersaturated with respect to calcite during biostimulation in 2016 but returned to near saturation in 2017.

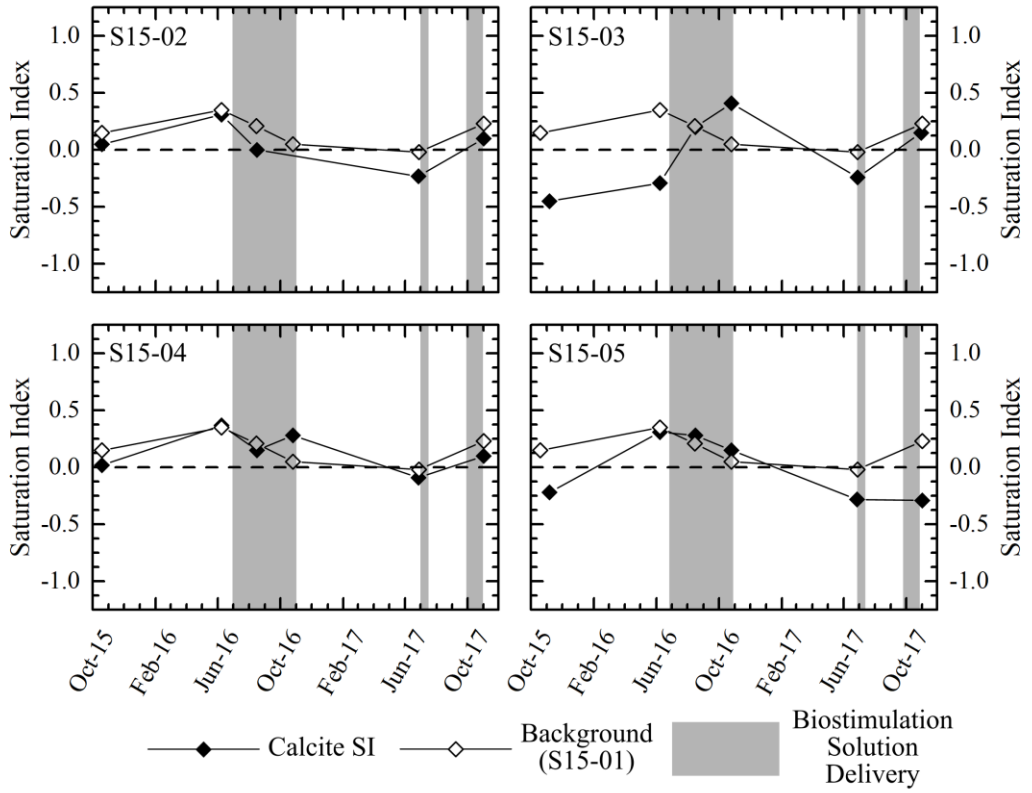

Figure 4.17. Saturation index of calcite during biostimulation. Grey bands indicate periods of biostimulation solution delivery.

The groundwater trended towards undersaturation with respect to dolomite (Figure 4.18) in some monitoring wells (S15-02, S15-04, and S15-04) but trended towards supersaturation in S15-03.

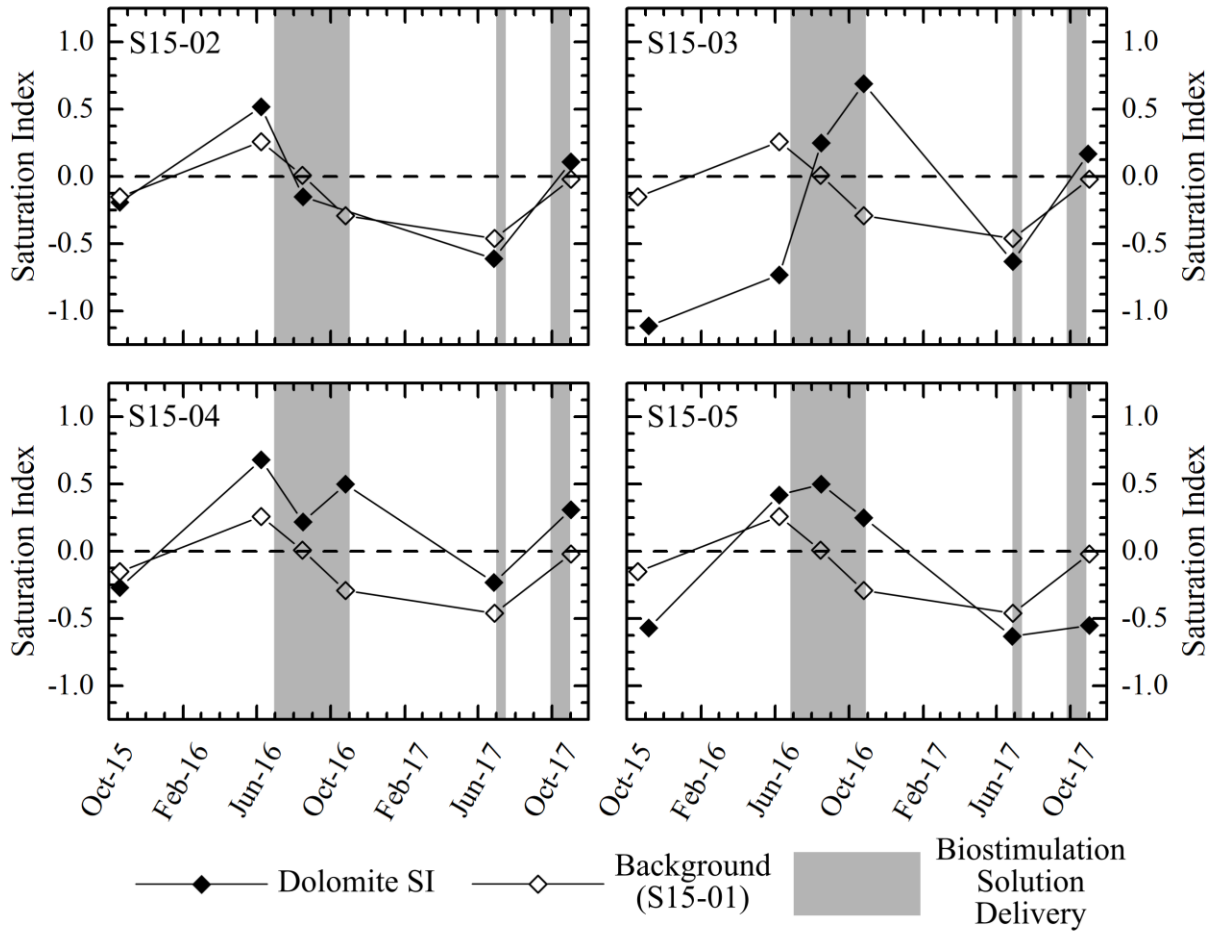

Figure 4.18. Saturation index of dolomite during biostimulation. Grey bands indicate periods of biostimulation solution delivery.

Gypsum (Figure 4.19) remained undersaturated in both the background and some contaminated monitoring wells (S15-02 and S15-04) but neared saturation in other contaminated monitoring wells (S15-03 and S15-05) during 2016 biostimulation. Groundwater in S15-04 neared saturation with respect to gypsum in 2017.

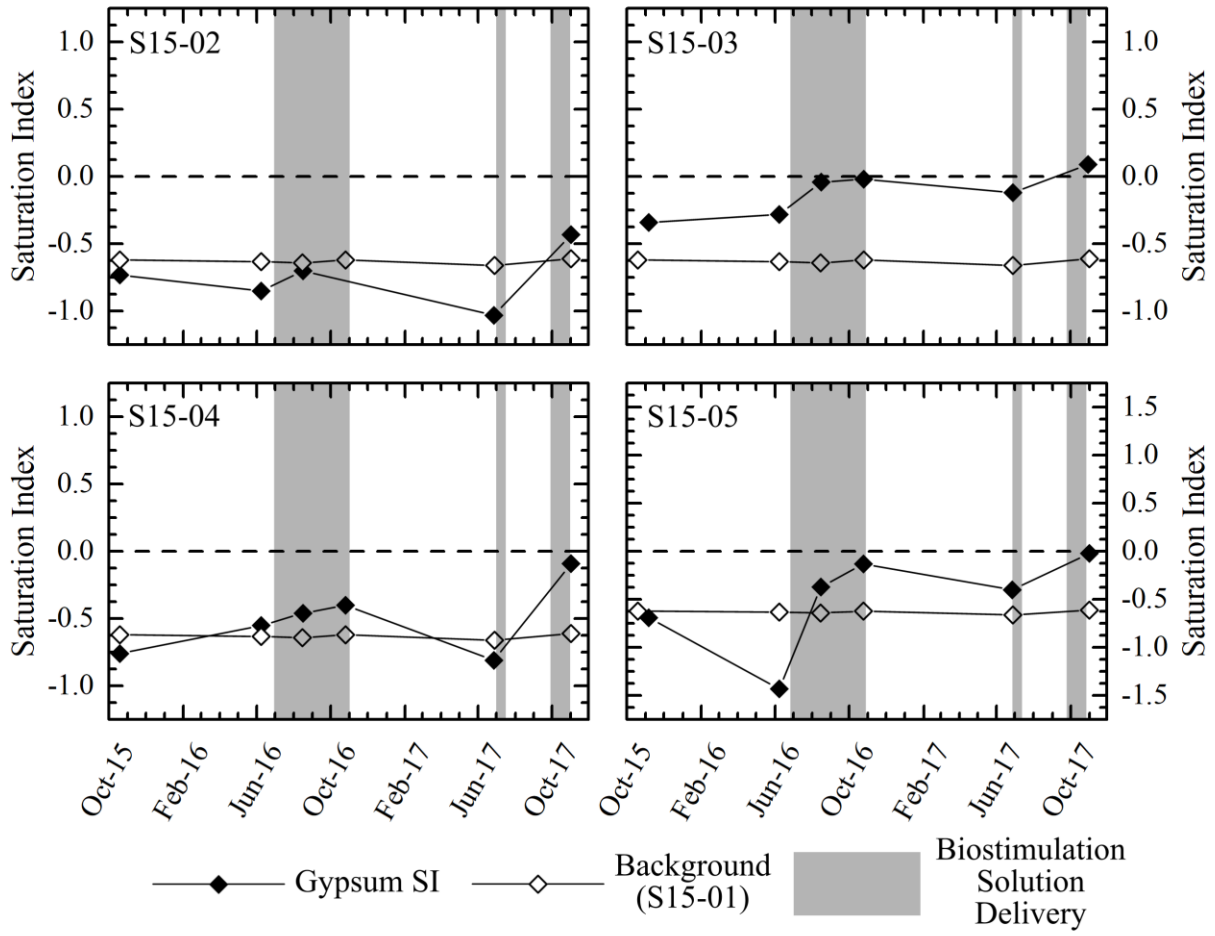

Figure 4.19. Saturation index of gypsum during biostimulation. Grey bands indicate periods of biostimulation solution delivery.

4.2.8 Soil Vapour Chemistry and Isotopes

Table 4.8 shows the composition of monitoring well and atmospheric vapour from samples collected prior to biostimulation (July 2016) and after a field season biostimulation (November 2016). The vapour from the contaminated wells became depleted in O_2 and slightly enriched with N_2 compared to the vapour of the background wells during biostimulation. The CO_2 component of vapour in the contaminated wells was lower when compared to the background well vapour.

Table 4.8. Monitoring well vapour composition. Results from GC analyses. ATM = atmosphere.

Well ID	Sample Date	Composition (%)			
		Ar	O_2	CO_2	N_2
ATM	15-Jul-16	0.932	21.1	0.041	78.0
ATM	17-Nov-16	0.916	21.1	0.043	77.9
S15-01	15-Jul-16	0.941	19.4	1.31	78.4
S15-01	17-Nov-16	0.932	20.0	1.30	77.8
S15-02	15-Jul-16	0.942	19.8	0.170	79.1
S15-02	17-Nov-16	0.946	17.6	0.130	81.3
S15-04	15-Jul-16	0.939	19.9	0.240	79.0
S15-04	17-Nov-16	0.947	17.2	0.140	81.7
S15-05	15-Jul-16	0.939	18.8	0.350	80.0
S15-05	17-Nov-16	0.957	16.0	0.190	82.9

CO_2 isotopic results (Table 4.9) from S15-01, S15-04, and S15-05 prior to biostimulation (July 2016) shows that the contaminated monitoring wells (S15-04 and S15-05) had a less negative $\delta^{13}C$ value and more negative $\delta^{18}O$ value compared to the background monitoring well.

Table 4.9. Isotopic fractionation of monitoring well vapour.

Well ID	Sample Date	$\delta^{13}C$ (‰)	$\delta^{18}O$ (‰)
S15-01	15-Jul-16	-21.3	-2.48
S15-01	17-Nov-16	-21.5	-2.72
S15-04	15-Jul-16	-20.0	-2.91
S15-05	15-Jul-16	-20.4	-2.11

4.4 Sediment Mineralogy

4.4.1 Powder X-ray Diffraction

PXRD results for 2015 and 2017 sediment samples (Figure 4.20) show that the mineral composition did not noticeably vary between sampling timepoints. According to semi-quantitative fitting results (Table B.1), the sediments primarily contain illite (50 ± 2 %; n = 47), quartz (28 ± 2 %; n = 47), albite (12 ± 1 %; n = 47), dolomite (5.0 ± 0.4 %; n = 47), kaolinite (3.6 ± 0.6 %; n = 47), and calcite (1.5 ± 0.1 %; n = 47). Gypsum was detected in one sediment sample (3.6 mBGL S17-04). It should be noted that overlapping peaks from silicates (e.g., illite) made it difficult to match other minerals that are potentially present in low abundance (e.g., magnetite).

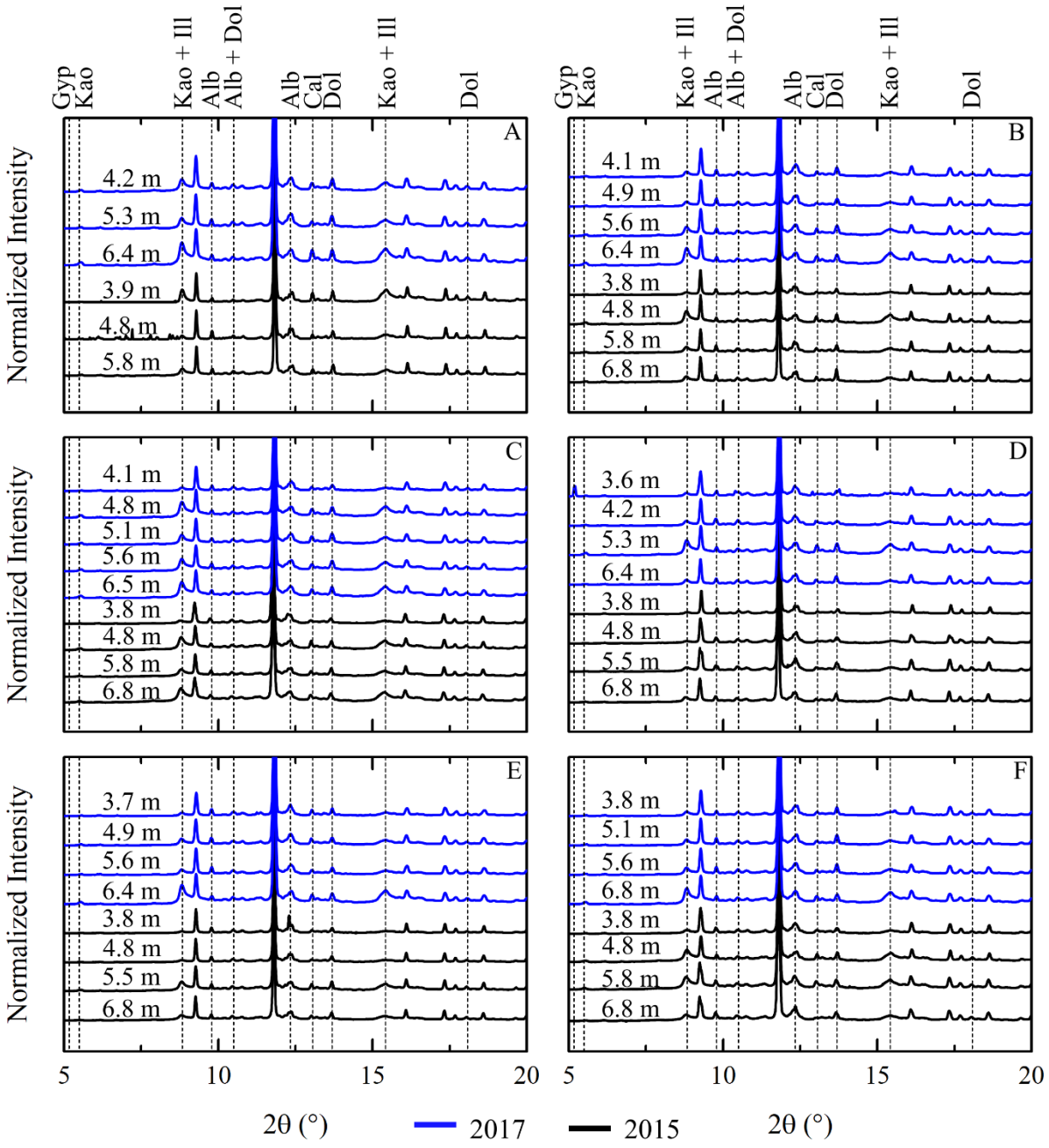

Figure 4.20. PXRD spectra for 2015 and 2017 soil samples. Spectra are shown from 5° to 20° with major non-quartz peaks labeled. Sub-figures: A) S15-01 & S17-01. B) S15-02 & S17-02. C) S15-03 & S17-03. D) S15-04 & S15-04. E) S15-05 & S17-05. F) S15-06 & S17-06.

4.4.2 X-ray Fluorescence

Full tabulated XRF results (Table B.2) for 2017 sediments are presented here. XRF data were not collected for 2015 samples.

Sulfur XRF

The average concentration of sulfur in the 2017 contaminated sediment samples was 0.036 ± 0.009 % (n = 25). This was elevated compared to the sulfur concentration in the background sediments (0.005 ± 0.002 %; n = 4). The trend of sulfur concentrations over depth for select 2017 boreholes (Figure 4.21) shows a peak in sulfur concentrations the sampling area where black staining was observed. However, there are some sulfur hot spots above and below these sampling areas (S17-03 and S17-04).

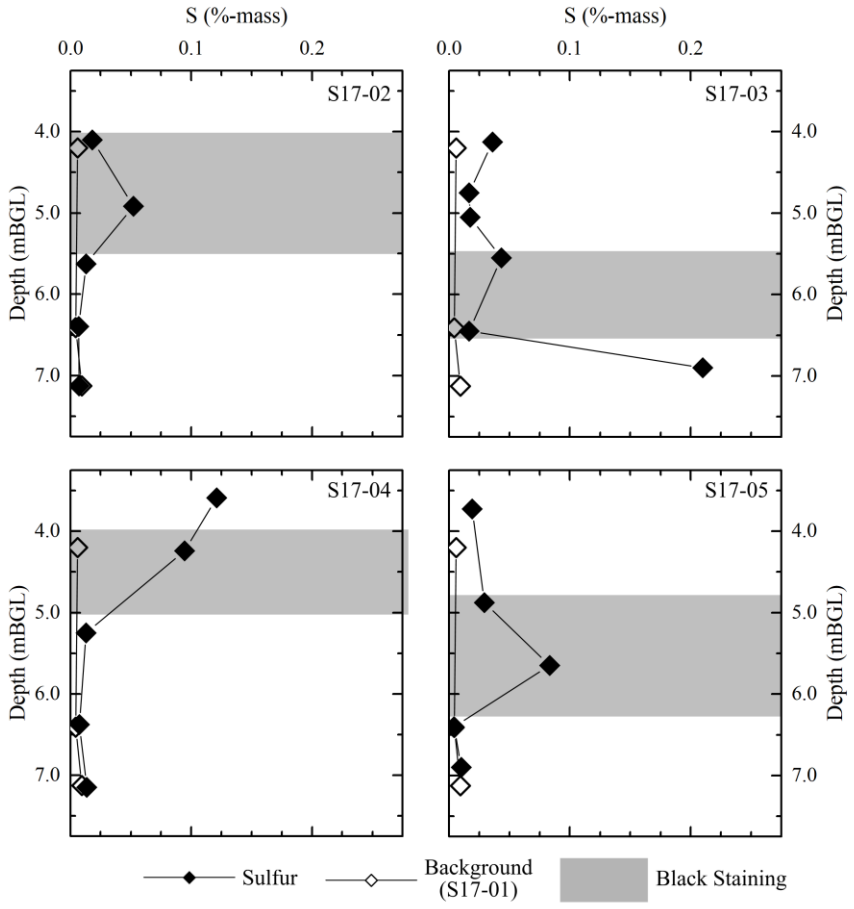

Figure 4.21. Sulfur XRF results from 2017 sediment samples. Grey bands indicate where black stains were observed in the soil.

Iron XRF

The average Fe concentration in 2017 contaminated sediments was 3.6 ± 0.1 % (n = 25). This was similar to the background Fe concentrations (3.7 ± 0.1 %; n = 4). Fe XRF results (Figure 4.22) for select 2017 sediment samples followed a different trend over depth. In the sampling area where black staining was observed, Fe concentrations were either depleted (S17-02), elevated (S17-04) or approximately the same (S17-03 & S17-05).

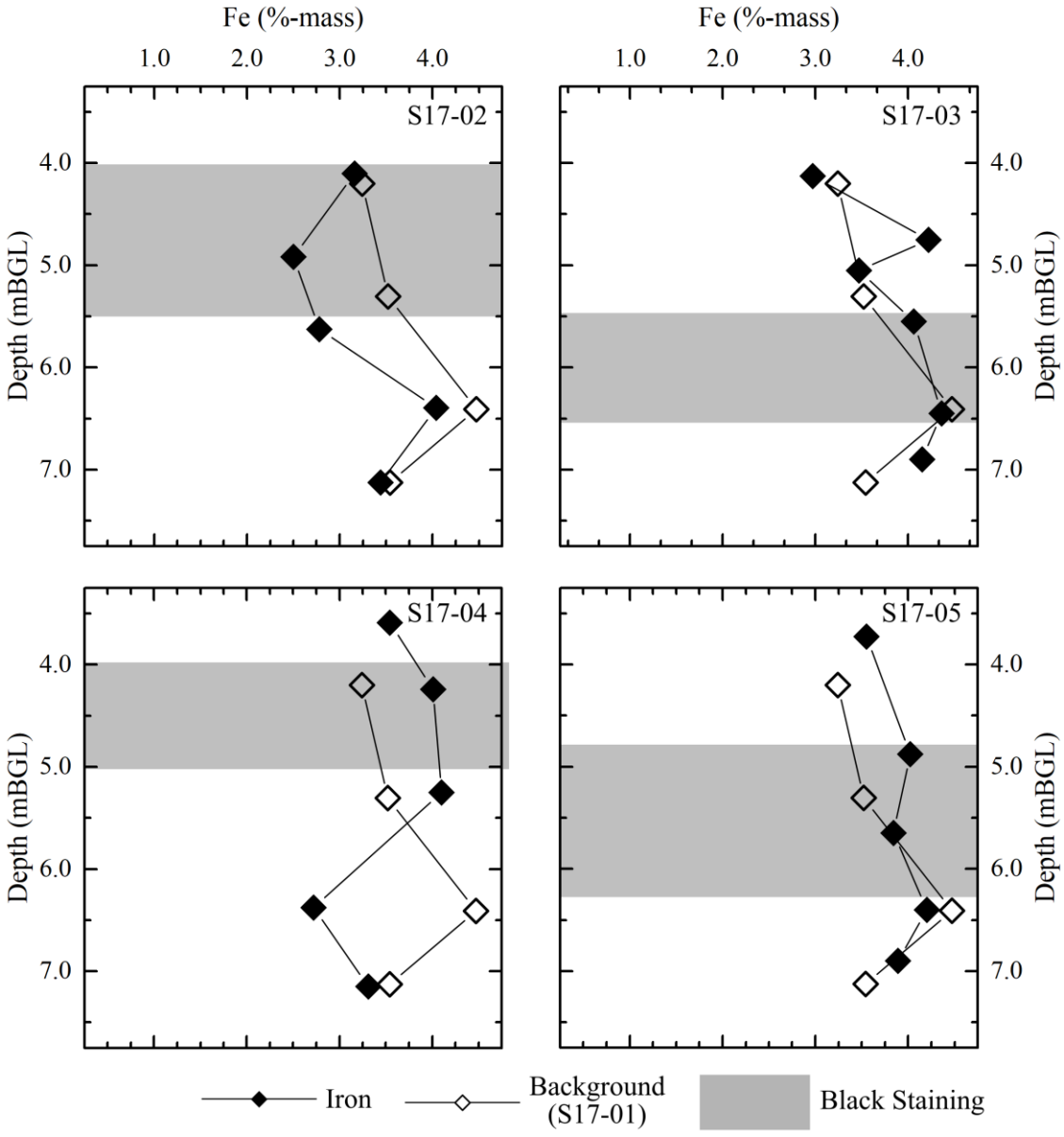

Figure 4.22. Fe XRF results from 2017 sediment samples. Grey bands indicate where black stains were observed in the soil.

Phosphorus XRF

Phosphorus in the 2017 contaminated sediments (0.10 ± 0.003 %; n = 25) was depleted slightly compared to the background sediments (0.12 ± 0.004 %; n = 4). The trend of phosphorus concentrations (Figure 4.23) in 2017 sediments is shows that the phosphorus concentrations are generally depleted compared to the background sediments over the sampled depth. However, in some boreholes (S17-04 and S17-05) the phosphorus concentration increased from approximately 5.5 to 7 mBGL.

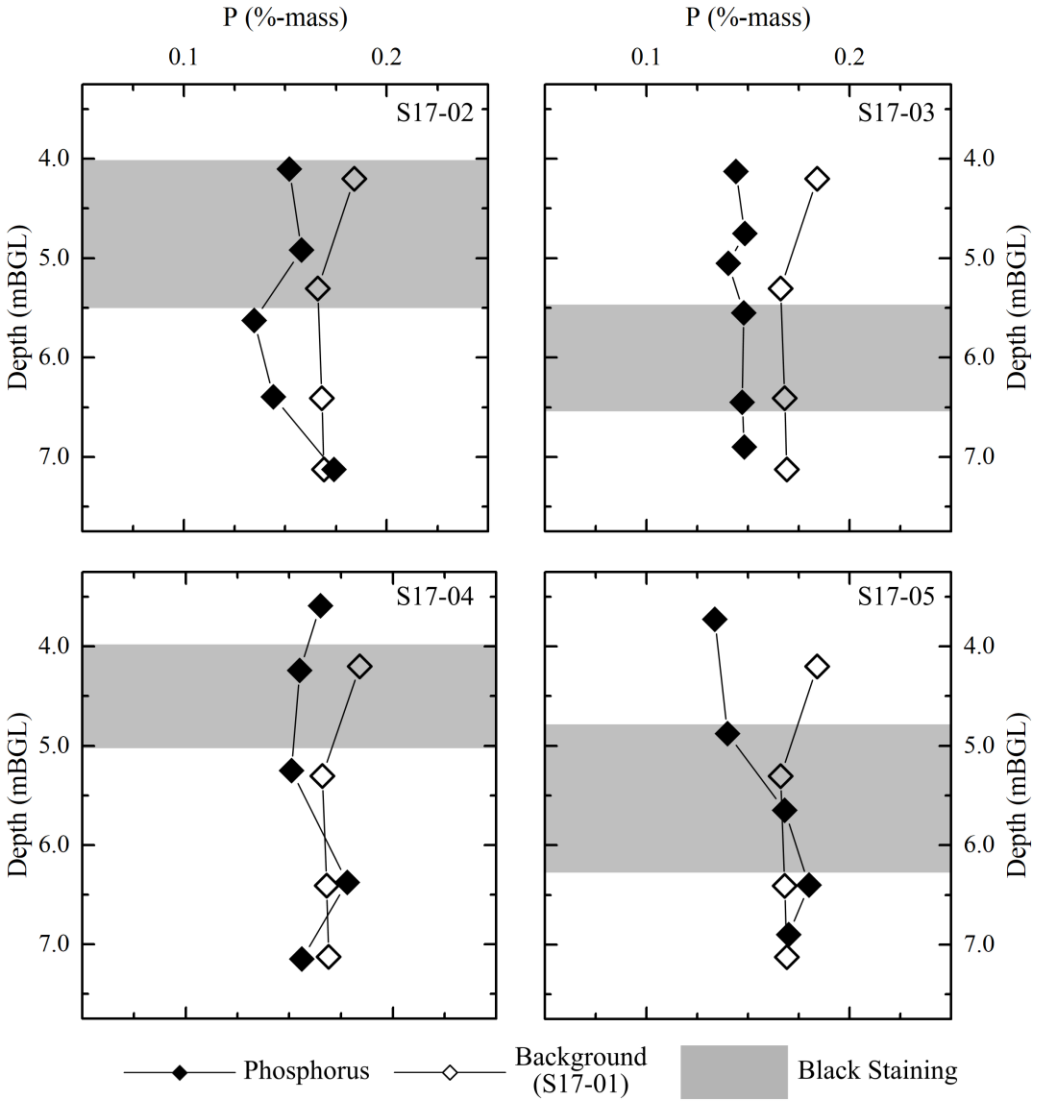

Figure 4.23. Phosphorus XRF results from 2017 sediment samples. Grey bands indicate where black stains were observed in the soil.

4.4.3 Sulfur X-ray Adsorption Spectroscopy

PCA was performed on sulfur K-edge XAS data (Figure 4.24 and Table B.3) and the results indicate that the spectra set contain either two or three principal components. Samples S15-03/S17-03, S15-04/S17-04, and S15-05/S17-05 all show a stronger second component and have three components. In comparison, S15-01/S17-01 and S15-02/S17-02 both show weaker second components and only have two components. The PCA results from the S15-02/S17-02 sample set has a smaller second peak in the first component in comparison to the other sample sets.

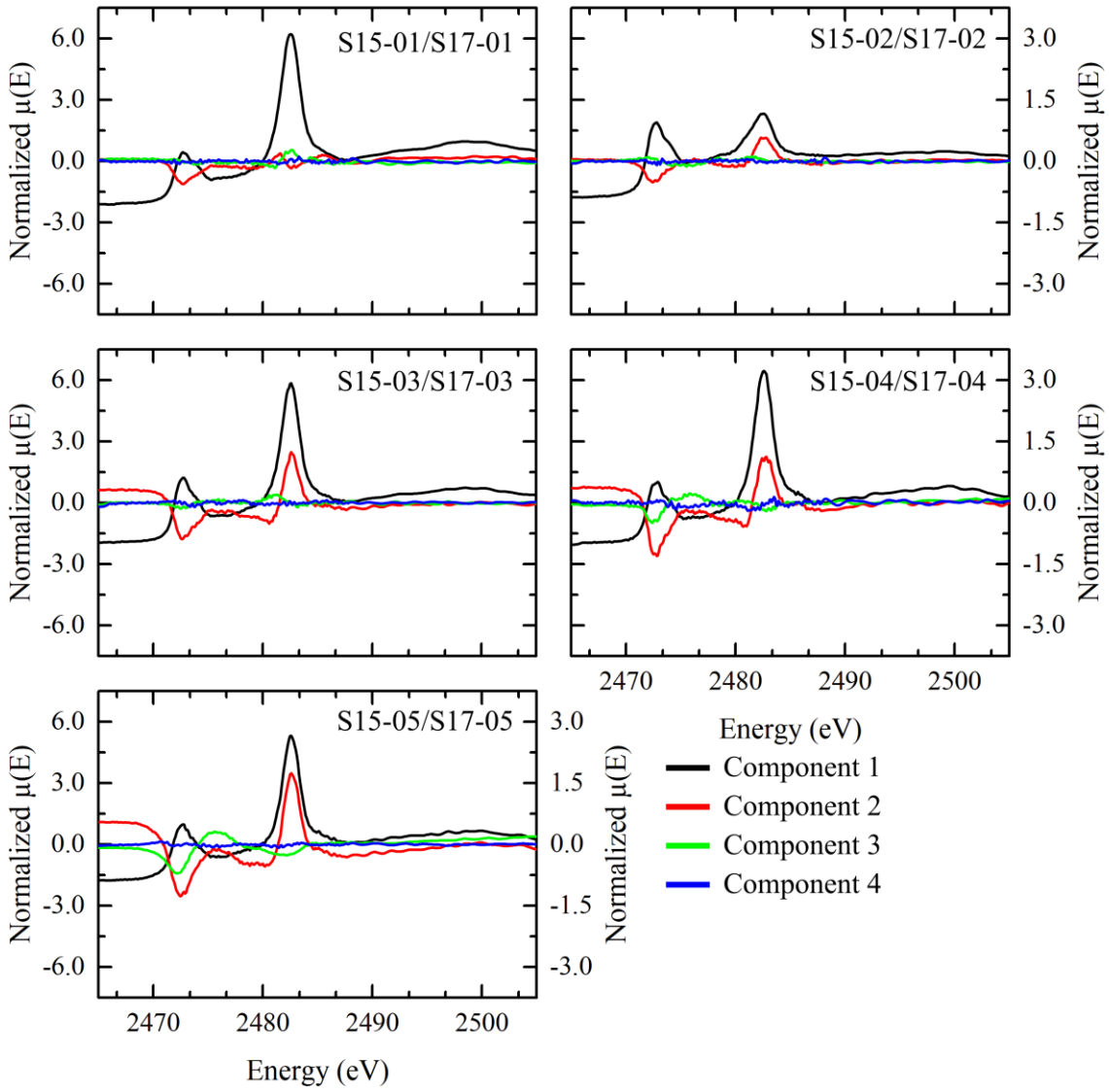

Figure 4.24. PCA results for sulfur XAS data. Component 1 is plotted on the left axis and components 2 – 4 plotted on the right axis.

Fits and normalized spectra data for sulfur K-edge XAS (Figure 4.25 and Table B.3) and the average sulfur mineralogy composition (Table 4.10) of background and PHC-contaminated sediments show that most spectra can initially be fitted with a combination of gypsum and reduced sulfur (elemental sulfur and L-cysteine). Some fits were improved by including sulfonate (S15-01 3.9 mBGL and S17-02 4.9 mBGL). Contaminated sediments were generally lower in gypsum and the main reduced sulfur compound was elemental sulfur according to the LCF. Some contaminated sediment samples (S15-03/S17-03 and S15-05/S17-05) may have had a slight increase in gypsum from 2015 to 2017.

Table 4.10. Average sulfur mineralogy composition determined by Sulfur XAS. ND = not detected.

Sampling Location	Sample Date	Gypsum (%)	Elemental Sulfur (%)	L-cysteine (%)
Background (n = 2)	October 2015	36 ± 1	44 ± 5	8 ± 8
Background (n = 2)	July 2017	43 ± 2	44 ± 1	12 ± 2
PHC-contaminated (n = 7)	October 2015	30 ± 7	50 ± 4	15 ± 4
PHC-contaminated (n = 8)	July 2017	25 ± 7	61 ± 6	7 ± 3

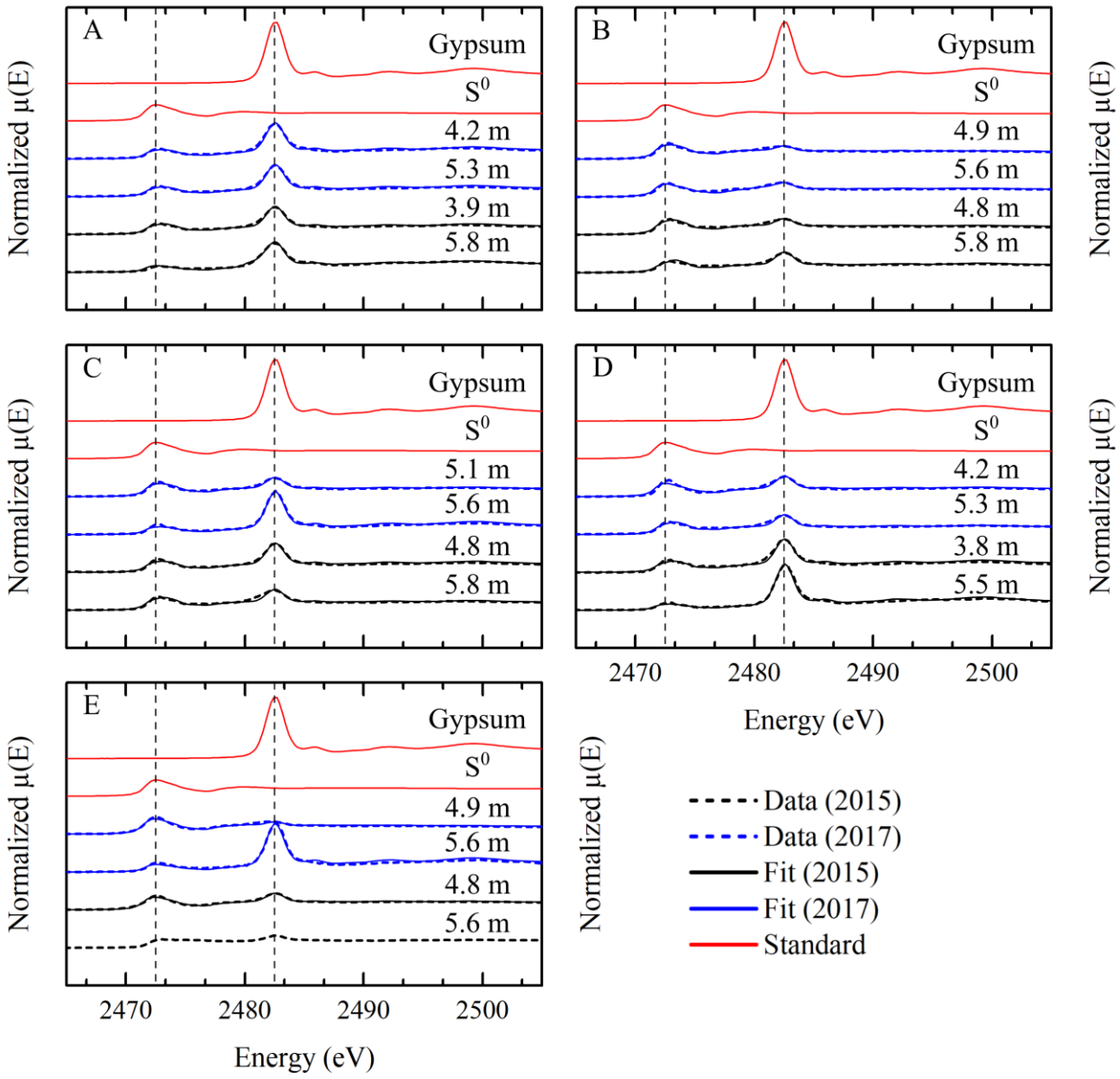

Figure 4.25. Normalized sulfur XAS fluorescence data and fit. Peak of gypsum and elemental sulfur shown. Sub-figures: A) S15-01 & S17-01. B) S15-02 & S17-02. C) S15-03 & S17-03. D) S15-04 & S15-04. E) S15-05 & S17-05.

Fits (e.g., Figure 4.26) were generally poor ($\chi^2 = 2.42 \pm 0.20$; n = 19) and this is likely due to the low sulfur concentrations in the sediment samples. One spectra (S15-05 5.6 mBGL) was not fit due to low data quality of the spectra.

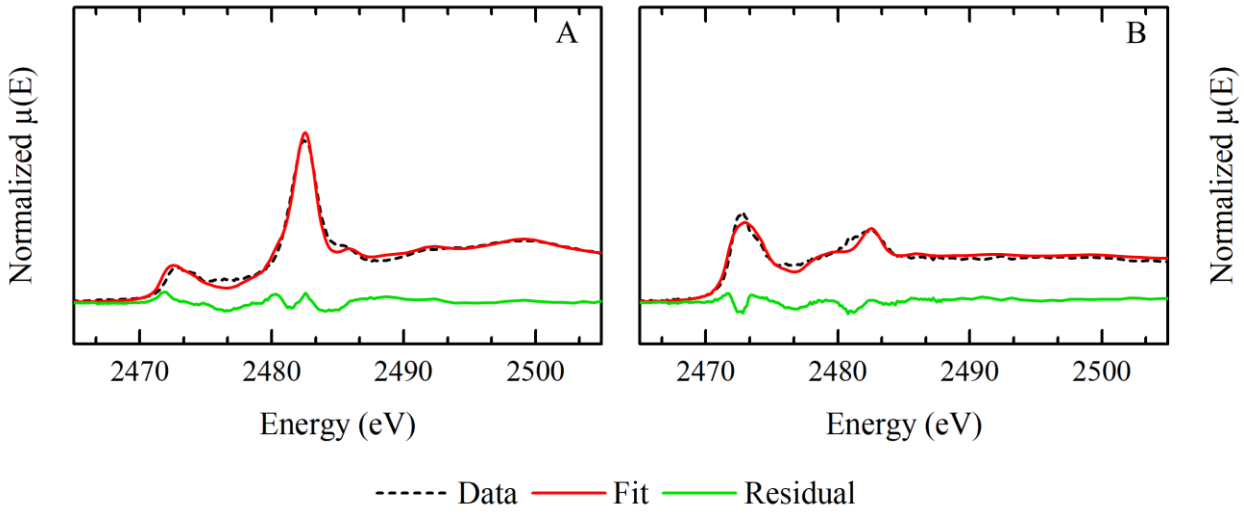

Figure 4.26. Typical residual from S XAS spectra fit. Sub-figures: A) S15-01 3.9 mBGL. B) S17-02 5.6 mBGL.

4.4.4 Iron X-ray Adsorption Spectroscopy

PCA was performed on collected Fe K-edge XAS data (Figure 4.27 and Table B.4) and the results show contaminated sediment sample sets usually have three distinct principal components but the S15-04/S17-04 sample set was closer to the background sediment sample set which had two components. The S15-05/S17-05 sample set was different compared to the other sample sets and had a stronger second principal component.

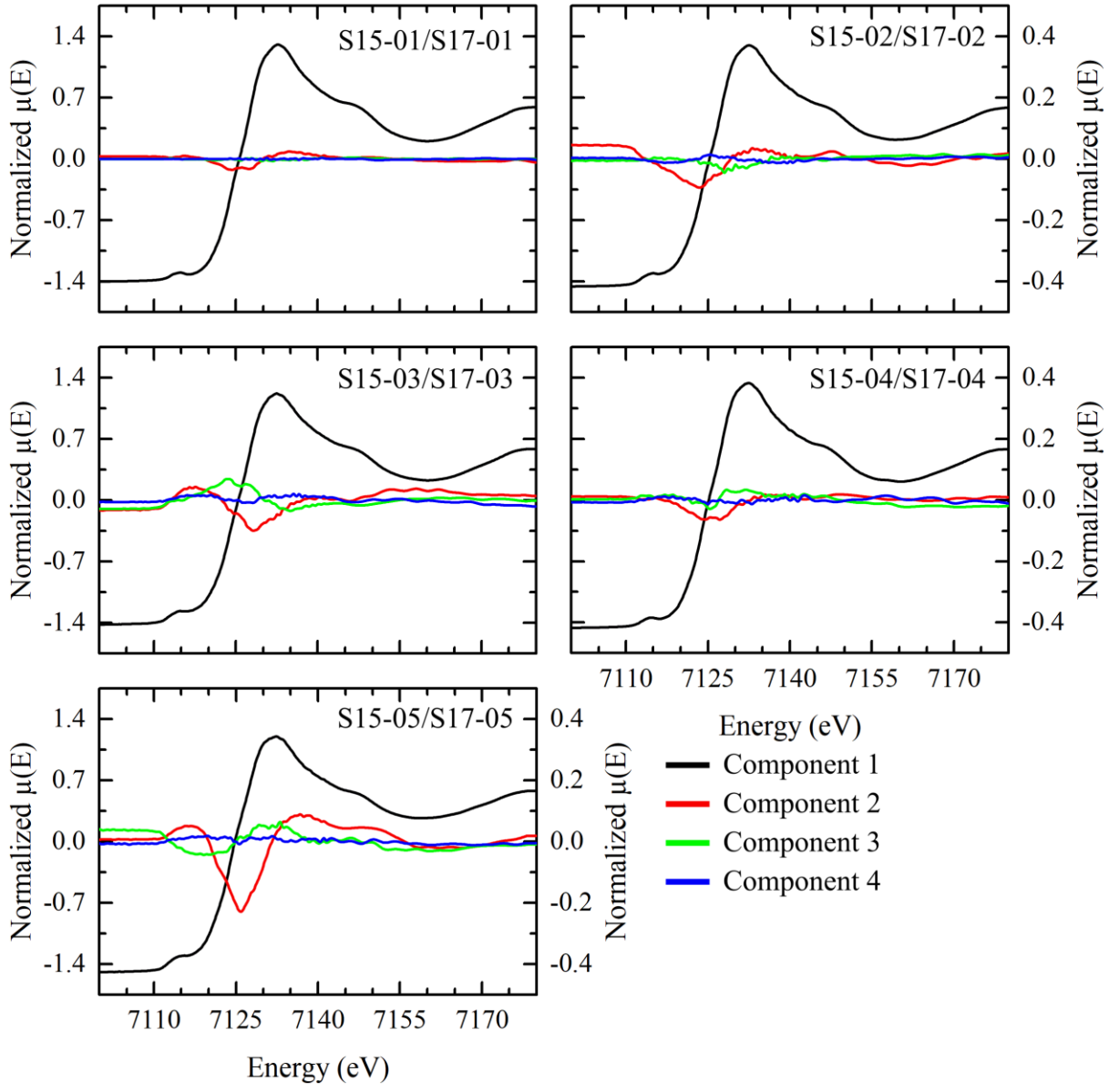

Figure 4.27. PCA results for Fe XAS data. Component 1 is plotted on the left axis and components 2 – 4 plotted on the right axis.

Fits and normalized spectra data for Fe XAS (Figure 4.28 and Table B.4) and the average Fe mineralogy composition (Table 4.11) of background and PHC-contaminated sediments show that prior to biostimulation (2015) sediments were not reduced and the spectra could be fit with an illite standard and Fe(III)-citrate standard (reference spectra presented in Figure B1). After biostimulation (2017) most sediments were reduced and were fit with a illite, Fe(III)-citrate, and pyrite standards. However, pyrite was not detected in S17-04 samples and these spectra could fit with only a Fe(III)-citrate and illite standard. It can be difficult or near impossible to differentiate between similar Fe-bearing materials in the near-edge region of XAS data (O'Day et al. 2004). For example, it can be almost impossible to differentiate between Fe(III)-citrate and Fe(III)-oxalate which are both forms of organic-Fe(III). Furthermore, the iron sulfide present in the sediment samples is likely not truly pyrite. Pyrite forms in sedimentary environments when amorphous iron monosulfide (FeS) is oxidized by elemental sulfur at high temperatures (Berner 1970). Therefore, it is assumed that Fe(III)-citrate generally represents organic-Fe(III) and that the pyrite reference standard is representative of FeS.

Table 4.11. Average Fe mineralogy composition determined by Fe XAS. ND = not detected.

Sampling Location	Sample Date	Illite (%)	Organic-Fe(III) (%)	FeS (%)
Background (n = 2)	October 2015	42 ± 3	58 ± 3	ND
Background (n = 2)	July 2017	39 ± 7	61 ± 7	ND
PHC-contaminated (n = 8)	October 2015	56 ± 6	48 ± 5	ND
PHC-contaminated (n = 8)	July 2017	53 ± 5	37 ± 2	10 ± 3

One spectra (S15-04 4.2 mBGL) was fit with Fe(III)-citrate and siderite reference standards, but the goodness of fit ($\chi^2 = 0.110$) was poor compared to other spectra fit.

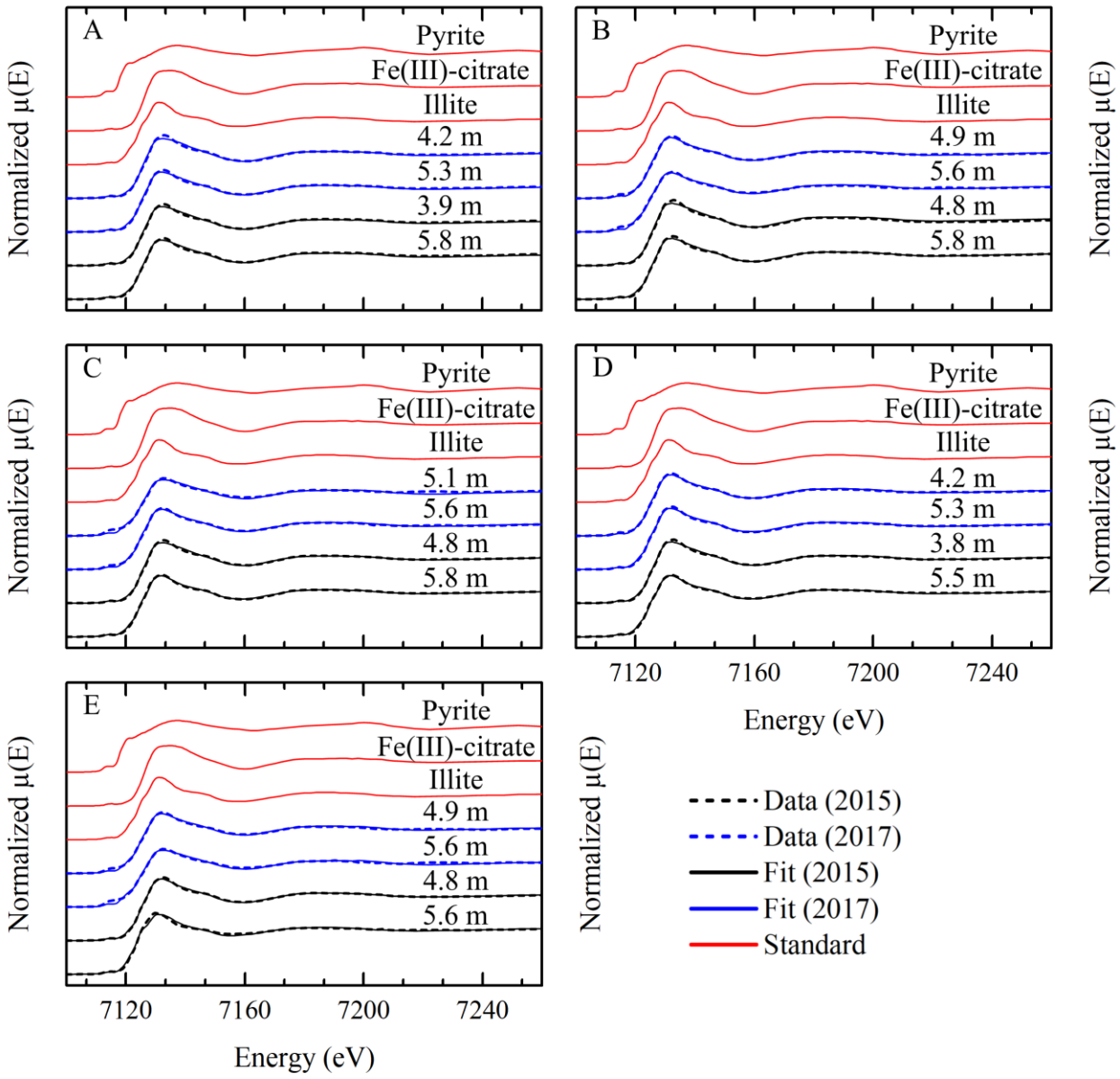

Figure 4.28. Normalized Fe XAS fluorescence data and fit. Sub-figures: A) S15-01 & S17-01. B) S15-02 & S17-02. C) S15-03 & S17-03. D) S15-04 & S15-04. E) S15-05 & S17-05.

Fits for Fe XAS (e.g., Figure 4.29) were generally good or acceptable ($\chi^2 = 0.044 \pm 0.005$; n = 20). The residual is typically minimal but fits near the pre-edge feature of spectra of reduced samples are less good and the residual is increased.

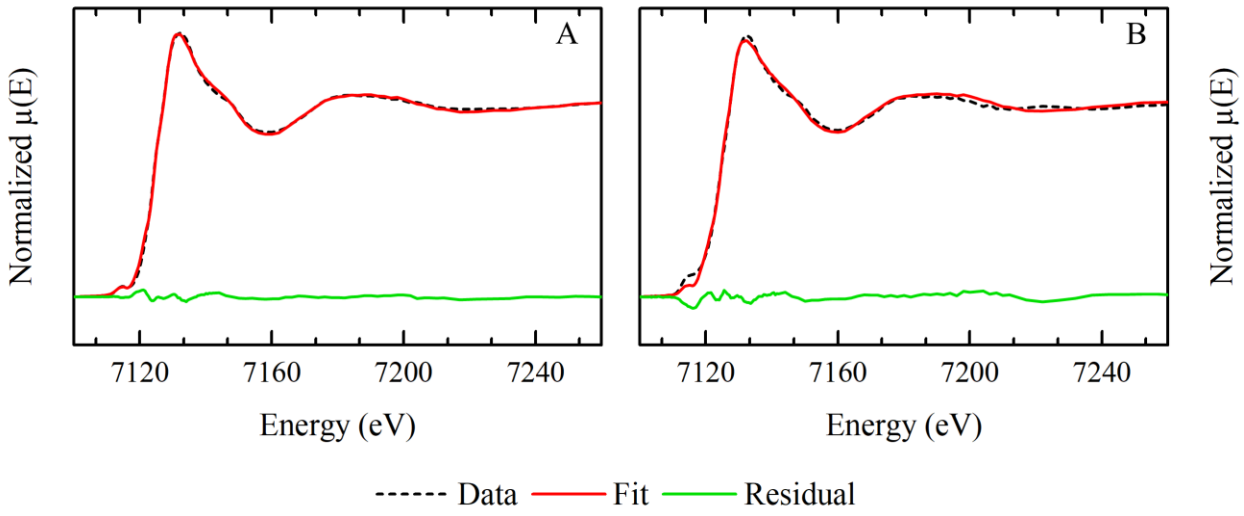

Figure 4.29. Typical residual from Fe XAS spectra fit. Sub-figures: A) S15-04 3.8 mBGL. B) S17-05 5.6 mBGL.

Wilke et al. (2001) reported that the Fe XAS pre-edge feature can provide useful information on Fe oxidation state, because it is especially sensitive to the proportion of Fe(II) and Fe(III). Furthermore, the shape and intensity of the pre-edge feature contains information on the bonding environment of elements (Bajt et al. 1994). Fe XAS data for S15-01/S17-01 (Figure 4.30), S15-02/S17-02 (Figure 4.31), and S15-04/S17-04 (Figure 4.32) show spectra collected from background (S15-01 and S17-01) and contaminated sediment samples from 2015 (S15-02 and S15-04) have a small pre-edge feature. In comparison, there is a distinct pre-edge feature in spectra collected from S17-02 samples and in all spectra collected from contaminated sediments other than samples from S17-04. This provides further evidence that 2017 sediment samples from S15-04 do not contain much Fe(II).

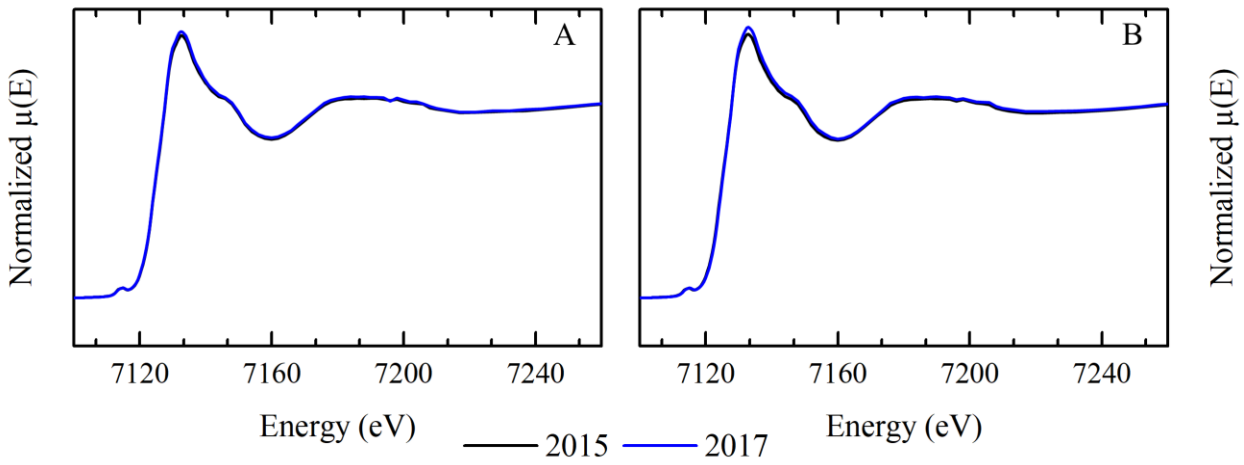

Figure 4.30. Fe XAS for S15-01 and S17-01 samples. Sub-figures: A) approximately 4 mBGL. B) approximately 5.5 mBGL.

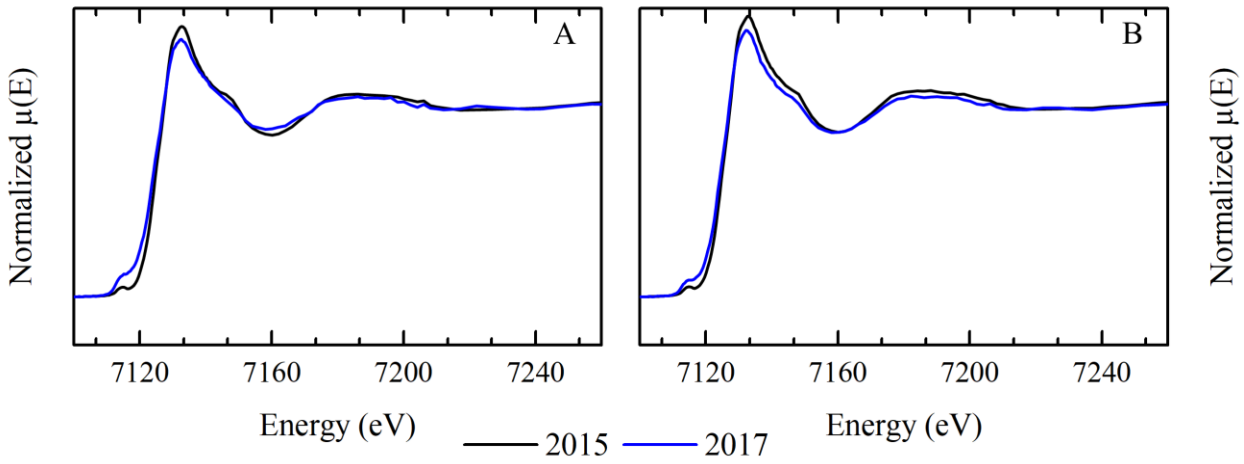

Figure 4.31. Fe XAS for S15-02 and S17-02 samples. Sub-figures: A) approximately 5 mBGL. B) approximately 5.5 mBGL.

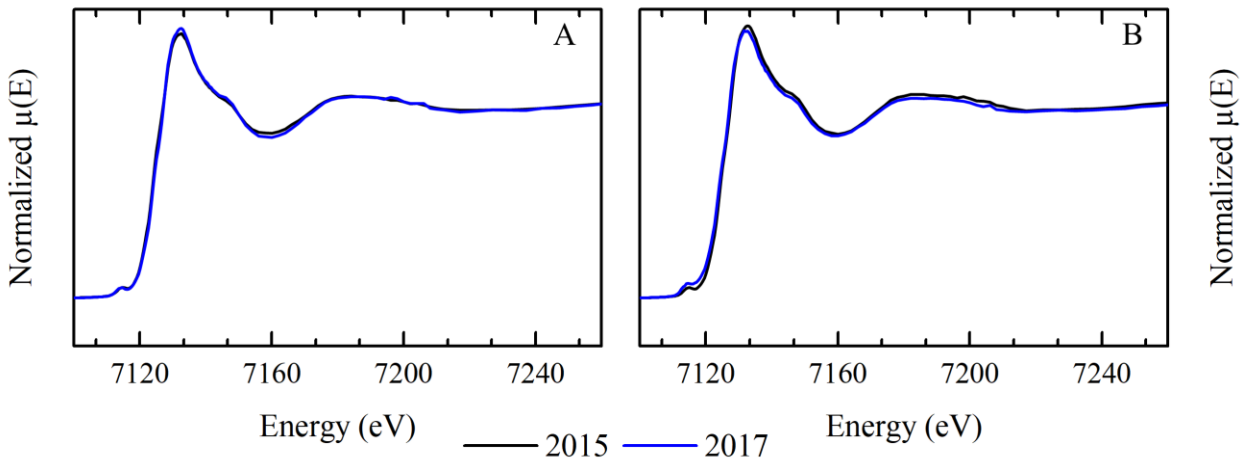

Figure 4.32. Fe XAS for S15-04 and S17-04 samples. Sub-figures: A) approximately 4 mBGL. B) approximately 5.5 mBGL.

4.5 Microbiology

4.5.1 General Microbiology Results

Alpha diversity calculations (Table 4.12) show the sequencing results provided good coverage of the community composition (Good's Coverage Estimator of 0.968 ± 0.002; n = 24) across all the samples. In general, the results show that some contaminated monitoring wells (S15-02, S15-04, and S15-05) were less diverse in terms of observed OTUs, Inverse Simpson Index, and Shannon Index when compared to the background monitoring well (S15-01) or other contaminated monitoring well (S15-03 and 11-03). Some contaminated monitoring wells (S15-03 and 11-03) were closer in diversity to the background monitoring well but still less diverse (e.g., Inverse Simpson Index is ten-fold higher in the background monitoring well). A similar trend can be observed in the estimates of species richness (Chao Estimator and Ace Estimator).

Table 4.12. Summary of alpha diversity calculations for the groundwater microbiology sample datasets. Note all data sets were subsampled to 34308 reads per dataset prior to calculations.

Well ID	Sample Date	Good's Coverage Estimator	Observed OTUs (97 % identity)	Inverse Simpson Index	Shannon Index	Chao Estimator	Ace Estimator
S15-01	8-Jun-16	0.976	1589	47.6	5.0	3376	4823
S15-01	15-Aug-16	0.961	2244	43.3	5.2	5466	8742
S15-01	25-Oct-16	0.954	2643	76.8	5.7	6601	10468
S15-01	28-Jun-17	0.956	2564	5.9	4.3	5917	9213
S15-02	8-Jun-16	0.993	388	4.3	2.0	1225	2383
S15-02	16-Aug-16	0.988	624	3.8	2.2	1957	3725
S15-02	27-Jun-17	0.957	2275	9.5	4.1	5891	10114
S15-03	8-Jun-16	0.966	1783	3.0	3.0	5075	9862
S15-03	16-Aug-16	0.965	1974	4.3	3.6	4946	8412
S15-03	25-Oct-16	0.962	2139	3.6	3.5	5326	8125
S15-03	28-Jun-17	0.950	2621	8.5	4.2	7426	12532
S15-04	8-Jun-16	0.972	1462	8.5	3.5	3935	6924
S15-04	16-Aug-16	0.984	846	6.7	2.9	2556	4820
S15-04	25-Oct-16	0.978	1181	12.6	3.6	3753	7157
S15-04	27-Jun-17	0.982	984	2.7	2.4	2677	4670
S15-05	8-Jun-16	0.970	1534	8.4	3.6	4387	7709
S15-05	16-Aug-16	0.980	1008	7.6	3.1	3493	7168
S15-05	25-Oct-16	0.973	1383	5.8	3.2	4434	8893
S15-05	27-Jun-17	0.969	1715	9.3	4.1	4391	7636

Table 4.12. Continued.

Well ID	Sample Date	Good's Coverage Estimator	Observed OTUs (97 % identity)	Inverse Simpson Index	Shannon Index	Chao Estimator	Ace Estimator
11-03	21-Oct-15	0.966	1903	11.4	4.3	5021	8359
11-03	10-Jun-16	0.973	1488	6.7	3.3	3780	6255
11-03	16-Aug-16	0.953	2487	31.7	5.0	7065	13271
11-03	1-Nov-16	0.961	2151	6.2	4.1	5685	9782
11-03	27-Jun-17	0.954	2431	26.4	4.8	6716	11897

Sequencing results of the S15 monitoring wells from October 2015 sampling timepoint came back as almost entirely *Pseudomonas* relatives (approximately 99 % *Pseudomonas* relatives). These results were deemed to be from a failed sequencing protocol and were not included in any further analyses. Another possibility is that these results were real and groundwater communities were altered in the construction area of the monitoring wells for a period of time before returning to their previous state.

4.5.2 Microbial Community Analysis

Genera level microbial community profiles for abundant genera (Figure 4.33) show the background monitoring well (S15-01) and the contaminated monitoring wells are dominated by different microbial taxa. The background monitoring well is dominated by relatives of unclassified Bacteria, unclassified *β-proteobacteria*, unclassified *Bacteroidetes*, and unclassified *Burkholderiales*. Minor amounts of *Pedobacter*, unclassified *Rhodocyclaceae*, unclassified *γ-proteobacteria*, and unclassified *Proteobacteria* are also present in the background monitoring well. Furthermore, the background microbial community profile does not appear to noticeably change throughout the sampling period of the study. The microbial community profile in the contaminated monitoring wells is mostly dominated by relatives of unclassified *Comamonadaceae*, *Desulfosporosinus*, and *Geobacter*. Other interesting genera in the contaminated monitoring wells are relatives of *Pseudoxanthomonas*, *Petrimonas*, and *Polaromonas*. These bacteria are ubiquitous in S15-02, S15-03, S15-04, and S15-05. In comparison to these monitoring wells, 11-03 appears to have a distinct community profile. Unclassified *Comamonadaceae* and *Desulfosporosinus* are still present in 11-03, but the microbial community profile also contains relatives of *Novosphingobium*, *Hydrocarboniphaga*,

Hydrogenophaga, unclassified *Anaerolineaceae*, *Desulfocapsa*, and *Sulfuricurvum*. Furthermore, the 11-03 community is also similar to the background well since it contained relatively larger proportions of unclassified *Bacteria* and unclassified *Bacteroidetes*. The S15-03 community also contained relatively larger proportions of unclassified Bacteria.

A few interesting trends and relationships can be noted from these results. Firstly, the proportion of unclassified *Comamonadaceae* appears to initially increase in S15-05 at the expense of *Geobacter* and *Desulfosporosinus*. This trend does not appear to occur in the other monitoring wells (e.g., S15-04). Secondly, relatives of *Pseudoxanthomonas* dominate S15-04 compared to the other monitoring wells and the proportion of this taxon increased after the initial biostimulation delivery (August 2016). *Pseudoxanthomonas* are also present in S15-05 at the first sampling timepoint (June 2016). Finally, it appears that relatives of *Petrimonas* are only present at a measurable abundance when *Pseudoxanthomonas* are also present (e.g., S15-04).

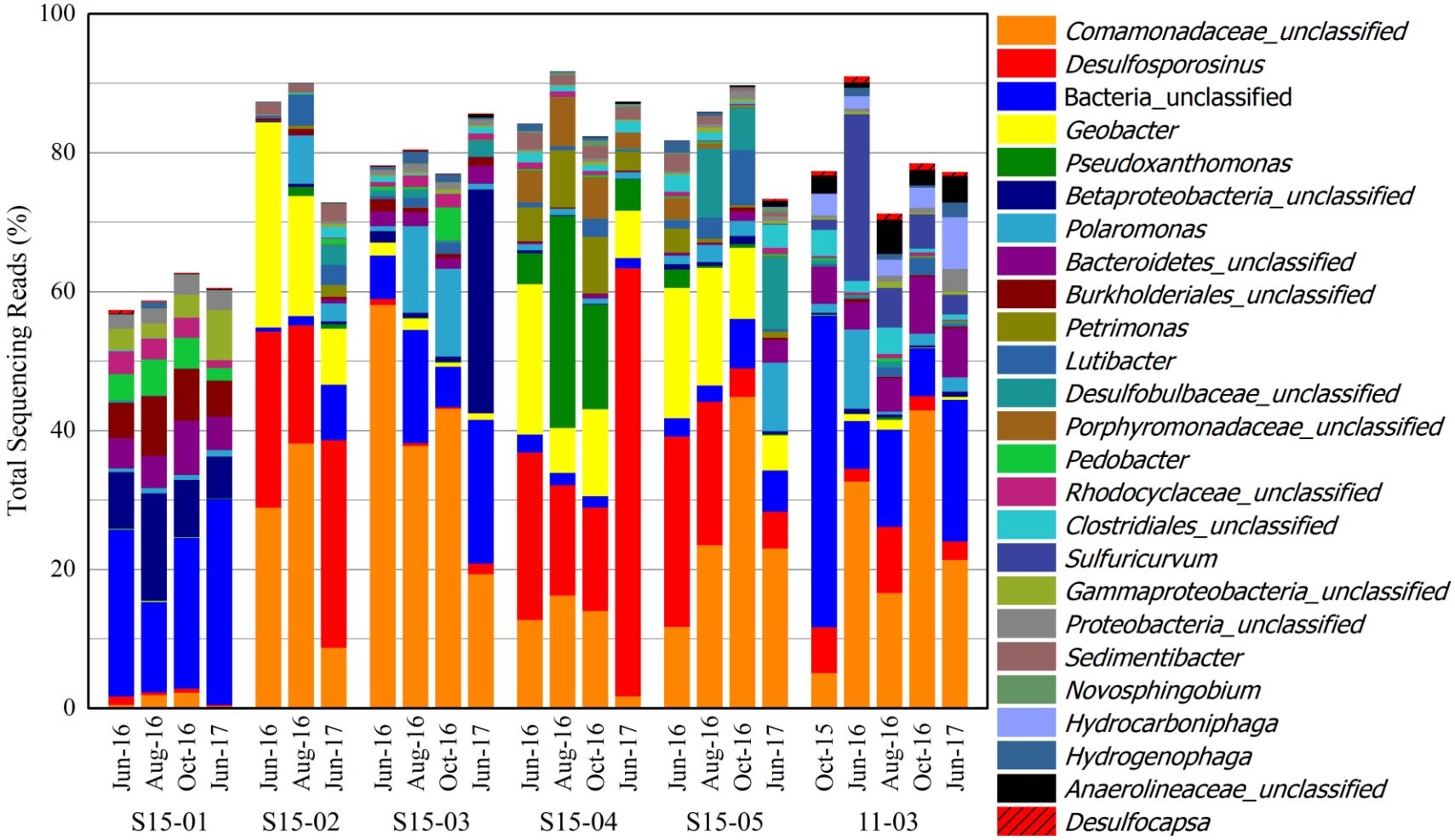

Figure 4.33. Microbial community profile (16S rRNA gene sequencing results) of groundwater samples from the background well (S15-01) and contaminated wells. Results are presented as a percentage of the total sequencing reads for that sample. The top ten most abundant genera and a selection of other abundant genera are presented.

Yue-Clayton Theta (Figure 4.34 and Figure 4.35) and Jaccard coefficients (Figure C1 in Appendix C) were both plotted using NMDS. The Yue-Clayton Theta coefficients had a stronger correlation ($R^2 = 0.724$) and lower stress-value (0.243) when compared to the Jaccard coefficients ($R^2 = 0.465$, stress-value 0.385). Therefore, I have more confidence in the results of the Yue-Clayton Theta NMDS plot for determining how the microbial community changes over time at this study site. A biplot combining the Yue-Clayton Theta NMDS and selected abundant and geochemically influential taxa from Spearman correlation axes calculations as vectors (Figure 4.34) shows similarities in the microbial community profiles and which directions of the plot are influenced by select taxa. Axis 1 of the plot is heavily influenced in the positive direction by unclassified *Comamonadaceae*. Taxa influencing Axis 2 include *Geobacter*, *Desulfosporosinus*, and *Sedimentibacter* in the positive direction. In the negative direction, Axis 2 is notably influenced by unclassified Bacteria.

Note that the community in the background monitoring well (S15-01) shows some variability over time that may represent seasonal variation. Thus, trends (Figure 4.34 and Figure 4.35) in contaminated monitoring wells may also be due to similar seasonal variations in the microbial communities and may not necessarily be induced by the biostimulation solution. Nevertheless, communities in contaminated wells do consistently appear in a different region of the Yue-Clayton Theta NMDS plot than the background monitoring well. In S15-04 and S15-05, the communities are initially clustered prior to biostimulation (June 2016) in an area of the plot influenced by *Desulfosporosinus* and *Sedimentibacter*. The initial community in S15-02 is in the same region of the NMDS plot but shifted slightly to the positive end of axis 1 since it has higher proportions of unclassified *Comamonadaceae* compared to the initial communities of S15-04 and S15-05. Over time, the community in S15-04 did not change dramatically and clustered near the initial position; however, the community in S15-05 migrated during the study toward the area of the plot where S15-03 initially clustered during biostimulation. This direction of the plot (positive direction of axis 1) is strongly influenced by unclassified *Comamonadaceae*. Results from S15-02 seems to initially follow the same path on the plot as the community in S15-05 but reverts toward the area where results from S15-04 and S15-05 initially clustered during the study (June 2016). The community in 11-03 appears to cluster in a large region below axis 1 partially influenced by unclassified Bacteria to the bottom left of the plot. The community in S15-03 enters this region of the plot after initially clustering very tightly around zero on axis 2.

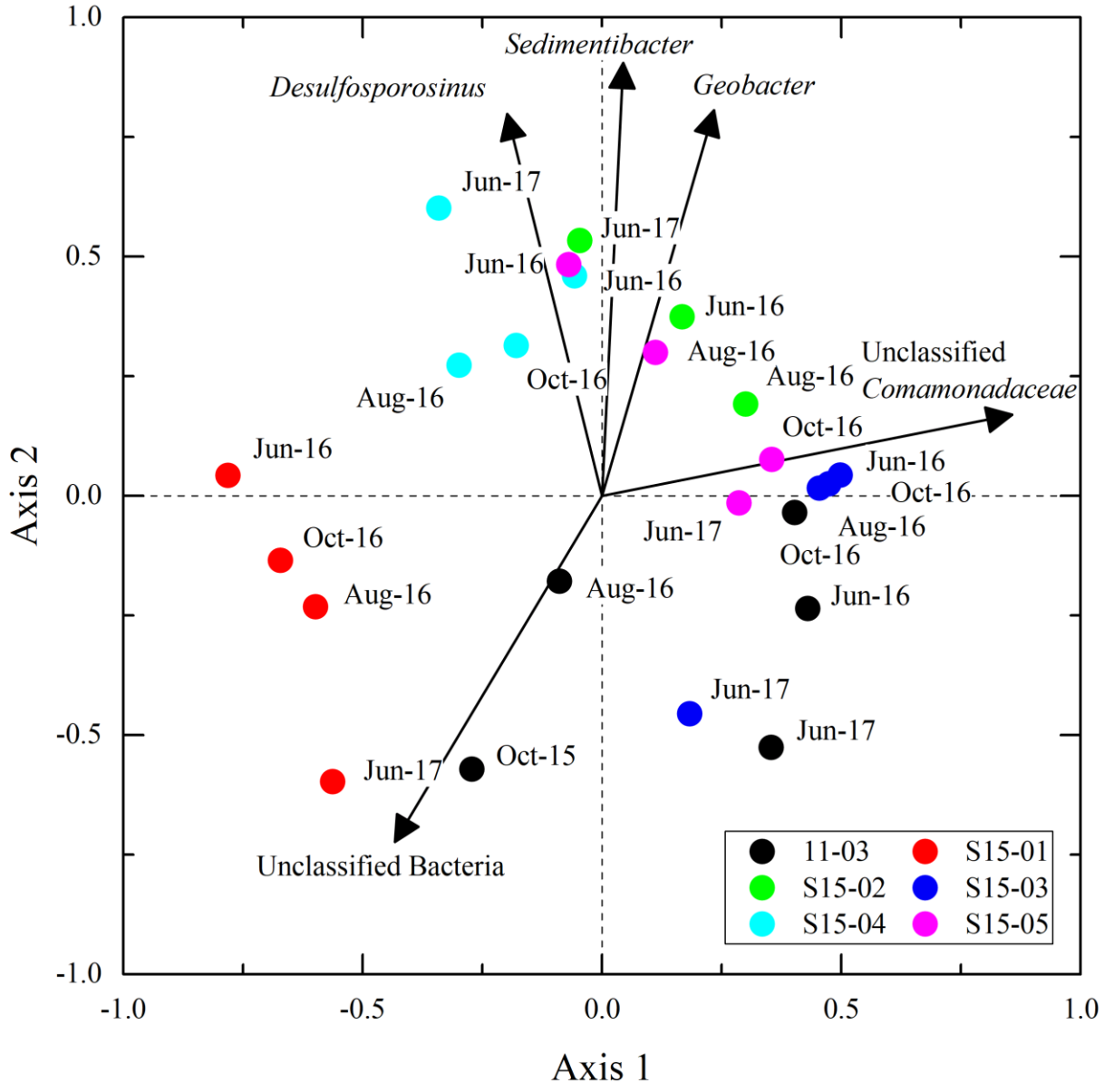

Figure 4.34. NMDS plot of Yue-Clayton Theta coefficients for microbial communities in groundwater samples, with Spearman correlations for select taxa plotted as vectors. The direction of the Spearman correlation vectors show which directions of the plot are influenced by each select taxon.

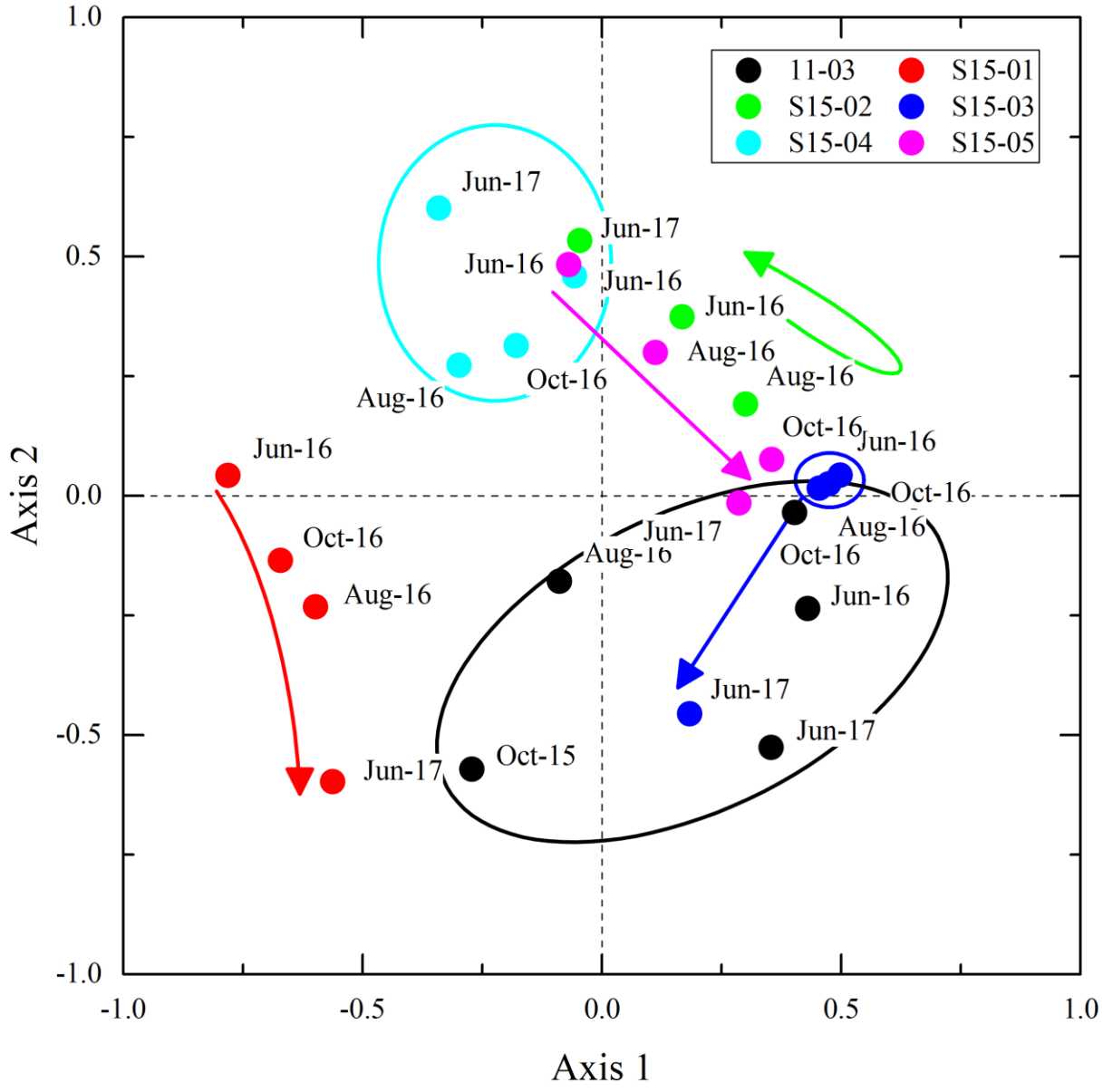

Figure 4.35. NMDS plot of Yue-Clayton Theta coefficients for microbial communities in groundwater samples. Observed trends and clustering in monitoring wells are noted by arrows and circles (colour corresponds to the monitoring well legend).

4.5.3 Microcosm Experiment

Surfactant Treatments

The trend of Fe(II) and Fe(III) concentrations (Figure 4.36 and Table C.2) in microcosm water over time for surfactant treatments and controls shows that all surfactant treatments increase the concentration of dissolved Fe(II) and Fe(III) compared to the sterile and untreated control. The unrefined biosurfactant may have stimulated more Fe(III) reduction compared to the refined product. All surfactant treatments remained near circumneutral pH.

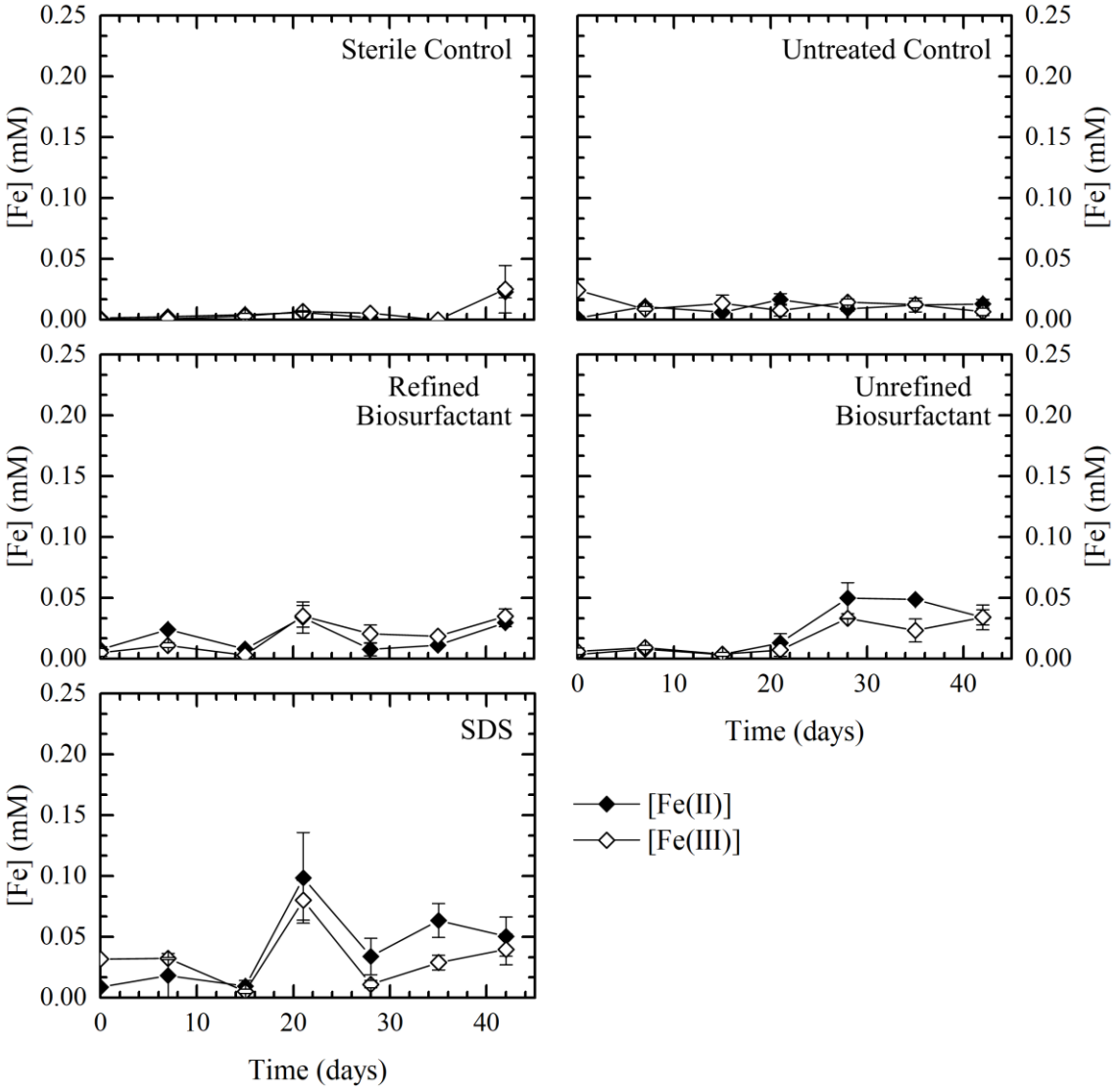

Figure 4.36. [Fe(II)] and [Fe(III)] over time in microcosms with surfactant treatments.

Malic Acid Treatments

The trend of Fe(II) and Fe(III) concentrations (Figure 4.37) in microcosm water over time for malic acid treatments and controls shows that both malic acid treatments increased the amount of dissolved Fe(II) and Fe(III) compared to the experimental controls. Both malic acid treatments dropped to approximately pH 2.5 at the start of the experiment. However, the alkalinity of the microcosm sediments buffered this over time to approximately pH 6 (Table C.2).

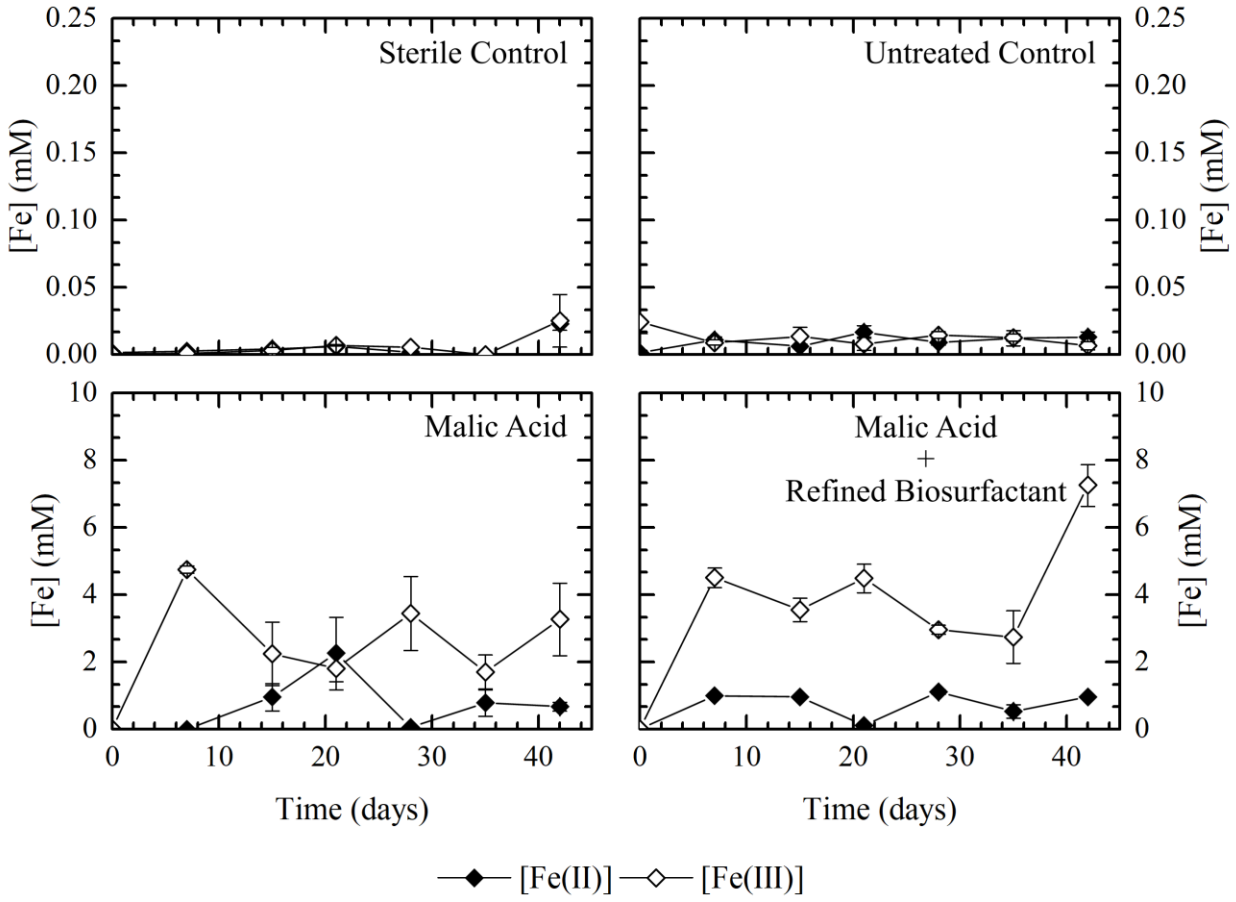

Figure 4.37. [Fe(II)] and [Fe(III)] over time in microcosms with malic acid treatment. Note: different vertical scale for controls compared to malic acid treatments.

CHAPTER 5 DISCUSSION

5.1 Remediation Progress

During the study period PHC concentrations decreased across the site, but because of the combined physical and biological remediation methods used at the site it is difficult to quantify to what degree the biostimulation solution enhanced PHC biodegradation. A portion of the PHCs were removed by physical extraction the MPE system during the study. However, the presence of metabolites (e.g., benzoate and benzylsuccinate) provides strong evidence that PHC biodegradation is occurring at the site. During the study, benzene decreased in all monitoring wells and the presence of benzoate (Figure 4.2) and phenol (Figure 4.3) are consistent with benzene biodegradation. Elevated concentrations of phenol compared to benzoate may suggest that benzene is biodegraded through a pathway that generates more phenol than benzoate (or phenol rather than benzoate) or that benzoate undergoes further biodegradation more rapidly than phenol and does not accumulate. Elevated concentrations of benzylsuccinate (Figure 4.4) and methylbenzylsuccinate (Figure 4.6) also provide strong evidence of toluene and xylene biodegradation.

CO_2 isotopic data ($\delta^{13}C$ and $\delta^{18}O$; Table 4.9) proved not to be as useful for assessing PHC biodegradation as the metabolite data. This is likely due to calcareous nature of the soil at the study site. Observed $\delta^{13}C$ results from CO_2 isotopic data in the contaminated region of the site were slightly more positive than the background values. Per literature sources, $\delta^{13}C$ values for PHC and BTEX compounds should be more negative than typical background soil values; however, carbonates typical have a slightly positive $\delta^{13}C$ value. Furthermore, the observed $\delta^{18}O$ values at the study site are very different than reported literature values. These CO_2 isotope results suggest that portions of the produced CO_2 at the site is dominated by carbonate dissolution and pH-buffering reactions. This is also supported by decreasing alkalinity (Figure 4.9) and increasing EC (Figure 4.10) during the study period, which suggests carbonate dissolution occurred and the produced alkalinity neutralized groundwater acidity. Dolomite is the

major carbonate mineral at the study site as evident from PXRD results (Figure 4.20) and elevated concentrations of Ca (Figure 4.12) and Mg (Figure 4.13).

The PHC data, specifically benzene concentrations, suggest that biodegradation was slower in some contaminated wells. For example, benzene concentrations in S15-02 and S15-04 decreased less than the benzene concentration in S15-05 (Figure 4.2 and Figure 4.3). One explanation for this difference in PHC biodegradation may be caused by differences in the microbial communities. As illustrated in the Yue-Clayton Theta NMDS plot (Figure 4.34 and Figure 4.35), the groundwater community in S15-05 was similar to S15-02 and S15-04, but after delivery of the biostimulation solution there was a change in the community and S15-05 became more similar to S15-03. This observed difference in the degree of benzene biodegradation and shift in the microbial community profile suggests that the different communities may have varying PHC remediation capabilities. Specifically, the microbial communities and biogeochemical processes occurring in S15-03 and S15-05 might be more conducive for PHC biodegradation compared to S15-02 and S15-04.

5.2 Biogeochemical Processes

5.2.1 Iron Reduction

Several lines of evidence (groundwater geochemistry, sediment mineralogy, and microbial community profiles) suggest that Fe(III) reduction is an important biogeochemical process occurring at the site. Groundwater geochemistry results show dissolved Fe (Figure 4.11) was elevated in the contaminated region of the site compared to the background monitoring well. Generally, these concentrations did not increase over the study period; however, soil mineralogy suggests that FeS (Figure 4.28) is an important sink for reduced Fe. The XANES results from sediment core showed FeS had formed in some areas of the site after the initial sediment sampling. Furthermore, the Fe XANES results suggest the dissolved Fe is derived from reduced organic-Fe(III). However, since the biostimulation solution also contained chelated Fe(III) it may also have contributed to the reduced Fe. Further to this, microbiology data suggests the biostimulation solution enhanced Fe(III)-reducer activity.

Relatives of *Geobacter* and *Comamonadaceae* (Figure 4.33) are the dominant Fe(III) reducers at the site and are likely responsible for the majority of observed Fe(III) reduction. *Geobacter* is a well-studied Fe(III) reducer that can couple benzene- and toluene oxidation to

Fe(III) reduction (Lovley et al. 1993; Zhang et al. 2012). The *Comamonadaceae* are a diverse family of bacteria that include nitrogen cyclers and Fe(III) reducers (Willems 2014). For example, *Rhodoferax* is a well-known Fe(III) reducer in the *Comamonadaceae* family (Finneran et al. 2003). The biostimulation solution used in the present study appears to have had a similar influence on the relationship between *Geobacter* and *Comamonadaceae* that Mouser et al. (2009) studied. During periods of biostimulation, the proportion of *Comamonadaceae* increased relative to *Geobacter* and other bacteria (Figure 4.33), suggesting the biostimulation solution may support a shift in the community towards populations that do not fix their own nitrogen. Furthermore, this trend of increasing *Comamonadaceae* might enhance benzene biodegradation as evident from benzene concentration data from different monitoring wells. Benzene concentrations in S15-05 decreased more than when compared to other contaminated monitoring wells (e.g., S15-02 and S15-04). The community in S15-05 also saw a shift towards relatives of *Comamonadaceae* (Figure 4.33, Figure 4.34, and Figure 4.35). The contaminated monitoring wells that saw less benzene biodegradation also saw lower proportions of *Comamonadaceae* relatives. The S15-03 community also had relatively high proportions of *Comamonadaceae* relatives, but benzene concentrations were already low. In summary, our results here provide evidence that *Comamonadaceae* are important to benzene biodegradation and increasing proportions of *Comamonadaceae* relatives may enhance PHC remediation.

Results collected from the field provides strong evidence that Fe(III) reduction is an important biogeochemical process related to PHC biodegradation. The microcosm experiment (Figure 4.36) completed as part of this thesis also suggests that Fe(III) reduction could be further enhanced by the addition of a biosurfactant. While a lack of PHC and metabolite data from the microcosm experiment means it is not conclusive that a biosurfactant would enhance PHC biodegradation, based on the nature of surfactants and history of surfactants being used in PHC remediation, it seems very likely that the biosurfactant used would enhance PHC remediation through either biological or physical mechanisms.

5.2.2 Sulfate Reduction

Increasing sulfide concentrations (Figure 4.15) and FeS formation (based on the iron XANES data) strongly suggest that Fe(III)- and sulfate reduction are both occurring during biostimulation at the study site. Although, it is not clear which process is most responsible for the observed decrease in PHC-contamination. It is possible that the main pathway of PHC

biodegradation occurs through sulfate reduction and concurrent abiotic Fe(III) reduction enhances PHC biodegradation by removing sulfide from the groundwater through FeS precipitation. This is the conclusion Beller et al. (1992) came to in their study on toluene oxidation under sulfate-reducing conditions.

The microbial community profile (Figure 4.33) shows the taxa most likely responsible for sulfate reduction at the study site are relatives of *Desulfosporosinus* and *Petrimonas*. These are both capable sulfur reducers found in PHC-contaminated environments (Robertson et al. 2001, Grabowski et al. 2005). Specifically, species of *Petrimonas* can reduce elemental sulfur (but not sulfate) and *Desulfosporosinus* can reduce sulfate. Relatives of *Desulfocapsa* and *Sulfuricurvum* are also sulfur-cycling bacteria that are present in low abundance but more dominant in 11-03 relative to other taxa. *Desulfocapsa* can disproportionate elemental sulfur and thiosulfate into hydrogen sulfide and sulfate (Finster et al. 1998). Furthermore, relatives of *Desulfocapsa* have been found at a tar-oil contaminated site and may have been related to toluene biodegradation at that site (Winderl et al. 2008). Relatives of *Sulfuricurvum* can couple sulfur oxidation (sulfide, elemental sulfur, and thiosulfate) to nitrate reduction (Kodama and Watanabe 2004). *Sulfuricurvum* has been isolated from PHC-contaminated sites but does not use hydrocarbons as an energy source (Kodama and Watanabe 2004). Therefore, it is not clear if its presence is related to PHC biodegradation directly. Relatives of *Desulfocapsa* and *Sulfuricurvum* were only present in low abundance in most of the monitoring wells or only in 11-03. It is possible these bacteria will play a more important role in PHC biodegradation as the site is remediated and groundwater approaches lower concentrations of PHCs as observed in 11-03. Certainly, their abundance in 11-03 suggests they grow more actively under these conditions.

Gypsum dissolution during biostimulation provides sulfate to these sulfate-reducing communities. Sulfur XANES data (Figure 4.25) shows the enhanced microbial activity at the site has resulted in a depletion of gypsum at some borehole sampling locations (e.g., S15-04). Furthermore, an increase in sulfate concentrations (Figure 4.14) and strong correlations with Ca (Table 4.5) provide evidence that gypsum dissolution occurred during biostimulation. However, gypsum dissolution did not appear to occur at every sampling location (e.g., S15-03). These locations likely saw less sulfate reduction and gypsum reprecipitated when the groundwater became supersaturated with Ca and sulfate, consistent with SI values for gypsum calculated using PHREEQC (Figure 4.19).

There was an interesting and noteworthy anomaly in the results for FeS in the sediment samples. Fe XANES results show FeS was present in the sediments after the biostimulation. However, FeS was not present in sulfur XANES and the two major sulfur compounds identified in the sediments were gypsum and elemental sulfur. This difference can likely be explained by a shallow x-ray penetration depth near the sulfur K-edge and partial oxidation of FeS sediment grains. A FeS sediment grain has an approximate adsorption length of 5 μm near the sulfur K-edge (calculation in Appendix B). Sediment samples were pulverized by hand and are likely larger than 5 μm in diameter. As the number of adsorption lengths of a sample increases, the percent of transmitted photons decreases (Calvin 2013). Furthermore, elemental sulfur is a key intermediate FeS oxidation product and can coat the surface of FeS grains (Burton et al. 2009). Therefore, it seems likely that the data collected from sulfur XANES is only showing the surface of the FeS sediment grains.

5.2.3 Denitrification

Since nitrate remained near or below detection during the study despite addition of the biostimulation solution (0.8 mM), it can be concluded that nitrate was consumed during the study as either an electron acceptor (possibly for PHC oxidation) or as a nutrient. In this study, it appears that nitrate is mainly used as a nutrient, based on the low abundance of denitrifying bacteria (Figure 4.33). However, there is some evidence of the roles denitrifying communities play in iron- and sulfur-cycling.

The microbial community analysis (Figure 4.33) shows the main bacteria potentially capable of denitrification are relatives of *Comamonadaceae*, *Petrimonas*, and *Pseudoxanthomonas*. *Novosphingobium* is also present at the site and can couple PHC oxidation to nitrate reduction (Sohn et al. 2004). However, relatives of this bacterium were only present in low abundance throughout the site. The *Comamonadaceae* are a diverse family of bacteria that contains both Fe(III) reducers and nitrogen cyclers; therefore, it is likely that some proportion of the unclassified *Comamonadaceae* in our samples are denitrifying bacteria. *Petrimonas* species can reduce nitrate to ammonium, in addition to reducing elemental sulfur to sulfide (Grabowski et al. 2005). The ammonium produced by *Petrimonas* may be used by Fe(III)-reducing *Comamonadaceae*, but this is likely a small influence compared to the ammonium in the biostimulation solution as they are in relatively low abundance. *Pseudoxanthomonas* is an aerobe capable of oxidizing BTEX compounds and reducing nitrite (but not nitrate) to N_2O (Thierry et

al. 2004, Kim et al. 2008). Relatives of *Pseudoxanthomonas*, which were dominant in S15-04 compared to other monitoring wells, may influence iron- and sulfur-cycling by facilitating FeS oxidation through nitrite reduction or their presence indicates nitrite is available for FeS oxidation. PHC biodegradation was limited where *Pseudoxanthomonas* was dominant (S15-04) compared to monitoring wells that had low abundance of *Pseudoxanthomonas* (e.g., S15-05). Therefore, this may suggest that FeS oxidation limits the potential of PHC biodegradation to some degree. This may occur because nutrient availability is decreased or that other microbes are better suited for PHC biodegradation.

Multiple lines of evidence from this study (sediment mineralogy and groundwater geochemistry) suggest that the nitrate portion of the biostimulation solution may have stimulated FeS oxidation near the injection wells. FeS was detected by Fe XANES (Figure 4.28) in every post-biostimulation sediment sample except for S17-04 samples. Furthermore, in S15-04 sulfate concentrations increased but were weakly correlated to Ca compared to the other monitoring wells (Figure 4.14 and Table 4.5). This evidence suggests that FeS oxidation contributes to sulfate in S15-04 in addition to sulfate from gypsum dissolution. The presence of *Petrimonas* in S15-04 further supports our interpretation that FeS oxidation occurred near the injection wells because *Petrimonas* growth is stimulated by elemental sulfur. This sampling location also happens to be the closest monitoring well directly downstream of the remediation injection wells used during the study. Postma et al. (1991) noted this biogeochemical reaction occurred quickly compared to the groundwater flow in their study. Similar slow groundwater flow compared to this biogeochemical reaction rate would explain why evidence of FeS oxidation was only observed immediately downstream of where the biostimulation solution was delivered.

Denitrifying activity may have caused an increase in the proportion of N_2 gas in the headspace of contaminated monitoring wells (Table 4.8). However, this may have occurred because of a decrease in O_2 gas in the headspace. Denitrification may also have increased the concentration of ammonia (Figure 4.16), but this cannot be proven conclusively since the biostimulation solution contains ammonia in the form of ferric-ammonium-citrate. Using these geochemistry results alone do not provide a clear picture of the influence denitrification has on PHC remediation at the site.

5.2.4 Aerobic Biodegradation

Dissolved oxygen at the site was typically low and anaerobic biogeochemistry (sulfate- and Fe(III) reduction) was dominant during the study period. However, aerobic biodegradation might become a more important process as the groundwater is remediated to lower PHC concentrations. The main aerobic bacteria present at the site are *Polaromonas* relatives which has been isolated from a coal-tar contaminated environment and confirmed to degrade PHCs (Jeon et al. 2004). *Polaromonas* is quite ubiquitous throughout the site but was only present in relatively high abundance in monitoring wells with lower levels of contamination (11-03, S15-03, and later timepoints of S15-05). This supports our conclusion that *Polaromonas* may be important for PHC biodegradation as the groundwater approaches lower levels of PHC-contamination. Another aerobic PHC-degrading bacteria present at the site are relatives of *Hydrocarboniphaga* (Palleroni et al. 2004). However, *Hydrocarboniphaga* was only present in low abundance in 11-03.

5.2.5 Fermentation

Fermentative bacteria at the study site were in relatively low abundance, especially when compared to Fe(III)- and sulfate reducers. In pristine environments, fermenters play a key-role in organic matter decomposition and provide fermentation products (e.g., acetate) to other anaerobic bacteria (Appelo and Postma 2005). However, this does not appear to be a major process contributing to PHC degradation at this study site. This suggests that the Fe(III)- and sulfate reducers present at the site can directly oxidize PHCs.

The main fermenting bacteria present in the data appears to be relatives of *Sedimentibacter*, *Petrimonas*, and *Anaerolineaceae*. *Sedimentibacter* is a fermenter that has been found in a tar-oil contaminated environment and is thought to be involved in the biodegradation of toluene (Weiss et al. 2002, Winderl et al. 2008). The Spearman correlations on the Yue-Clayton Theta NMDS plot (Figure 4.34) also illustrates that *Sedimentibacter* relatives are a taxa that heavily influenced the position of the microbial communities in the plot. Grabowski et al. (2005) who isolated and characterized *Petrimonas sulfuriphila*, found that *Petrimonas* uses simple sugars (e.g., glucose) in its metabolism to produce fermentation products (e.g., acetate). The *Anaerolineaceae* are a family of bacteria that have been found in PHC-contaminated environments and anaerobic digesters used to treat wastewater sludge (Liang et al. 2015, McIlroy et al. 2017). This family is associated with environments where PHC biodegradation is occurring and they have an interesting syntrophic relationship with methanogens. Liang et al. (2016) found

that *Anaerolineaceae* were one of the dominant bacteria present in a methanogenic culture that actively degraded alkanes. They theorized that *Anaerolineaceae* played a key-role in the initial activation step of the alkane degradation and provided fermentation products (e.g., acetate) to methanogens.

5.3 Conceptual Model

The conceptual model (Figure 5.1) developed here illustrates how the different components of the biostimulation solution influenced the biogeochemistry in the contaminated region of the site based on the mineralogical, geochemical, and microbiological data collected in this study. The citrate and the phosphate components of the biostimulation solution have a universal effect on the microbiology and could influence any portion of the biogeochemistry. Phosphorus is an essential nutrient and citrate can stimulate Fe(III) reduction and increase the bioavailability of phosphorus (Chen et al. 2017; Bulmer et al. 2018). Citrate is also a component of the citric acid cycle used in cellular respiration and could be used as a simple carbon source by bacteria which could stimulate microbial growth (Madigan et al. 2014).

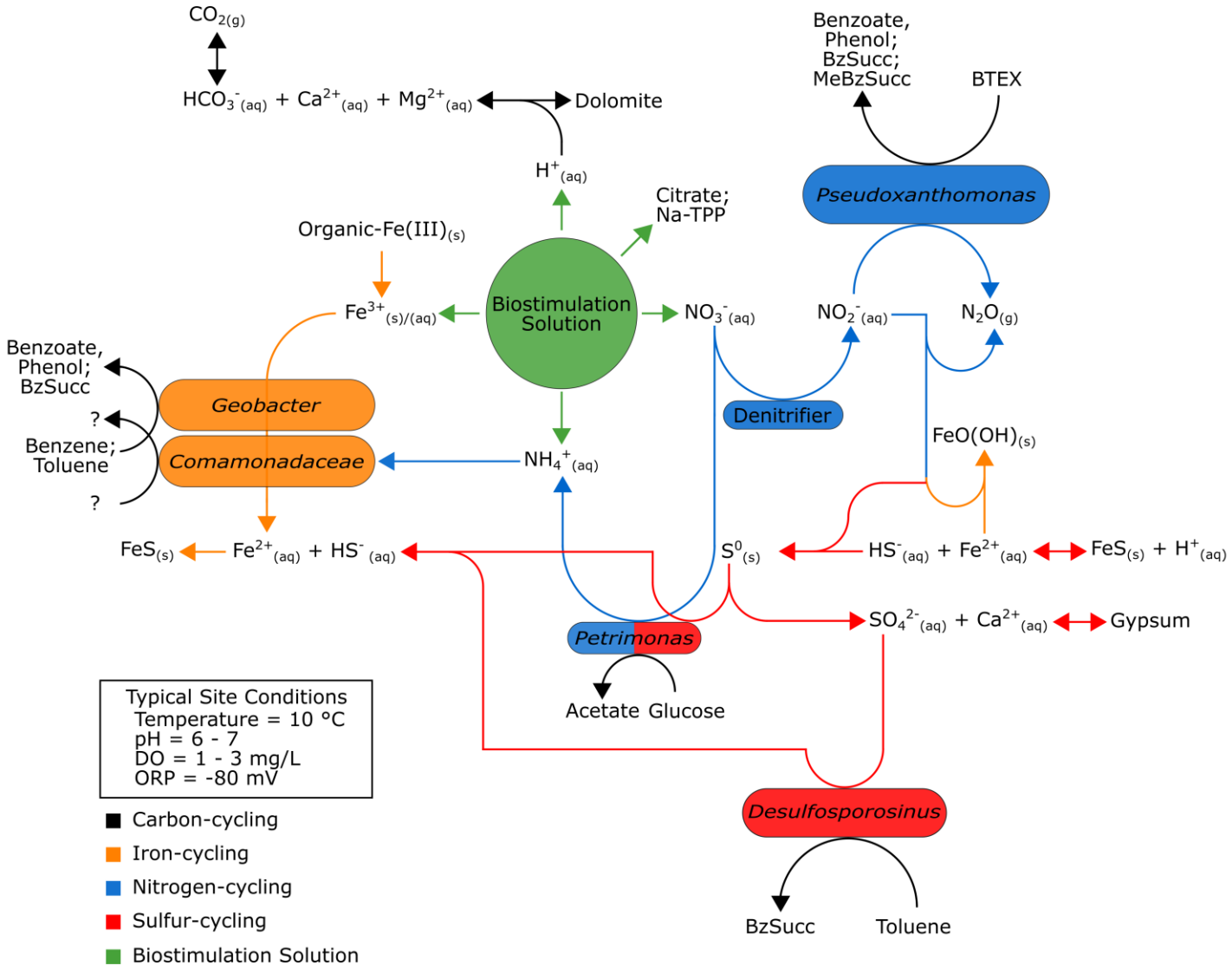

Figure 5.1. Proposed conceptual model of anaerobic biogeochemistry at the PHC-contaminated region of the study site. Note: geochemical reactions shown are unbalanced, simplified conceptual reactions.

CHAPTER 6 CONCLUSIONS AND RECOMMENDATIONS

6.1 Conclusions

A combination of physical and biological remediation methods was used to remediate a PHC-contaminated site in Saskatoon, SK. Contaminated groundwater was extracted using a MPE system and amended with a biostimulation solution and re-injected into the subsurface. The biostimulation solution contained nitrate added as nitric acid, sodium tripolyphosphate, and ferric-ammonium-citrate. The combined physical and biological remediation methods caused a measurable decrease in PHC contamination at the site. Using geochemical, mineralogical, and microbiological methods I assessed the biogeochemical pathways of the enhanced remediation at the site. This novel approach provided unique insights into the biogeochemistry of PHC biodegradation. Metabolite results collected throughout the study provided strong evidence that observed decreases in PHC concentrations were produced through biodegradation. The conceptual model developed in this thesis demonstrates how this biostimulation solution influences PHC biodegradation through different biogeochemical pathways at the study site.

The major pathways of PHC biodegradation appear to be Fe(III) reduction (*Geobacter* and unclassified *Comamonadaceae*) and sulfate reduction (*Desulfosporosinus*). In contrast, denitrification does not appear to be related to PHC biodegradation. Nitrite-reducing *Pseudoxanthomonas* relatives can degrade BTEX compounds, but here there is evidence suggesting they are related to FeS oxidation by nitrite. Thus, they are likely influencing both iron- and sulfur-cycling at this site through FeS oxidation. This FeS oxidation possibly decreases potential PHC biodegradation by consuming nitrate that could otherwise be used as a nutrient or coupled to PHC oxidation. Compared to nitrate, the ferric-ammonium-citrate component of the biostimulation solution appears to have influenced Fe(III)-reducer activity and the proportions of relatives of *Geobacter* and *Comamonadaceae*; however, it is not clear how this relationship affects rates or degree of PHC biodegradation. *Geobacter* species can degrade benzene and toluene but it is not clear how or if relatives of *Comamonadaceae* degrade PHCs in this system. However, it does appear that increasing proportions of unclassified *Comamonadaceae* in our

samples were related to enhanced PHC biodegradation, and this is compelling evidence that these microbes may be an important part of the PHC degrading community.

6.2 Recommendations and Future Work

Based on the findings reported in this thesis, the following recommendations and future works are suggested to further elucidate the biogeochemical effects of the biostimulation solution and improve remediation strategies for the region.

1) **Expand knowledge of groundwater microbial communities at the site.** Sequencing and analyzing samples from other monitoring wells that have similar geochemistry to monitoring wells sequenced in this study will further expand our knowledge of the relationship between observed communities and geochemical conditions. For example, 11-10 is geochemically similar to both 11-03 and S15-01 (the background monitoring well). Sequencing samples from this monitoring well will provide useful information on communities that exist in areas of the site that are intermediate between low contamination and background conditions.
2) **Study the effects of the biostimulation solution on sediment microbial communities.** This present study was only concerned with the effects of the biostimulation solution on groundwater communities. Sequencing and analyzing DNA from sediment samples will elucidate the effects of biostimulation on sediment microbial communities. Comparing these results to the groundwater communities found in this thesis will also provide useful information in the differences or similarities between sediment and groundwater communities.
3) **Isolate and characterize the unclassified *Comamonadaceae* found in our study.** Confirming the PHC biodegradation and Fe(III) reduction potential of the unclassified *Comamonadaceae* will fill in a knowledge gap of its role in PHC biodegradation.
4) **Conduct a flow-through column experiment with the biostimulation solution.** Sampling for microbiology and geochemistry over a high-resolution distance would provide useful information of observed biogeochemical trends spatially.
5) **Test the biostimulation solution without nitric acid.** Our conclusions here support that the nitric acid portion of the biostimulation solution causes FeS oxidation and that ammonia increases the proportions of unclassified *Comamonadaceae*. Removing the nitric acid from the biostimulation solution may improve remediation strategies.

REFERENCES

Aggarwal, P.K., Fuller, M.E., Gurgas, M.M., Manning, J.F., and Dillon, M.A. 1997. Use of Stable Oxygen and Carbon Isotope Analyses for Monitoring the Pathways and Rates of Intrinsic and Enhanced in Situ Biodegradation. Environmental Science & Technology, 31(2): 590–596. doi:10.1021/ES960562B.

Appelo, C.A.J., and Postma, D. 2005. Groundwater, Geochemistry, and Pollution. 2nd edition. A.A. Balkema Publishers, Leiden, NL.

Atekwana, E.A., Atekwana, E., Legall, F.D., and Krishnamurthy, R.V. 2005. Biodegradation and mineral weathering controls on bulk electrical conductivity in a shallow hydrocarbon contaminated aquifer. Journal of Contaminant Hydrology, 80(3): 149–167. doi:10.1016/j.jconhyd.2005.06.009.

ATSDR. 1999. Toxicological Profile for Total Petroleum Hydrocarbons.

Bajt, S., Sutton, S.R., and Delaney, J.S. 1994. X-ray microprobe analysis of iron oxidation states in silicates and oxides using X-ray absorption near edge structure (XANES). Geochimica et Cosmochimica Acta, 58(23): 5209–5214. doi:10.1016/0016-7037(94)90305-0.

Ball, J.W., and Nordstrom, D.K. 1991. User's Manual for WATEQ4F, with revised thermodynamic data base and test cases for calculating speciation of major, trace, and redox elements in natural waters. U.S. Geological Survey Water-Resources Investigations Report, 91–183(1): 1–188. Available from http://wwwbrr.cr.usgs.gov/projects/GWC_chemtherm/pubs/wq4fdoc.pdf.

Bekins, B.A., Cozzarelli, I.M., Godsy, E.M., Warren, E., Essaid, H.I., and Tuccillo, M.E. 2001. Progression of natural attenuation processes at a crude oil spill site: II. Controls on spatial distribution of microbial populations. Journal of Contaminant Hydrology, 53(3): 387–406. doi:10.1016/S0169-7722(01)00175-9.

Bell, P.E., Mills, A.L., and Herman, J.S. 1987. Biogeochemical Conditions Favoring Magnetite Formation during Anaerobic Iron Reduction. Applied and Environmental Microbiology, 53(11): 2610–2616.

Beller, H.R. 2000. Metabolic indicators for detecting in situanaerobic alkylbenzene degradation. Biodegradation, 11(2–3): 125–139. doi:10.1023/A:1011109800916.

Beller, H.R., Ding, W.-H., and Reinhard, M. 1995. Byproducts of Anaerobic Alkylbenzene Metabolism Useful as indicators of in Situ Bioremediation. Environmental Science & Technology, 29(11): 2864–2870.

Beller, H.R., Grbic-Galic, D., and Reinhard, M. 1992. Microbial degradation of toluene under sulfate-reducing conditions and the influence of iron on the process. Applied and Environmental Microbiology, 58(3): 786–793. Available from http://www.ncbi.nlm.nih.gov/pubmed/1575481.

Berner, R.A. 1970. Sedimentary pyrite formation. American Journal of Science, 268(1): 1–23. doi:10.2475/ajs.268.1.1.

Bethke, C.M., Sanford, R.A., Kirk, M.F., Jin, Q., and Flynn, T.M. 2011. The thermodynamic ladder in geomicrobiology. American Journal of Science, 311(3): 183–210. doi:10.2475/03.2011.01.

Blicher-Mathiesen, G., McCarty, G.W., and Nielsen, L.P. 1998. Denitrification and degassing in groundwater estimated from dissolved dinitrogen and argon. Journal of Hydrology, 208(1–2): 16–24. doi:10.1016/S0022-1694(98)00142-5.

Bonneville, S., Van Cappellen, P., and Behrends, T. 2004. Microbial reduction of iron(III) oxyhydroxides: effects of mineral solubility and availability. Chemical Geology, 212(3): 255–268. doi:10.1016/j.chemgeo.2004.08.015.

Bosch, J., Lee, K.-Y., Jordan, G., Kim, K.-W., and Meckenstock, R.U. 2012. Anaerobic, Nitrate-Dependent Oxidation of Pyrite Nanoparticles by Thiobacillus denitrificans. Environmental Science & Technology, 46(4): 2095–2101. doi:10.1021/es2022329.

Bottinga, Y., and Craig, H. 1968. Oxygen isotope fractionation between CO_2 and water, and the isotopic composition of marine atmospheric CO_2. Earth and Planetary Science Letters, 5(1): 285–295. doi:10.1016/S0012-821X(68)80054-8.

Bulmer, D., Kar, G., Hamilton, J., Siciliano, S., and Peak, D. 2018. Extent and Mechanism of Interaction between Phosphate and Citrate in a Calcareous Soil. Soil Science Society of America Journal, 82(2): 315. doi:10.2136/sssaj2017.08.0289.

Burton, E.D., Bush, R.T., Sullivan, L.A., Hocking, R.K., Mitchell, D.R.G., Johnston, S.G., Fitzpatrick, R.W., Raven, M., McClure, S., and Jang, L.Y.Y. 2009. Iron-monosulfide oxidation in natural sediments: Resolving microbially mediated S transformations using XANES, electron microscopy, and selective extractions. Environmental Science & Technology, 43(9): 3128–3134. doi:10.1021/es8036548.

Calvin, S. 2013. XAFS for Everyone. 1st edition. CRC Press, Boca Raton, FL.

CCME. 2008. Canada-Wide Standard for Petroleum Hydrocarbons (PHC) in Soil: Scientific Rationale Supporting Technical Document.

Chen, K.F., Chang, Y.C., and Chiou, W.T. 2016. Remediation of diesel-contaminated soil using in situ chemical oxidation (ISCO) and the effects of common oxidants on the indigenous microbial community: a comparison study. Journal of Chemical Technology & Biotechnology, 91(6): 1877–1888. doi:10.1002/jctb.4781.

Chen, T., Philips, C., Hamilton, J., Chartbrand, B., Grosskleg, J., Bradshaw, K., Carlson, T., Timlick, K., Peak, D., and Siciliano, S.D. 2017. Citrate Addition Increased Phosphorus Bioavailability and Enhanced Gasoline Bioremediation. Journal of Environment Quality, 46(5): 975–983. doi:10.2134/jeq2017.02.0064.

Christiansen, E.A. 1968. Pleistocene stratigraphy of the Saskatoon area, Saskatchewan, Canada. Canadian Journal of Earth Sciences, 5(5): 1167–1173. doi:10.1139/e68-114.

Christiansen, E.A. 1992. Pleistocene stratigraphy of the Saskatoon area, Saskatchewan, Canada: an update. Canadian Journal of Earth Sciences, 29(8): 1767–1778. doi:10.1139/e92-139.

Christofi, N., and Ivshina, I.B. 2002. Microbial surfactants and their use in field studies of soil remediation. Journal of Applied Microbiology, 93(6): 915–929. doi:10.1046/j.1365-2672.2002.01774.x.

Cleveland, C.C., and Liptzin, D. 2007. C:N:P stoichiometry in soil: is there a “Redfield ratio” for the microbial biomass? Biogeochemistry, 85(3): 235–252. doi:10.1007/s10533-007-9132-0.

Cozzarelli, I.M., Baedecker, M.J., Eganhouse, R.P., and Goerlitz, D.F. 1994. The geochemical evolution of low-molecular-weight organic acids derived from the degradation of petroleum contaminants in groundwater. Geochimica et Cosmochimica Acta, 58(2): 863–877. doi:10.1016/0016-7037(94)90511-8.

Degens, E.T., and Epstein, S. 1964. Oxygen and carbon isotope ratios in coexisting calcites and dolomites from recent and ancient sediments. Geochimica et Cosmochimica Acta, 28(1): 23–44. doi:10.1016/0016-7037(64)90053-5.

Deshpande, S., Shiau, B.J., Wade, D., Sabatini, D.A., and Harwell, J.H. 1999. Surfactant selection for enhancing ex situ soil washing. Water Research, 33(2): 351–360. doi:10.1016/S0043-1354(98)00234-6.

European Synchrotron Radiation Facility (ESRF). (n.d.). ID21 Sulfur XANES spectra database home. Available from http://www.esrf.eu/home/UsersAndScience/Experiments/XNP/ID21/php.html [accessed 22 January 2018].

Finneran, K.T., Johnsen, C. V., and Lovley, D.R. 2003. Rhodoferax ferrireducens sp. nov., a psychrotolerant, facultatively anaerobic bacterium that oxidizes acetate with the reduction of Fe(III). International Journal of Systematic and Evolutionary Microbiology, 53(3): 669–673. doi:10.1099/ijs.0.02298-0.

Finster, K., Liesack, W., and Thamdrup, B. 1998. Elemental sulfur and thiosulfate disproportionation by Desulfocapsa sulfoexigens sp. nov., a new anaerobic bacterium isolated from marine surface sediment. Applied and Environmental Microbiology, 64(1): 119–125. Available from http://www.ncbi.nlm.nih.gov/pubmed/9435068.

Fischer, W. 1988. Microbiological reactions of iron in soil. *In* Iron in Soil and Clay Minerals. *Edited by* J.W. Stucki, B.A. Goodman, and U. Schwertmann. D. Reidel Publishing Company. pp. 715–748.

Flynn, T.M., O’Loughlin, E.J., Mishra, B., DiChristina, T.J., and Kemner, K.M. 2014. Sulfur-mediated electron shuttling during bacterial iron reduction. Science, 344(6187): 1039–1042. doi:10.1126/science.1252066.

Fredrickson, J.K., Zachara, J.M., Kennedy, D.W., Dong, H., Onstott, T.C., Hinman, N.W., and Li, S. 1998. Biogenic iron mineralization accompanying the dissimilatory reduction of hydrous ferric oxide by a groundwater bacterium. Geochimica et Cosmochimica Acta, 62(19): 3239–3257. doi:10.1016/S0016-7037(98)00243-9.

Gieg, L.M., and Suflita, J.M. 2002. Detection of Anaerobic Metabolites of Saturated and Aromatic Hydrocarbons in Petroleum-Contaminated Aquifers. Environmental Science & Technology, 36(17): 3755–3762. doi:10.1021/ES0205333.

Government of Saskatchewan. 2016. Saskatchewan Environmental Quality Guidelines. Available from https://envrbrportal.crmp.saskatchewan.ca/seqg-search/ [accessed 23 October 2018].

Grabowski, A., Tindall, B.J., Bardin, V., Blanchet, D., and Jeanthon, C. 2005. Petrimonas sulfuriphila gen. nov., sp. nov., a mesophilic fermentative bacterium isolated from a biodegraded oil reservoir. International Journal of Systematic and Evolutionary Microbiology, 55(3): 1113–1121. doi:10.1099/ijs.0.63426-0.

Hamilton, J.G., Grosskleg, J., Hilger, D., Bradshaw, K., Carlson, T., Siciliano, S.D., and Peak, D. 2018. Chemical speciation and fate of tripolyphosphate after application to a calcareous soil. Geochemical Transactions, 19(1): 1–11. doi:10.1186/s12932-017-0046-z.

Hedrich, S., Schlömann, M., and Barrie Johnson, D. 2011. The iron-oxidizing proteobacteria. Microbiology, 157(6): 1551–1564. doi:10.1099/mic.0.045344-0.

Hoefs, J. 2009. Stable Isotope Geochemistry. 6th edition. Springer, Berlin, DE.

Hunkeler, D., Andersen, N., Aravena, R., Bernasconi, S.M., and Butler, B.J. 2001. Hydrogen and Carbon Isotope Fractionation during Aerobic Biodegradation of Benzene. Environmental Science & Technology, 35(17): 3462–3467. doi:10.1021/ES0105111.

Hunkeler, D., Meckenstock, R.U., Lollar, T., Schmidt, C., and Wilson, J.T. 2009. A Guide for Assessing Biodegradation and Source Identification of Organic Groundwater Contaminants Using Compound Specific Isotope Analysis (CSIA). Washington, USA. Available from https://cfpub.epa.gov/si/si_public_record_report.cfm?dirEntryId=202171.

Janssen, P.H. 2006. Identifying the Dominant Soil Bacterial Taxa in Libraries of 16S rRNA and 16S rRNA Genes. Applied and Environmental Microbiology, 72(3): 1719–1728. doi:10.1128/AEM.72.3.1719–1728.2006.

Jeon, C.O., Park, W., Ghiorse, W.C., and Madsen, E.L. 2004. Polaromonas naphthalenivorans sp. nov., a naphthalene-degrading bacterium from naphthalene-contaminated sediment. International Journal of Systematic and Evolutionary Microbiology, 54(1): 93–97. doi:10.1099/ijs.0.02636-0.

Kelley, C.A., Hammer, B.T., and Coffin, R.B. 1997. Concentrations and Stable Isotope Values of BTEX in Gasoline-Contaminated Groundwater. Environmental Science & Technology, 31(9): 2469–2472. doi:10.1021/ES960635R.

Kim, J.M., Le, N.T., Chung, B.S., Park, J.H., Bae, J.-W., Madsen, E.L., and Jeon, C.O. 2008. Influence of soil components on the biodegradation of benzene, toluene, ethylbenzene, and o-, m-, and p-xylenes by the newly isolated bacterium Pseudoxanthomonas spadix BD-a59. Applied and Environmental Microbiology, 74(23): 7313–7320. doi:10.1128/AEM.01695-08.

Kirk, M.F., Jin, Q., and Haller, B.R. 2016. Broad-Scale Evidence That pH Influences the Balance Between Microbial Iron and Sulfate Reduction. Groundwater, 54(3): 406–413. doi:10.1111/gwat.12364.

Kodama, Y., and Watanabe, K. 2004. Sulfuricurvum kujiense gen. nov., sp. nov., a facultatively anaerobic, chemolithoautotrophic, sulfur-oxidizing bacterium isolated from an underground crude-oil storage cavity. International Journal of Systematic and Evolutionary Microbiology, 54(6): 2297–2300. doi:10.1099/ijs.0.63243-0.

Krembs, F.J., Siegrist, R.L., Crimi, M.L., Furrer, R.F., and Petri, B.G. 2010. ISCO for Groundwater Remediation: Analysis of Field Applications and Performance. Ground Water Monitoring & Remediation, 30(4): 42–53. doi:10.1111/j.1745-6592.2010.01312.x.

Liang, B., Wang, L.-Y., Mbadinga, S.M., Liu, J.-F., Yang, S.-Z., Gu, J.-D., and Mu, B.-Z. 2015. Anaerolineaceae and Methanosaeta turned to be the dominant microorganisms in alkanes-dependent methanogenic culture after long-term of incubation. AMB Express, 5(1): 37. doi:10.1186/s13568-015-0117-4.

Liang, B., Wang, L.-Y., Zhou, Z., Mbadinga, S.M., Zhou, L., Liu, J.-F., Yang, S.-Z., Gu, J.-D., and Mu, B.-Z. 2016. High Frequency of Thermodesulfovibrio spp. and Anaerolineaceae in Association with Methanoculleus spp. in a Long-Term Incubation of n-Alkanes-Degrading Methanogenic Enrichment Culture. Frontiers in Microbiology, 7(1): 1431–1444. doi:10.3389/fmicb.2016.01431.

Lovley, D.R. 1993. Dissimilatory metal reduction. Annual Review of Microbiology, 47(1): 263–290. doi:10.1146/annurev.micro.47.1.263.

Lovley, D.R., Giovannoni, S.J., White, D.C., Champine, J.E., Phillips, E.J.P., Gorby, Y.A., and Goodwin, S. 1993. Geobacter metallireducens gen. nov. sp. nov., a microorganism capable of coupling the complete oxidation of organic compounds to the reduction of iron and other metals. Archives of Microbiology, 159(4): 336–344. Springer-Verlag. doi:10.1007/BF00290916.

Madigan, M.T., Martinko, J.M., Bender, K.S., and Buckley, D.H. 2014. Brock's Biology of Microorganisms. 13th edition. Pearson.

Mahmoudi, N., Slater, G.F., and Fulthorpe, R.R. 2011. Comparison of commercial DNA extraction kits for isolation and purification of bacterial and eukaryotic DNA from PAH-contaminated soils. Canadian Journal of Microbiology, 57(8): 623–628. doi:10.1139/w11-049.

Makkar, R.S., and Rockne, K.J. 2003. Comparison of synthetic surfactants and biosurfactants in enhancing biodegradation of polycyclic aromatic hydrocarbons. Environmental Toxicology and Chemistry, 22(10): 2280–2292. doi:10.1897/02-472.

Mao, D., Lookman, R., Van De Weghe, H., Weltens, R., Vanermen, G., Brucker, N. De, and Diels, L. 2009. Combining HPLC-GCXGC, GCXGC/ToF-MS, and Selected Ecotoxicity Assays for Detailed Monitoring of Petroleum Hydrocarbon Degradation in Soil and Leaching Water. Environmental Science & Technology, 43(20): 7651–7657. doi:10.1021/es9015603.

Marley, M.C., Hazebrouck, D.J., and Walsh, M.T. 1992. The Application of In Situ Air Sparging as an Innovative Soils and Ground Water Remediation Technology. Ground Water Monitoring & Remediation, 12(2): 137–145. doi:10.1111/j.1745-6592.1992.tb00044.x.

McIlroy, S.J., Kirkegaard, R.H., Dueholm, M.S., Fernando, E., Karst, S.M., Albertsen, M., and Nielsen, P.H. 2017. Culture-Independent Analyses Reveal Novel Anaerolineaceae as Abundant Primary Fermenters in Anaerobic Digesters Treating Waste Activated Sludge. Frontiers in Microbiology, 8(1): 1134–1144. doi:10.3389/fmicb.2017.01134.

McLean, J.S., Lee, J.U., and Beveridge, T.. J. 2002. Interactions of bacteria and environmental metals, fine-grained mineral development and bioremediation strategies. *In* IUPAC Series on Analytical and Physical Chemistry of Environmental Systems. *Edited by* P.M. Huang, J.-M. Bollag, and N. Senesi. Wiley. pp. 227–262.

Melbye, A.G., Brakstad, O.G., Hokstad, J.N., Gregersen, I.K., Hansen, B.H., Booth, A.M., Rowland, S.J., and Tollefsen, K.E. 2009. Chemical and toxicological characterization of an unresolved complex mixture-rich biodegraded crude oil. Environmental Toxicology and Chemistry, 28(9): 1815–1824. doi:10.1897/08-545.1.

Molins, S., Mayer, K.U., Amos, R.T., and Bekins, B.A. 2010. Vadose zone attenuation of organic compounds at a crude oil spill site — Interactions between biogeochemical reactions and multicomponent gas transport. Journal of Contaminant Hydrology, 112(1–4): 15–29. doi:10.1016/J.JCONHYD.2009.09.002.

Mouser, P.J., N'Guessan, A.L., Holmes, D.E., Williams, K.H., Wilkins, M.J., Long, P.E., Lovley, D.R., N'Guessan, A.L., Elifantz, H., Holmes, D.E., Williams, K.H., Wilkins, M.J., Long, P.E., and Lovley, D.R. 2009. Influence of Heterogeneous Ammonium Availability on Bacterial Community Structure and the Expression of Nitrogen Fixation and Ammonium Transporter Genes during in Situ Bioremediation of Uranium-Contaminated Groundwater. Environmental Science & Technology, 43(12): 4386–4392. doi:10.1021/es8031055.

Mulligan, C., Yong, R., and Gibbs, B. 2001. Surfactant-enhanced remediation of contaminated soil: a review. Engineering Geology, 60(1–4): 371–380. doi:10.1016/S0013-7952(00)00117-4.

Munch, J.C., and Ottow, J.C.G. 1980. Preferential reduction of amorphous to crystalline iron oxides by bacterial activitity. Soil Science, 129(1): 15–21. doi:10.1097/00010694-198001000-00004.

O'Day, P.A., Rivera, N., Root, R., and Carroll, S.A. 2004. X-ray absorption spectroscopic study of Fe reference compounds for the analysis of natural sediments. American Mineralogist, 89(4): 572–585. doi:10.2138/am-2004-0412.

O'Neil, R.A., Holmes, D.E., Coppi, M. V., Adams, L.A., Larrahondo, M.J., Ward, J.E., Nevin, K.P., Woodard, T.L., Vrionis, H.A., N'Guessan, A.L., and Lovley, D.R. 2008. Gene transcript analysis of assimilatory iron limitation in Geobacteraceae during groundwater bioremediation. Environmental Microbiology, 10(5): 1218–1230. doi:10.1111/j.1462-2920.2007.01537.x.

Palleroni, N.J., Port, A.M., Chang, H.-K., and Zylstra, G.J. 2004. Hydrocarboniphaga effusa gen. nov., sp. nov., a novel member of the gamma-proteobacteria active in alkane and aromatic hydrocarbon degradation. International Journal of Systematic and Evolutionary Microbiology, 54(4): 1203–1207. doi:10.1099/ijs.0.03016-0.

Parada, C.B., Long, A., and Davis, S.N. 1983. Stable-isotopic composition of soil carbon dioxide in the Tucson basin, Arizona, U.S.A. Chemical Geology, 41(1): 219–236. doi:10.1016/S0009-2541(83)80020-5.

Parkhurst, D.L., and Appelo, C.A.J. 1999. User's Guide To PHREEQC (version 2) — a Computer Program for Speciation, and Inverse Geochemical Calculations. doi:Rep. 99-4259.

Pérez-Rodríguez, M., Prieto, G., Rega, C., Varela, L.M., Sarmiento, F., and Mosquera, V. 1998. A Comparative Study of the Determination of the Critical Micelle Concentration by Conductivity and Dielectric Constant Measurements. Langmuir, 14(16): 4422–4426. doi:10.1021/LA980296A.

Ponsin, V., Mouloubou, O.R., Prudent, P., and Höhener, P. 2014. Does phosphate enhance the natural attenuation of crude oil in groundwater under defined redox conditions? Journal of Contaminant Hydrology, 169(1): 4–18. doi:10.1016/j.jconhyd.2014.04.003.

Postma, D., Boesen, C., Kristiansen, H., and Larsen, F. 1991. Nitrate Reduction in an Unconfined Sandy Aquifer: Water Chemistry, Reduction Processes, and Geochemical Modeling. Water Resources Research, 27(8): 2027–2045. doi:10.1029/91WR00989.

Prommer, H., Davis, G.B., and Barry, D.A. 1999. Geochemical changes during biodegradation of petroleum hydrocarbons: field investigations and biogeochemical modelling. Organic Geochemistry, 30(6): 423–435. doi:10.1016/S0146-6380(99)00027-3.

Ravel, B., and Newville, M. 2005. ATHENA, ARTEMIS, HEPHAESTUS: Data analysis for X-ray absorption spectroscopy using IFEFFIT. Journal of Synchrotron Radiation, 12(4): 537–541. doi:10.1107/S0909049505012719.

Reardon, E.J., Allison, G.B., and Fritz, P. 1979. Seasonal chemical and isotopic variations of soil CO2 at Trout Creek, Ontario. Journal of Hydrology, 43(1–4): 355–371. doi:10.1016/0022-1694(79)90181-1.

Robertson, W.J., Bowman, J.P., Mee, B.J., Franzmann, P.D., and Mee, B.J. 2001. Desulfosporosinus meridiei sp . nov ., a spore- forming sulfate-reducing bacterium isolated from gasolene-contaminated groundwater. International Journal of Systematic and Evolutionary Microbiology, 51(1): 133–140. doi:10.1099/00207713-51-1-133.

Roden, E.E. 2003. Fe(III) Oxide Reactivity Toward Biological versus Chemical Reduction. Environmental Science & Technology, 37(7): 1319–1324. doi:10.1021/es026038o.

Russell, D.L. 2012. Remediation Manual for Contaminated Sites. 1st edition. CRC Press, New York, NY.

Saul, D.J., Aislabie, J.M., Brown, C.E., Harris, L., and Foght, J.M. 2005. Hydrocarbon contamination changes the bacterial diversity of soil from around Scott Base, Antarctica. FEMS Microbiology Ecology, 53(1): 141–155. doi:10.1016/j.femsec.2004.11.007.

Schippers, A., and Jørgensen, B.B. 2002. Biogeochemistry of pyrite and iron sulfide oxidation in marine sediments. Geochimica et Cosmochimica Acta, 66(1): 85–92. doi:10.1016/S0016-7037(01)00745-1.

Schloss, P.D., Westcott, S.L., Ryabin, T., Hall, J.R., Hartmann, M., Hollister, E.B., Lesniewski, R.A., Oakley, B.B., Parks, D.H., Robinson, C.J., Sahl, J.W., Stres, B., Thallinger, G.G., Van Horn, D.J., and Weber, C.F. 2009. Introducing mothur: Open-Source, Platform-Independent, Community-Supported Software for Describing and Comparing Microbial Communities. Applied and Environmental Microbiology, 75(23): 7537–7541. doi:10.1128/AEM.01541-09.

Shan, C., Falta, R.W., and Javandel, I. 1992. Analytical solutions for steady state gas flow to a soil vapor extraction well. Water Resources Research, 28(4): 1105–1120. doi:10.1029/91WR02986.

Siciliano, S.D., Chen, T., Phillips, C., Hamilton, J., Hilger, D., Chartrand, B., Grosskleg, J., Bradshaw, K., Carlson, T., and Peak, D. 2016. Total Phosphate Influences the Rate of Hydrocarbon Degradation but Phosphate Mineralogy Shapes Microbial Community Composition in Cold-Region Calcareous Soils. Environmental Science & Technology, 50(10): 5197–5206. doi:10.1021/acs.est.5b05911.

Smith, V.H., Graham, D.W., and Cleland, D.D. 1998. Application of Resource-Ratio Theory to Hydrocarbon Biodegradation. Environmental Science & Technology, 32(21): 3386–3395. doi:10.1021/es9805019.

Sohn, J.H., Kwon, K.K., Kang, J.-H., Jung, H.-B., and Kim, S.-J. 2004. Novosphingobium pentaromativorans sp. nov., a high-molecular-mass polycyclic aromatic hydrocarbon-degrading bacterium isolated from estuarine sediment. International Journal of Systematic and Evolutionary Microbiology, 54(5): 1483–1487. doi:10.1099/ijs.0.02945-0.

Van Stempvoort, D.R., Millar, K., and Lawrence, J.R. 2009. Accumulation of short-chain fatty acids in an aquitard linked to anaerobic biodegradation of petroleum hydrocarbons. Applied Geochemistry, 24(1): 77–85. doi:10.1016/J.APGEOCHEM.2008.11.004.

Stookey, L.L. 1970. Ferrozine---a new spectrophotometric reagent for iron. Analytical Chemistry, 42(7): 779–781. doi:10.1021/ac60289a016.

Suthersan, S.S., Horst, J., Schnobrich, M., Welty, N., and McDonough, J. 2017. Remediation Engineering: Design Concepts. 2nd edition. CRC Press, New York, NY.

Thierry, S., Macarie, H., Iizuka, T., Geißdörfer, W., Assih, E.A., Spanevello, M., Verhe, F., Thomas, P., Fudou, R., Monroy, O., Labat, M., and Ouattara, A.S. 2004. Pseudoxanthomonas mexicana sp. nov. and Pseudoxanthomonas japonensis sp. nov., isolated from diverse environments, and emended descriptions of the genus Pseudoxanthomonas Finkmann et al. 2000 and of its type species. International Journal of Systematic and Evolutionary Microbiology, 54(6): 2245–2255. doi:10.1099/ijs.0.02810-0.

Toby, B.H., and Von Dreele, R.B. 2013. GSAS-II : the genesis of a modern open-source all purpose crystallography software package. Journal of Applied Crystallography, 46(2): 544–549. doi:10.1107/S0021889813003531.

Torrentó, C., Urmeneta, J., Otero, N., Soler, A., Viñas, M., and Cama, J. 2011. Enhanced denitrification in groundwater and sediments from a nitrate-contaminated aquifer after addition of pyrite. Chemical Geology, 287(1–2): 90–101. doi:10.1016/J.CHEMGEO.2011.06.002.

Torsvik, V., Goksøyr, J., and Daae, F.L. 1990a. High diversity in DNA of soil bacteria. Applied and Environmental Microbiology, 56(3): 782–787. Available from http://www.ncbi.nlm.nih.gov/pubmed/2317046.

Torsvik, V., Salte, K., Sørheim, R., and Goksøyr, J. 1990b. Comparison of phenotypic diversity and DNA heterogeneity in a population of soil bacteria. Applied and Environmental Microbiology, 56(3): 776–781. Available from http://www.ncbi.nlm.nih.gov/pubmed/2180371.

Toth, C.R.A., and Gieg, L.M. 2018. Time Course-Dependent Methanogenic Crude Oil Biodegradation: Dynamics of Fumarate Addition Metabolites, Biodegradative Genes, and Microbial Community Composition. Frontiers in Microbiology, 8: 2610–2826. Frontiers. doi:10.3389/fmicb.2017.02610.

Tsai, Y., and Olson, B.H. 1992. Rapid Method for Separation of Bacterial DNA from Humic Substances in Sediments for Polymerase Chain Reaction. 58(7): 2292–2295.

Tuccillo, M.E., Cozzarelli, I.M., and Herman, J.S. 1999. Iron reduction in the sediments of a hydrocarbon-contaminated aquifer. Applied Geochemistry, 14(5): 655–667. doi:10.1016/S0883-2927(98)00089-4.

Tyagi, M., da Fonseca, M.M.R., and de Carvalho, C.C.C.R. 2011. Bioaugmentation and biostimulation strategies to improve the effectiveness of bioremediation processes. Biodegradation, 22(2): 231–241. doi:10.1007/s10532-010-9394-4.

Ulrich, A.C., Beller, H.R., and Edwards, E.A. 2005. Metabolites Detected during Biodegradation of 13C6-Benzene in Nitrate-Reducing and Methanogenic Enrichment Cultures. Environmental Science & Technology, 39(17): 6681–6691. doi:10.1021/ES050294U.

Viollier, E., Englett, P.W., Hunter, K., Roychoudhury, A.N., and Van Cappellen, P. 2000. The ferrozine method revisted: Fe(II)/Fe(III) determination in natural waters. Applied Geochemistry, 15(6): 785–790. doi:http://dx.doi.org/10.1016/S0883-2927(99)00097-9.

Webb, S.M. 2005. SIXPack a Graphical User Interface for XAS Analysis Using IFEFFIT. Physica Scripta, 2005(T115): 1011–1014. doi:10.1238/Physica.Topical.115a01011.

Wei, L., Chen, C., and Xu, Z. 2010. Citric acid enhances the mobilization of organic phosphorus in subtropical and tropical forest soils. Biology and Fertility of Soils, 46(7): 765–769. doi:10.1007/s00374-010-0464-x.

Weiss, N., Wiegel, J., Andreesen, J.R., Breitenstein, A., Haertig, C., and Lechner, U. 2002. Reclassification of Clostridium hydroxybenzoicum as Sedimentibacter hydroxybenzoicus gen. nov., comb. nov., and description of Sedimentibacter saalensis sp. nov.. International Journal of Systematic and Evolutionary Microbiology, 52(3): 801–807. doi:10.1099/00207713-52-3-801.

Wilke, M., Farges, F., Petit, P.-E.P., Brown, G.E., and Martin, F. 2001. Oxidation state and coordination of Fe in minerals: An Fe K-XANES spectroscopic study. American Mineralogist, 86(5): 714–730. doi:10.2138/am-2001-5-612.

Willems, A. 2014. The Family Comamonadaceae. *In* The Prokaryotes. Springer Berlin Heidelberg, Berlin, DE. pp. 777–851. doi:10.1007/978-3-642-30197-1_238.

Winderl, C., Anneser, B., Griebler, C., Meckenstock, R.U., and Lueders, T. 2008. Depth-resolved quantification of anaerobic toluene degraders and aquifer microbial community patterns in distinct redox zones of a tar oil contaminant plume. Applied and Environmental Microbiology, 74(3): 792–801. doi:10.1128/AEM.01951-07.

Xiong, W., Mathies, C., Bradshaw, K., Carlson, T., Tang, K., and Wang, Y. 2012. Benzene removal by a novel modification of enhanced anaerobic biostimulation. Water Research, 46(15): 4721–4731. doi:10.1016/j.watres.2012.06.036.

Yeh, H.-W., and Epstein, S. 1981. Hydrogen and carbon isotopes of petroleum and related organic matter. Geochimica et Cosmochimica Acta, 45(5): 753–762. doi:10.1016/0016-7037(81)90046-6.

Zachara, J.M., Kukkadapu, R.K., Gassman, P.L., Dohnalkova, A., Fredrickson, J.K., and Anderson, T. 2004. Biogeochemical transformation of Fe minerals in a petroleum-contaminated aquifer. Geochimica et Cosmochimica Acta, 68(8): 1791–1805. doi:10.1016/j.gca.2003.09.022.

Zhang, T., Bain, T.S., Nevin, K.P., Barlett, M.A., and Lovley, D.R. 2012. Anaerobic benzene oxidation by Geobacter species. Applied and Environmental Microbiology, 78(23): 8304–8310. doi:10.1128/AEM.02469-12.

APPENDIX A: Groundwater Monitoring Results

Table A.1. Groundwater elevation data. Datum set at 9 mBGL (typical depth of a borehole at the site).

Well ID	Sample Date	Ground Surface (mASL)	Groundwater Table (mASL)	Groundwater Table (mBGL)	Groundwater Table (mAD)
11-03	20-Oct-15	493.5	489.5	4.0	5.0
11-03	10-Jun-16	493.5	489.8	3.7	5.3
11-03	16-Aug-16	493.5	489.4	4.1	4.9
11-03	1-Nov-16	493.5	489.1	4.4	4.6
11-03	27-Jun-17	493.5	490.2	3.3	5.7
11-03	30-Oct-17	493.5	490.0	3.5	5.5
S15-01	19-Oct-15	493.2	490.0	3.2	5.8
S15-01	8-Jun-16	493.2	490.3	2.9	6.1
S15-01	15-Aug-16	493.2	490.2	2.9	6.1
S15-01	25-Oct-16	493.2	490.3	2.9	6.1
S15-01	28-Jun-17	493.2	490.1	3.0	6.0
S15-01	1-Nov-17	493.2	490.2	3.0	6.0
S15-02	19-Oct-15	493.4	486.2	7.2	1.8
S15-02	8-Jun-16	493.4	490.0	3.4	5.6
S15-02	16-Aug-16	493.4	490.0	3.4	5.6
S15-02	27-Jun-17	493.4	490.0	3.4	5.6
S15-02	1-Nov-17	493.4	490.4	3.0	6.0
S15-03	6-Nov-15	493.4	488.9	4.4	4.6
S15-03	8-Jun-16	493.4	489.9	3.4	5.6
S15-03	16-Aug-16	493.4	489.9	3.4	5.6
S15-03	25-Oct-16	493.4	490.4	3.0	6.0
S15-03	28-Jun-17	493.4	490.0	3.4	5.6
S15-03	30-Oct-17	493.4	490.5	2.9	6.1
S15-04	19-Oct-15	493.5	487.4	6.1	2.9
S15-04	8-Jun-16	493.5	489.9	3.5	5.5
S15-04	16-Aug-16	493.5	490.1	3.4	5.6
S15-04	25-Oct-16	493.5	489.9	3.6	5.4
S15-04	27-Jun-17	493.5	490.1	3.3	5.7
S15-04	1-Nov-17	493.5	490.4	3.1	5.9

Table A.1. Continued.

Well ID	Sample Date	Ground Surface (mASL)	Groundwater Table (mASL)	Groundwater Table (mBGL)	Groundwater Table (mAD)
S15-05	6-Nov-15	493.4	489.0	4.4	4.6
S15-05	8-Jun-16	493.4	489.9	3.5	5.5
S15-05	16-Aug-16	493.4	490.0	3.5	5.5
S15-05	25-Oct-16	493.4	489.8	3.6	5.4
S15-05	27-Jun-17	493.4	490.0	3.5	5.5
S15-05	1-Nov-17	493.4	490.3	3.1	5.9
S15-06	19-Oct-15	493.4	489.1	4.4	4.6
S15-06	10-Jun-16	493.4	489.7	3.7	5.3
S15-06	16-Aug-16	493.4	489.6	3.9	5.1
S15-06	1-Nov-16	493.4	490.1	3.3	5.7
S15-06	27-Jun-17	493.4	489.7	3.7	5.3
S15-06	30-Oct-17	493.4	489.8	3.7	5.3

Table A.2. Groundwater BTEX concentrations.

Well ID	Sample Date	Benzene		Toluene		Ethylbenzene		Xylenes, Total	
		(mg/L)	(mM)	(mg/L)	(mM)	(mg/L)	(mM)	(mg/L)	(mM)
11-03	20-Oct-15	2.5	3.2E-02	0.018	2.0E-04	0.36	3.4E-03	0.39	3.7E-03
11-03	10-Jun-16	1.7	2.2E-02	0.012	1.3E-04	0.15	1.4E-03	0.34	3.2E-03
11-03	16-Aug-16	1.7	2.2E-02	0.018	2.0E-04	0.26	2.4E-03	0.44	4.1E-03
11-03	1-Nov-16	1.3	1.7E-02	0.015	1.6E-04	0.19	1.8E-03	0.33	3.1E-03
11-03	27-Jun-17	1.1	1.4E-02	0.0085	9.2E-05	0.16	1.5E-03	0.30	2.8E-03
11-03	30-Oct-17	1.8	2.3E-02	0.009	9.8E-05	0.34	3.2E-03	0.35	3.3E-03
S15-01	19-Oct-15	<0.00040	<0.00040	<0.00040	<0.00040	<0.00040	<0.00040	<0.00080	<0.00080
S15-01	8-Jun-16	<0.00040	<0.00040	<0.00040	<0.00040	<0.00040	<0.00040	<0.00080	<0.00080
S15-01	15-Aug-16	<0.00040	<0.00040	<0.00040	<0.00040	<0.00040	<0.00040	<0.00080	<0.00080
S15-01	25-Oct-16	<0.00040	<0.00040	<0.00040	<0.00040	<0.00040	<0.00040	<0.00080	<0.00080
S15-01	28-Jun-17	0.0013	1.7E-05	<0.00040	<0.00040	0.00045	4.2E-06	<0.00080	<0.00080
S15-01	1-Nov-17	<0.00040	<0.00040	<0.00040	<0.00040	<0.00040	<0.00040	<0.00080	<0.00080
S15-02	19-Oct-15	13	0.17	21	0.23	2.3	2.2E-02	14	0.13
S15-02	8-Jun-16	15	0.19	17	0.18	1.9	1.8E-02	12	0.11
S15-02	16-Aug-16	15	0.19	15	0.16	2.4	2.3E-02	14	0.13
S15-02	27-Jun-17	11	0.14	3.1	3.4E-02	1.5	1.4E-02	5.2	4.9E-02
S15-02	1-Nov-17	9.8	0.13	4.7	5.1E-02	1.4	1.3E-02	5.2	4.9E-02
S15-03	6-Nov-15	3	3.8E-02	1.9	2.1E-02	0.20	1.9E-03	3.2	3.0E-02
S15-03	8-Jun-16	3.3	4.2E-02	0.220	2.4E-03	0.26	2.4E-03	0.85	8.0E-03
S15-03	16-Aug-16	1.7	2.2E-02	0.089	9.7E-04	0.20	1.9E-03	0.54	5.1E-03
S15-03	25-Oct-16	0.59	7.6E-03	0.024	2.6E-04	0.01	5.6E-05	0.18	1.7E-03
S15-03	28-Jun-17	0.20	2.6E-03	0.032	3.5E-04	0.14	1.3E-03	0.13	1.2E-03
S15-03	30-Oct-17	0.82	1.0E-02	0.015	1.6E-04	6.9E-03	6.5E-05	0.14	1.3E-03

Table A.2. Continued

Well ID	Sample Date	Benzene		Toluene		Ethylbenzene		Xylenes, Total	
		(mg/L)	(mM)	(mg/L)	(mM)	(mg/L)	(mM)	(mg/L)	(mM)
S15-04	19-Oct-15	18	0.23	26	0.28	2.3	2.2E-02	15	0.14
S15-04	8-Jun-16	11	0.14	9.2	0.10	1.3	1.2E-02	8.2	7.7E-02
S15-04	16-Aug-16	14	0.18	7.6	8.2E-02	1.7	1.6E-02	8.9	8.4E-02
S15-04	25-Oct-16	7.8	0.10	4.0	4.3E-02	0.94	8.9E-03	5.9	5.6E-02
S15-04	27-Jun-17	12	0.15	0.80	8.7E-03	1.4	1.3E-02	3.3	3.1E-02
S15-04	1-Nov-17	8.1	0.10	1.70	1.8E-02	0.82	7.7E-03	3.3	3.1E-02
S15-05	6-Nov-15	11	0.14	17	0.18	2.0	1.9E-02	14	0.13
S15-05	8-Jun-16	10	0.13	2.7	2.9E-02	1.8	1.7E-02	6.8	6.4E-02
S15-05	16-Aug-16	6.0	7.7E-02	0.86	9.3E-03	1.2	1.1E-02	4.0	3.8E-02
S15-05	25-Oct-16	4.5	5.8E-02	0.39	4.2E-03	0.91	8.6E-03	2.2	2.1E-02
S15-05	27-Jun-17	5.6	7.2E-02	0.39	4.2E-03	1.0	9.4E-03	1.8	1.7E-02
S15-05	1-Nov-17	0.64	8.2E-03	0.028	3.0E-04	0.10	9.0E-04	0.26	2.4E-03
S15-06	19-Oct-15	<0.00040	<0.00040	0.0020	2.2E-05	0.0011	1.0E-05	0.014	1.3E-04
S15-06	10-Jun-16	0.0081	1.0E-04	<0.00040	<0.00040	0.0009	8.6E-06	0.0019	1.8E-05
S15-06	16-Aug-16	0.0420	5.4E-04	0.0410	4.4E-04	0.0030	2.8E-05	0.0180	1.7E-04
S15-06	1-Nov-16	0.0025	3.2E-05	0.0023	2.5E-05	<0.00040	<0.00040	0.0016	1.5E-05
S15-06	27-Jun-17	0.0099	1.3E-04	<0.00040	<0.00040	1.4	1.3E-02	0.0015	1.4E-05
S15-06	30-Oct-17	<0.00040	<0.00040	<0.00040	<0.00040	<0.00040	<0.00040	<0.00080	<0.00080

Table A.3. Groundwater CCME PHC concentrations.

Well ID	Sample Date	CCME F1-BTEX (mg/L)	CCME F2 (mg/L)
11-03	20-Oct-15	<1.0	0.28
11-03	10-Jun-16	0.65	0.36
11-03	16-Aug-16	0.91	0.27
11-03	1-Nov-16	<0.50	0.14
11-03	27-Jun-17	0.83	0.20
11-03	30-Oct-17	0.77	0.26
S15-01	19-Oct-15	<0.10	<0.10
S15-01	8-Jun-16	<0.10	<0.10
S15-01	15-Aug-16	<0.10	<0.10
S15-01	25-Oct-16	<0.10	<0.10
S15-01	28-Jun-17	<0.10	<0.10
S15-01	1-Nov-17	<0.10	<0.10
S15-02	19-Oct-15	11	2
S15-02	8-Jun-16	<5	2.6
S15-02	16-Aug-16	<10	2.2
S15-02	27-Jun-17	11	1.6
S15-02	1-Nov-17	7.3	1.1
S15-03	6-Nov-15	<1	0.72
S15-03	8-Jun-16	0.66	0.39
S15-03	16-Aug-16	1.1	0.41
S15-03	25-Oct-16	0.27	0.16
S15-03	28-Jun-17	1.1	0.24
S15-03	30-Oct-17	0.36	<0.10
S15-04	19-Oct-15	12	2.8
S15-04	8-Jun-16	4.0	3.2
S15-04	16-Aug-16	<10	0.41
S15-04	25-Oct-16	2.6	2.7
S15-04	27-Jun-17	9.0	2.0
S15-04	1-Nov-17	2.8	1.6

Table A.3. Continued.

Well ID	Sample Date	CCME F1-BTEX (mg/L)	CCME F2 (mg/L)
S15-05	6-Nov-15	<2	4.7
S15-05	8-Jun-16	4.7	2.2
S15-05	16-Aug-16	5.8	1.3
S15-05	25-Oct-16	2.9	1.2
S15-05	27-Jun-17	5.8	1.1
S15-05	1-Nov-17	0.68	<0.10
S15-06	19-Oct-15	<0.10	<0.10
S15-06	10-Jun-16	<0.10	<0.10
S15-06	16-Aug-16	<0.10	<0.10
S15-06	1-Nov-16	<0.10	<0.10
S15-06	27-Jun-17	<0.10	<0.10
S15-06	30-Oct-17	<0.10	<0.10

Table A.4. Metabolite results. ND = not detected.

Well ID	Sample Date	Benzoate (nM)	Phenol (nM)	Cresol, Total (nM)	Toluate, Total (nM)	BzSucc (nM)	MeBzSucc (nM)
11-03	10-Jun-16	234	165	ND	45	ND	ND
11-03	16-Aug-16	ND	ND	ND	ND	ND	ND
11-03	27-Jun-17	106	55	20	ND	ND	ND
11-03	31-Oct-17	82	35	21	ND	ND	ND
S15-01	8-Jun-16	8	31	ND	ND	ND	ND
S15-01	15-Aug-16	20	20	ND	ND	ND	ND
S15-01	28-Jun-17	196	89	ND	ND	ND	ND
S15-01	1-Nov-17	322	29	ND	ND	ND	ND
S15-02	8-Jun-16	274	904	107	864	36	ND
S15-02	16-Aug-16	166	646	93	ND	20	ND
S15-02	27-Jun-17	207	634	157	318	272	559
S15-02	1-Nov-17	510	505	233	766	137	254
S15-03	8-Jun-16	69	537	38	61	ND	ND
S15-03	16-Aug-16	226	54	ND	ND	ND	ND
S15-03	28-Jun-17	133	126	61	ND	ND	ND
S15-03	31-Oct-17	85	39	61	ND	ND	ND
S15-04	8-Jun-16	ND	1800	786	2848	19	ND
S15-04	16-Aug-16	ND	1932	240	ND	3	ND
S15-04	27-Jun-17	489	2702	1192	1364	ND	188
S15-04	1-Nov-17	189	505	271	423	ND	79
S15-05	8-Jun-16	ND	1412	183	462	1	ND
S15-05	16-Aug-16	113	531	236	209	1	ND
S15-05	27-Jun-17	269	561	460	464	39	95
S15-05	1-Nov-17	113	58	105	92	18	24
S15-06	10-Jun-16	33	31	ND	ND	ND	ND
S15-06	16-Aug-16	3	13	97	ND	ND	ND
S15-06	27-Jun-17	46	22	29	ND	ND	ND
S15-06	31-Oct-17	253	26	19	ND	ND	ND

Table A.5. Groundwater field chemistry.

Well ID	Sample Date	Temp	pH	Alk - $CaCO_3$		DO	ORP	pe	EC	
		(°C)	-	(mg/L)	(mM)	(mg/L)	(mV)	-	(µS/cm)	(mS/cm)
11-03	20-Oct-15	8.8	6.8	790	7.9	8.6	125	2.2	3183	3.2
11-03	10-Jun-16	8.8	7.1	750	7.5	1.5	-60	-1.1	2552	2.6
11-03	16-Aug-16	10	6.5	800	8.0	1.4	-57	-1.0	2524	2.5
11-03	1-Nov-16	7.7	6.6	740	7.4	3.1	-114	-2.0	3211	3.2
11-03	27-Jun-17	7.9	6.5	710	7.1	3.9	-91	-1.6	3229	3.2
11-03	30-Oct-17	7.9	6.6	780	7.8	3.2	-90	-1.6	3072	3.1
S15-01	19-Oct-15	7.1	6.8	530	5.3	7.2	244	4.4	1467	1.5
S15-01	8-Jun-16	7.8	7.0	540	5.4	0.85	150	2.7	1504	1.5
S15-01	15-Aug-16	9.6	6.7	560	5.6	1.0	65	1.2	1615	1.6
S15-01	25-Oct-16	7.2	6.7	470	4.7	1.4	94	1.7	1521	1.5
S15-01	28-Jun-17	6.4	6.6	520	5.2	2.4	35	0.63	1607	1.6
S15-01	1-Nov-17	5.1	6.9	540	5.4	2.6	-39	-0.71	1522	1.5
S15-02	19-Oct-15	8.5	6.5	830	8.3	3.3	216	3.9	1733	1.7
S15-02	8-Jun-16	9.7	6.8	820	8.2	1.3	-98	-1.7	1851	1.9
S15-02	16-Aug-16	9.9	6.4	840	8.4	2.0	-133	-2.4	2028	2.0
S15-02	27-Jun-17	9.5	6.3	890	8.9	2.0	-158	-2.8	1991	2.0
S15-02	1-Nov-17	6.7	6.7	750	7.5	2.6	-172	-3.1	2763	2.8
S15-03	6-Nov-15	8.0	6.4	240	2.4	0.85	136	2.4	1867	1.9
S15-03	8-Jun-16	10	6.6	340	3.4	1.1	-54	-1.0	2583	2.6
S15-03	16-Aug-16	13	6.7	460	4.6	0.91	-78	-1.4	3465	3.5
S15-03	25-Oct-16	9.0	7.1	380	3.8	1.6	17	0.31	4760	4.8
S15-03	28-Jun-17	7.1	6.5	480	4.8	1.8	-65	-1.2	2581	2.6
S15-03	30-Oct-17	7.4	6.9	380	3.8	2.5	17	0.30	3872	3.9

Table A.5. Continued.

Well ID	Sample Date	Temp	pH	Alk - $CaCO_3$		DO	ORP	pe	EC	
		(°C)	-	(mg/L)	(mM)	(mg/L)	(mV)	-	(µS/cm)	(mS/cm)
S15-04	19-Oct-15	11	6.5	780	7.8	1.2	205	3.6	1898	1.9
S15-04	8-Jun-16	11	6.8	960	9.6	0.93	-128	-2.3	2165	2.2
S15-04	16-Aug-16	13	6.5	930	9.3	1.6	-161	-2.8	2366	2.4
S15-04	25-Oct-16	12	6.7	850	8.5	2.0	-119	-2.1	2294	2.3
S15-04	27-Jun-17	10	6.2	1300	13	2.3	-170	-3.0	2474	2.5
S15-04	1-Nov-17	8.0	6.7	790	7.9	2.8	-167	-3.0	3648	3.6
S15-05	6-Nov-15	10	6.5	570	5.7	0.59	68	1.2	1509	1.5
S15-05	8-Jun-16	11	6.8	970	9.7	0.67	-150	-2.7	1660	1.7
S15-05	16-Aug-16	13	6.8	660	6.6	1.2	-128	-2.2	2509	2.5
S15-05	25-Oct-16	11	6.7	620	6.2	1.9	-112	-2.0	2909	2.9
S15-05	27-Jun-17	10	6.2	850	8.5	1.3	-140	-2.5	2732	2.7
S15-05	1-Nov-17	7.2	6.7	310	3.1	2.3	-77	-1.4	3093	3.1
S15-06	19-Oct-15	11	6.8	380	3.8	3.0	214	3.8	1085	1.1
S15-06	10-Jun-16	10	7.0	330	3.3	0.92	37	0.66	2598	2.6
S15-06	16-Aug-16	12	6.9	380	3.8	3.1	27	0.47	1666	1.7
S15-06	1-Nov-16	9.6	7.2	360	3.6	1.3	-23	-0.40	2224	2.2
S15-06	27-Jun-17	10	6.5	400	4.0	0.93	58	1.0	2881	2.9
S15-06	30-Oct-17	9.1	6.9	420	4.2	1.44	-2.6	-0.046	3141	3.1

Table A.6. Groundwater concentrations of major cations.

Well ID	Sample Date	Ca		Fe_T		Mg		Mn_T		K		Na	
		(mg/L)	(mM)	(mg/L)	(mM)	(mg/L)	(mM)	(mg/L)	(mM)	(mg/L)	(mM)	(mg/L)	(mM)
11-03	20-Oct-15	410	10	1.3	2.3E-02	230	9.5	6.6	0.12	9.0	0.23	160	7.0
11-03	10-Jun-16	390	9.7	0.50	9.0E-03	220	9.0	5.5	0.10	8.3	0.21	160	7.0
11-03	16-Aug-16	390	9.7	0.38	6.8E-03	200	8.2	6.1	0.11	8.1	0.21	140	6.1
11-03	1-Nov-16	410	10	0.43	7.7E-03	200	8.2	5.4	0.10	9.8	0.25	120	5.2
11-03	27-Jun-17	450	11	0.62	1.1E-02	310	13	5.2	9.5E-02	8.8	0.23	140	6.1
11-03	30-Oct-17	420	10	0.68	1.2E-02	270	11	5.4	9.8E-02	8.8	0.23	200	8.7
S15-01	19-Oct-15	330	8.2	0.16	2.9E-03	97	4.0	0.42	7.6E-03	9.7	0.25	15	0.65
S15-01	8-Jun-16	330	8.2	0.18	3.2E-03	100	4.1	0.25	4.6E-03	7.0	0.18	14	0.61
S15-01	15-Aug-16	370	9.2	0.19	3.4E-03	110	4.5	0.23	4.2E-03	7.7	0.20	18	0.78
S15-01	25-Oct-16	330	8.2	0.14	2.5E-03	110	4.5	0.21	3.8E-03	7.6	0.19	17	0.74
S15-01	28-Jun-17	330	8.2	0.13	2.3E-03	110	4.5	0.12	2.2E-03	6.9	0.18	16	0.70
S15-01	1-Nov-17	320	8.0	0.13	2.3E-03	100	4.1	0.12	2.2E-03	7.0	0.18	15	0.65
S15-02	19-Oct-15	320	8.0	0.41	7.3E-03	130	5.3	1.8	3.3E-02	12	0.31	67	2.9
S15-02	8-Jun-16	270	6.7	5.7	1.0E-01	160	6.6	5.5	0.10	6.9	0.18	78	3.4
S15-02	16-Aug-16	330	8.2	8.5	1.5E-01	180	7.4	5.4	0.10	8.0	0.20	92	4.0
S15-02	27-Jun-17	250	6.2	20	3.6E-01	140	5.8	5.0	9.1E-02	6.9	0.18	90	3.9
S15-02	1-Nov-17	330	8.2	13	2.3E-01	230	9.5	4.4	8.0E-02	9.4	0.24	150	6.5
S15-03	6-Nov-15	330	8.2	7.1E-02	1.3E-03	160	6.6	2.2	4.0E-02	10	0.26	110	4.8
S15-03	8-Jun-16	370	9.2	3.2	5.7E-02	190	7.8	3.8	6.9E-02	8.2	0.21	140	6.1
S15-03	16-Aug-16	610	15	3.4	6.1E-02	280	12	4.9	8.9E-02	11	0.28	180	7.8
S15-03	25-Oct-16	570	14	0.41	7.3E-03	320	13	4.2	7.6E-02	9.6	0.25	210	9.1
S15-03	28-Jun-17	460	11	2.4	4.3E-02	270	11	4.5	8.2E-02	7.9	0.20	150	6.5
S15-03	30-Oct-17	630	16	0.38	6.8E-03	380	16	2.1	3.8E-02	7.1	0.18	290	13

Table A.6. Continued.

Well ID	Sample Date	Ca		Fe_T		Mg		Mn_T		K		Na	
		(mg/L)	(mM)	(mg/L)	(mM)	(mg/L)	(mM)	(mg/L)	(mM)	(mg/L)	(mM)	(mg/L)	(mM)
S15-05	06-Nov-15	240	6.0	<0.060	<0.060	130	5.3	1.6	2.9E-02	8.5	0.22	140	6.1
S15-05	08-Jun-16	210	5.2	14	2.5E-01	94	3.9	3.1	5.6E-02	5.9	0.15	120	5.2
S15-05	16-Aug-16	360	9.0	12	2.1E-01	210	8.6	3.8	6.9E-02	6.5	0.17	160	7.0
S15-05	25-Oct-16	460	11	10	1.8E-01	280	12	4.4	8.0E-02	7.3	0.19	150	6.5
S15-05	27-Jun-17	370	9.2	15	2.7E-01	230	9.5	4.9	8.9E-02	5.7	0.15	150	6.5
S15-06	19-Oct-15	200	5.0	0.13	2.3E-03	61	2.5	0.70	1.3E-02	8.3	0.21	54	2.3
S15-06	10-Jun-16	520	13	<0.060	<0.060	210	8.6	0.46	8.4E-03	12	0.31	140	6.1
S15-06	16-Aug-16	300	7.5	0.16	2.9E-03	93	3.8	1.4	2.5E-02	8.7	0.22	75	3.3
S15-06	01-Nov-16	270	6.7	0.13	2.3E-03	110	4.5	1.3	2.4E-02	8.8	0.23	94	4.1
S15-06	27-Jun-17	480	12	0.28	5.0E-03	230	9.5	2.2	4.0E-02	11	0.28	170	7.4

Table A.7. Groundwater concentrations of major anions.

Well ID	Sample Date	Cl		ΣH_2S		SO_4	
		(mg/L)	(mM)	(mg/L)	(mM)	(mg/L)	(mM)
11-03	20-Oct-15	140	3.9	0.12	3.7E-03	1300	14
11-03	10-Jun-16	140	3.9	4.5E-02	1.4E-03	1400	15
11-03	16-Aug-16	130	3.7	8.4E-03	2.6E-04	1200	12
11-03	1-Nov-16	130	3.7	8.5E-02	2.7E-03	1100	11
11-03	27-Jun-17	180	5.1	1.9E-02	5.9E-04	2100	22
11-03	30-Oct-17	140	3.9	<0.0019	<0.0019	1800	19
S15-01	19-Oct-15	190	5.4	<0.0019	<0.0019	470	4.9
S15-01	8-Jun-16	190	5.4	<0.0019	<0.0019	440	4.6
S15-01	15-Aug-16	150	4.2	<0.0019	<0.0019	410	4.3
S15-01	25-Oct-16	210	5.9	<0.0019	<0.0019	460	4.8
S15-01	28-Jun-17	230	6.5	<0.0019	<0.0019	410	4.3
S15-01	1-Nov-17	220	6.2	0.0067	2.1E-04	470	4.9
S15-02	19-Oct-15	170	4.8	<0.0019	<0.0019	390	4.1
S15-02	8-Jun-16	210	5.9	0.33	1.0E-02	360	3.7
S15-02	16-Aug-16	240	6.8	0.85	2.7E-02	460	4.8
S15-02	27-Jun-17	210	5.9	2.9	9.0E-02	240	2.5
S15-02	1-Nov-17	440	12	0.44	1.4E-02	1000	10
S15-03	6-Nov-15	200	5.6	1.1E-02	3.4E-04	1100	11
S15-03	8-Jun-16	310	8.7	<0.0019	<0.0019	1300	14
S15-03	16-Aug-16	340	9.6	5.6E-03	1.7E-04	1900	20
S15-03	25-Oct-16	350	9.9	<0.0038	<0.0038	2100	22
S15-03	28-Jun-17	230	6.5	<0.0019	<0.0019	1800	19
S15-03	30-Oct-17	430	12	<0.0019	<0.0019	2800	29
S15-04	19-Oct-15	91	2.6	3.5E-02	1.1E-03	400	4.2
S15-04	8-Jun-16	62	1.7	0.50	1.6E-02	770	8.0
S15-04	16-Aug-16	61	1.7	1.7	5.3E-02	850	8.8
S15-04	25-Oct-16	110	3.1	1.1	3.4E-02	1000	10
S15-04	27-Jun-17	180	5.1	0.68	2.1E-02	410	4.3
S15-04	1-Nov-17	130	3.7	0.35	1.1E-02	2700	28

Table A.7. Continued.

Well ID	Sample Date	Cl		ΣH_2S		SO_4	
		(mg/L)	(mM)	(mg/L)	(mM)	(mg/L)	(mM)
S15-05	6-Nov-15	170	4.8	4.2E-02	1.3E-03	560	5.8
S15-05	8-Jun-16	120	3.4	0.52	1.6E-02	99	1.0
S15-05	16-Aug-16	120	3.4	0.26	8.1E-03	1100	11
S15-05	25-Oct-16	160	4.5	0.24	7.5E-03	1900	20
S15-05	27-Jun-17	200	5.6	7.4E-02	2.3E-03	1000	10
S15-05	1-Nov-17	89	2.5	1.6E-02	5.0E-04	2800	29
S15-06	19-Oct-15	35	1.0	<0.0019	<0.0019	1000	10
S15-06	10-Jun-16	120	3.4	<0.0019	<0.0019	1800	19
S15-06	16-Aug-16	55	1.6	<0.0019	<0.0019	780	8.1
S15-06	1-Nov-16	51	1.4	<0.0019	<0.0019	780	8.1
S15-06	27-Jun-17	120	3.4	<0.0019	<0.0019	1800	19
S15-06	30-Oct-17	170	4.8	<0.0019	<0.0019	2100	22

Table A.8. Groundwater nutrient concentrations.

Well ID	Sample Date	NH_3 - N		NO_2 - N		NO_3 - N		P_T	
		(mg/L)	(mM)	(mg/L)	(mM)	(mg/L)	(mM)	(mg/L)	(mM)
11-03	20-Oct-15	0.310	2.2E-02	<0.010	<0.010	<0.020	<0.020	0.0240	7.7E-04
11-03	10-Jun-16	0.081	5.8E-03	<0.010	<0.010	<0.020	<0.020	0.0160	5.2E-04
11-03	16-Aug-16	0.072	5.1E-03	<0.010	<0.010	0.130	9.3E-03	0.0190	6.1E-04
11-03	1-Nov-16	0.150	1.1E-02	<0.010	<0.010	<0.020	<0.020	0.0150	4.8E-04
11-03	27-Jun-17	0.320	2.3E-02	<0.050	<0.050	<0.050	<0.050	<0.0030	<0.0030
11-03	30-Oct-17	0.160	1.1E-02	<0.010	<0.010	<0.010	<0.010	0.010	3.2E-04
S15-01	19-Oct-15	0.380	2.7E-02	0.053	3.8E-03	2.3	0.16	0.0420	1.4E-03
S15-01	8-Jun-16	0.081	5.8E-03	<0.010	<0.010	0.65	4.6E-02	0.0100	3.2E-04
S15-01	15-Aug-16	0.480	3.4E-02	0.030	2.1E-03	0.64	4.6E-02	0.0140	4.5E-04
S15-01	25-Oct-16	0.120	8.6E-03	0.021	1.5E-03	0.71	5.1E-02	0.0062	2.0E-04
S15-01	28-Jun-17	0.070	5.0E-03	<0.010	<0.010	0.70	5.0E-02	0.0081	2.6E-04
S15-01	1-Nov-17	<0.015	<0.015	<0.010	<0.010	1.10	7.9E-02	0.0085	2.7E-04
S15-02	19-Oct-15	0.200	1.4E-02	0.019	1.4E-03	0.120	8.6E-03	0.020	6.5E-04
S15-02	8-Jun-16	<0.050	<0.050	<0.010	<0.010	<0.010	<0.010	0.041	1.3E-03
S15-02	16-Aug-16	0.130	9.3E-03	<0.010	<0.010	<0.010	<0.010	0.070	2.3E-03
S15-02	27-Jun-17	0.150	1.1E-02	<0.010	<0.010	0.015	1.1E-03	0.120	3.9E-03
S15-02	1-Nov-17	0.180	1.3E-02	<0.010	<0.010	0.031	2.2E-03	0.046	1.5E-03
S15-03	6-Nov-15	0.086	6.1E-03	<0.010	<0.010	0.011	7.9E-04	0.007	2.4E-04
S15-03	8-Jun-16	0.100	7.1E-03	<0.010	<0.010	<0.010	<0.010	0.027	8.7E-04
S15-03	16-Aug-16	0.380	2.7E-02	<0.010	<0.010	<0.010	<0.010	0.030	9.7E-04
S15-03	25-Oct-16	0.310	2.2E-02	0.007	4.9E-04	0.900	6.4E-02	0.017	5.5E-04
S15-03	28-Jun-17	0.440	3.1E-02	0.039	2.8E-03	<0.010	<0.010	0.055	1.8E-03
S15-03	30-Oct-17	0.310	2.2E-02	0.054	3.9E-03	3.5	2.5E-01	<0.0030	<0.0030

Table A.8. Continued.

Well ID	Sample Date	NH_3 - N		NO_2 - N		NO_3 - N		P_T	
		(mg/L)	(mM)	(mg/L)	(mM)	(mg/L)	(mM)	(mg/L)	(mM)
S15-04	19-Oct-15	0.660	4.7E-02	0.15	1.1E-02	0.086	6.1E-03	0.038	1.2E-03
S15-04	8-Jun-16	0.074	5.3E-03	<0.010	<0.010	<0.010	<0.010	0.026	8.4E-04
S15-04	16-Aug-16	0.130	9.3E-03	<0.010	<0.010	<0.010	<0.010	0.028	9.0E-04
S15-04	25-Oct-16	0.054	3.9E-03	0.011	7.9E-04	0.014	1.0E-03	0.013	4.2E-04
S15-04	27-Jun-17	0.160	1.1E-02	<0.010	<0.010	0.024	1.7E-03	<0.030	<0.030
S15-04	1-Nov-17	0.340	2.4E-02	<0.010	<0.010	0.025	1.8E-03	0.077	2.5E-03
S15-05	6-Nov-15	0.110	7.9E-03	<0.010	<0.010	<0.010	<0.010	0.014	4.5E-04
S15-05	8-Jun-16	0.190	1.4E-02	0.018	1.3E-03	0.051	3.6E-03	0.031	1.0E-03
S15-05	16-Aug-16	0.270	1.9E-02	0.025	1.8E-03	0.029	2.1E-03	0.013	4.2E-04
S15-05	25-Oct-16	0.180	1.3E-02	<0.010	<0.010	0.012	8.6E-04	<0.0030	<0.0030
S15-05	27-Jun-17	0.310	2.2E-02	<0.010	<0.010	<0.010	<0.010	0.150	4.8E-03
S15-05	1-Nov-17	0.220	1.6E-02	0.038	2.7E-03	0.50	3.6E-02	8.8E-03	2.8E-04
S15-06	19-Oct-15	0.190	1.4E-02	<0.010	<0.010	0.063	4.5E-03	0.0044	1.4E-04
S15-06	10-Jun-16	0.100	7.1E-03	0.021	1.5E-03	0.049	3.5E-03	0.0055	1.8E-04
S15-06	16-Aug-16	0.360	2.6E-02	<0.010	<0.010	0.040	2.9E-03	0.0130	4.2E-04
S15-06	1-Nov-16	0.180	1.3E-02	0.017	1.2E-03	2.00	1.4E-01	0.0049	1.6E-04
S15-06	27-Jun-17	0.200	1.4E-02	<0.010	<0.010	0.62	4.4E-02	0.0760	2.5E-03
S15-06	30-Oct-17	0.110	7.9E-03	<0.010	<0.010	0.25	1.8E-02	<0.0030	<0.0030

Table A.9. Saturation Indices (calcite, dolomite, gypsum, FeS, mackinawite, and pyrite) and charge balance error calculated in PHREEQC. n.d = no data.

Well ID	Sample Date	Charge Balance (% error)	Calcite $CaCO_3$	Dolomite $CaMg(CO_3)_2$	Gypsum $CaSO_4{:}2H_2O$	Amorphous FeS	Mackinawite FeS	Pyrite FeS_2
11-03	20-Oct-15	-2.7	0.31	0.48	-0.24	-0.54	0.20	20
11-03	10-Jun-16	-4.3	0.57	1.0	-0.25	-0.91	-0.17	13
11-03	16-Aug-16	-3.2	0.06	-0.04	-0.30	-2.7	-2.0	9.5
11-03	1-Nov-16	1.9	0.12	0.02	-0.30	-1.5	-0.72	9.9
11-03	27-Jun-17	-11	-0.08	-0.22	-0.10	-2.3	-1.5	9.0
11-03	30-Oct-17	-5.6	0.06	0.04	-0.16	n.d	n.d	n.d
S15-01	19-Oct-15	12	0.15	-0.15	-0.62	n.d	n.d	n.d
S15-01	8-Jun-16	0.33	0.35	0.26	-0.63	n.d	n.d	n.d
S15-01	15-Aug-16	10	0.21	0.01	-0.64	n.d	n.d	n.d
S15-01	25-Oct-16	3.4	0.05	-0.29	-0.62	n.d	n.d	n.d
S15-01	28-Jun-17	2.1	-0.02	-0.46	-0.66	n.d	n.d	n.d
S15-01	1-Nov-17	-3.9	0.23	-0.02	-0.61	n.d	n.d	n.d
S15-02	19-Oct-15	0.89	0.05	-0.19	-0.73	n.d	n.d	n.d
S15-02	8-Jun-16	1.5	0.31	0.52	-0.85	0.63	1.4	13
S15-02	16-Aug-16	4.8	0.00	-0.15	-0.70	0.57	1.3	12
S15-02	27-Jun-17	0.54	-0.23	-0.61	-1.0	1.1	1.8	12
S15-02	1-Nov-17	-7.1	0.10	0.11	-0.43	0.84	1.6	11
S15-03	6-Nov-15	2.6	-0.45	-1.1	-0.34	-3.0	-2.3	16
S15-03	8-Jun-16	-3.0	-0.29	-0.73	-0.28	n.d	n.d	n.d
S15-03	16-Aug-16	4.0	0.20	0.25	-0.04	-1.5	-0.73	10
S15-03	25-Oct-16	3.3	0.41	0.69	-0.02	n.d	n.d	n.d
S15-03	28-Jun-17	-1.7	-0.24	-0.63	-0.12	n.d	n.d	n.d
S15-03	30-Oct-17	-2.4	0.15	0.17	0.09	n.d	n.d	n.d

Table A.9. Continued.

Well ID	Sample Date	Charge Balance (% error)	Calcite $CaCO_3$	Dolomite $CaMg(CO_3)_2$	Gypsum $CaSO_4{:}2H_2O$	Amorphous FeS	Mackinawite FeS	Pyrite FeS_2
S15-04	19-Oct-15	1.9	0.02	-0.27	-0.76	-2.4	-1.6	20
S15-04	8-Jun-16	0.44	0.37	0.68	-0.55	1.2	1.9	13
S15-04	16-Aug-16	6.0	0.15	0.22	-0.46	1.1	1.8	12
S15-04	25-Oct-16	5.4	0.28	0.50	-0.40	1.4	2.1	1.0
S15-04	27-Jun-17	1.8	-0.09	-0.23	-0.81	0.32	1.1	9.8
S15-04	1-Nov-17	-8.5	0.10	0.31	-0.09	0.50	1.2	11
S15-05	6-Nov-15	2.4	-0.22	-0.57	-0.69	n.d	n.d	n.d
S15-05	8-Jun-16	-1.4	0.31	0.42	-1.4	1.1	1.9	12
S15-05	16-Aug-16	5.3	0.28	0.50	-0.37	0.82	1.6	12
S15-05	25-Oct-16	-4.0	0.15	0.25	-0.13	0.50	1.2	12
S15-05	27-Jun-17	1.9	-0.28	-0.63	-0.40	-0.78	-0.04	8.7
S15-05	1-Nov-17	-9.5	-0.29	-0.55	-0.02	-2.9	-2.1	8.2
S15-06	19-Oct-15	-31	-0.19	-0.75	-0.50	n.d	n.d	n.d
S15-06	10-Jun-16	3.1	0.26	0.26	-0.06	n.d	n.d	n.d
S15-06	16-Aug-16	1.9	0.15	-0.06	-0.46	n.d	n.d	n.d
S15-06	1-Nov-16	4.5	0.31	0.36	-0.50	n.d	n.d	n.d
S15-06	27-Jun-17	2.4	-0.25	-0.68	-0.10	n.d	n.d	n.d
S15-06	30-Oct-17	-0.55	0.17	0.23	-0.06	n.d	n.d	n.d

Table A.10. Saturation Indices (magnetite, siderite, and vivianite) calculated in PHREEQC. n.d = no data.

Well ID	Sample Date	Magnetite Fe_3O_4	Siderite $FeCO_3$	Vivianite $Fe_3(PO_4)_2{:}8H_2O$
11-03	20-Oct-15	10	-0.10	-5.3
11-03	10-Jun-16	4.9	-0.23	-6.1
11-03	16-Aug-16	0.31	-0.87	-7.9
11-03	1-Nov-16	-1.2	-0.77	-7.6
11-03	27-Jun-17	-1.2	-0.82	n.d
11-03	30-Oct-17	0.0	-0.62	-7.6
S15-01	19-Oct-15	12	-1.1	-7.1
S15-01	8-Jun-16	10	-0.83	-7.7
S15-01	15-Aug-16	5.7	-0.99	-8.0
S15-01	25-Oct-16	6.0	-1.2	-7.1
S15-01	28-Jun-17	2.7	-1.3	-9.3
S15-01	1-Nov-17	1.9	-1.1	-8.5
S15-02	19-Oct-15	9.9	-0.81	-7.7
S15-02	8-Jun-16	4.9	0.67	-2.6
S15-02	16-Aug-16	1.1	0.49	-2.8
S15-02	27-Jun-17	-0.23	0.68	-1.9
S15-02	1-Nov-17	1.6	0.77	-2.0
S15-03	6-Nov-15	5.6	-1.9	-10
S15-03	8-Jun-16	3.8	-0.17	-4.4
S15-03	16-Aug-16	4.8	0.13	-4.0
S15-03	25-Oct-16	7.8	-0.55	-6.2
S15-03	28-Jun-17	1.5	-0.37	-4.7
S15-03	30-Oct-17	5.5	-0.88	n.d
S15-04	19-Oct-15	8.8	-1.1	-8.0
S15-04	8-Jun-16	5.1	1.1	-1.9
S15-04	16-Aug-16	1.6	0.75	-3.0
S15-04	25-Oct-16	14	-2.7	n.d
S15-04	27-Jun-17	-1.3	0.71	n.d
S15-04	1-Nov-17	1.2	0.53	-2.4

Table A.10. Continued.

Well ID	Sample Date	Magnetite Fe_3O_4	Siderite $FeCO_3$	Vivianite $Fe_3(PO_4)_2{:}8H_2O$
S15-05	6-Nov-15	n.d	n.d	n.d
S15-05	8-Jun-16	4.1	1.1	-1.8
S15-05	16-Aug-16	5.2	0.92	-2.8
S15-05	25-Oct-16	4.3	0.62	n.d
S15-05	27-Jun-17	-0.63	0.41	-2.5
S15-05	1-Nov-17	1.2	-0.92	-7.4
S15-06	19-Oct-15	11	-1.2	-7.1
S15-06	10-Jun-16	n.d	n.d	n.d
S15-06	16-Aug-16	6.1	-0.97	-7.6
S15-06	1-Nov-16	5.9	-0.85	-8.0
S15-06	27-Jun-17	3.7	-1.3	-7.1
S15-06	30-Oct-17	4.8	-0.90	n.d

Table A.11. PHREEQC sensitivity analysis.

Well ID	Sample Date	Measured pe -	Calculated pe -	Redox Couple	Calcite		Dolomite	
					Measured pe	Calculated pe	Measured pe	Calculated pe
S15-01	19-Oct-15	4.4	6.9957	N(-3)/N(3)	0.15	0.15	-0.15	-0.15
S15-01	8-Jun-16	2.7	7.3499	N(-3)/N(5)	0.35	0.35	0.26	0.26
S15-01	15-Aug-16	1.2	6.8639	N(-3)/N(3)	0.21	0.21	0.01	0.21
S15-01	25-Oct-16	1.7	7.0852	N(-3)/N(3)	0.05	0.05	-0.29	-0.29
S15-01	28-Jun-17	0.63	7.8649	N(-3)/N(5)	-0.02	-0.02	-0.46	-0.46
S15-01	1-Nov-17	-0.71	-2.6015	S(-2)/S(6)	0.23	0.23	-0.02	-0.02
S15-04	19-Oct-15	3.6	7.1767	N(-3)/N(3)	0.02	0.02	-0.27	-0.27
S15-04	8-Jun-16	-2.3	-2.8267	S(-2)/S(6)	0.37	0.37	0.68	0.68
S15-04	16-Aug-16	-2.8	-2.5578	S(-2)/S(6)	0.15	0.15	0.22	0.22
S15-04	25-Oct-16	-2.1	-2.7451	S(-2)/S(6)	0.28	0.28	0.50	0.50
S15-04	27-Jun-17	-3.0	-2.1189	S(-2)/S(6)	-0.09	-0.09	-0.23	-0.23
S15-04	1-Nov-17	-3.0	-2.5576	S(-2)/S(6)	0.10	0.10	0.31	0.31
S15-05	6-Nov-15	1.2	15.1462	O(-2)/O(0)	-0.22	-0.22	-0.57	-0.57
S15-05	8-Jun-16	-2.7	-2.9017	S(-2)/S(6)	0.31	0.31	0.42	0.42
S15-05	16-Aug-16	-2.2	-2.8125	S(-2)/S(6)	0.28	0.28	0.50	0.50
S15-05	25-Oct-16	-2.0	-2.6302	S(-2)/S(6)	0.15	0.15	0.25	0.25
S15-05	27-Jun-17	-2.5	-1.9213	S(-2)/S(6)	-0.28	-0.28	-0.63	-0.63
S15-05	1-Nov-17	-1.4	-2.2449	S(-2)/S(6)	-0.29	-0.29	-0.55	-0.55

Table A.11. Continued.

Well ID	Sample Date	Measured pe -	Calculated pe -	Redox Couple	Gypsum	
					Measured pe	Calculated pe
S15-01	19-Oct-15	4.4	6.9957	N(-3)/N(3)	-0.62	-0.62
S15-01	8-Jun-16	2.7	7.3499	N(-3)/N(5)	-0.63	-0.63
S15-01	15-Aug-16	1.2	6.8639	N(-3)/N(3)	-0.64	-0.64
S15-01	25-Oct-16	1.7	7.0852	N(-3)/N(3)	-0.62	-0.62
S15-01	28-Jun-17	0.63	7.8649	N(-3)/N(5)	-0.66	-0.66
S15-01	1-Nov-17	-0.71	-2.6015	S(-2)/S(6)	-0.61	-0.61
S15-04	19-Oct-15	3.6	7.1767	N(-3)/N(3)	-0.76	-0.76
S15-04	8-Jun-16	-2.3	-2.8267	S(-2)/S(6)	-0.55	-0.55
S15-04	16-Aug-16	-2.8	-2.5578	S(-2)/S(6)	-0.46	-0.46
S15-04	25-Oct-16	-2.1	-2.7451	S(-2)/S(6)	-0.40	-0.40
S15-04	27-Jun-17	-3.0	-2.1189	S(-2)/S(6)	-0.81	-0.81
S15-04	1-Nov-17	-3.0	-2.5576	S(-2)/S(6)	-0.09	-0.09
S15-05	6-Nov-15	1.2	15.1462	O(-2)/O(0)	-0.69	-0.69
S15-05	8-Jun-16	-2.7	-2.9017	S(-2)/S(6)	-1.4	-1.4
S15-05	16-Aug-16	-2.2	-2.8125	S(-2)/S(6)	-0.37	-0.37
S15-05	25-Oct-16	-2.0	-2.6302	S(-2)/S(6)	-0.13	-0.13
S15-05	27-Jun-17	-2.5	-1.9213	S(-2)/S(6)	-0.40	-0.40
S15-05	1-Nov-17	-1.4	-2.2449	S(-2)/S(6)	-0.02	-0.02

Table A.12. Pearson's r correlation values for select geochemical parameters. Positive correlations are marked in green and negative correlations are marked in red.

Well ID	n	Alk Ca	Alk Mg+Ca	Mg Ca	SO_4 Ca
11-03	4	-0.818	-0.779	0.898	0.836
S15-01	4	0.648	0.435	0.333	-0.544
S15-02	3	-0.467	-0.573	0.961	0.945
S15-03	4	0.448	0.460	0.847	0.876
S15-04	4	-0.617	-0.438	0.513	0.704
S15-05	4	-0.862	-0.842	0.995	0.987
S15-05	4	-0.194	-0.108	0.950	0.987

Table A.12. Continued.

Well ID	n	Na Ca	Na Mg	Fe_T NH_3-N	SO_4 Fe_T
11-03	4	-0.289	0.155	0.841	0.941
S15-01	4	0.683	0.878	0.665	-0.185
S15-02	3	0.402	0.132	0.740	-0.792
S15-03	4	0.834	0.871	-0.162	-0.647
S15-04	4	0.280	0.947	0.202	-0.605
S15-05	4	0.799	0.819	0.567	-0.750
S15-05	4	0.875	0.982	0.460	-0.025

APPENDIX B: Mineralogy Results

Table B.1. PXRD results. ND = not detected.

Borehole ID	Sample Date	Core Interval	Depth (mBGL)	Quartz	Albite	Illite	Kaolinite	Dolomite	Calcite	Gypsum
S15-01	15-Oct-15	3.75 - 4 m	3.9	25%	10%	58%	ND	4%	2%	ND
S15-01	15-Oct-15	4.5 - 5 m	4.8	29%	12%	53%	ND	4%	1%	ND
S15-01	15-Oct-15	5.5 - 6 m	5.8	30%	8%	50%	5%	5%	2%	ND
S17-01	10-Jul-17	3 - 4.5 m	4.2	24%	11%	52%	6%	5%	1%	ND
S17-01	10-Jul-17	4.5 - 6 m	5.3	23%	11%	54%	6%	5%	1%	ND
S17-01	10-Jul-17	6 - 6.75 m	6.4	20%	10%	53%	9%	5%	2%	ND
S15-02	15-Oct-15	3.5 - 4 m	3.8	32%	10%	53%	ND	4%	1%	ND
S15-02	15-Oct-15	4.5 - 5 m	4.8	24%	8%	55%	7%	5%	1%	ND
S15-02	15-Oct-15	5.5 - 6 m	5.8	30%	11%	54%	ND	3%	2%	ND
S15-02	15-Oct-15	6.5 - 7 m	6.8	29%	11%	53%	ND	5%	2%	ND
S17-02	11-Jul-17	3 - 4.5 m	4.1	23%	13%	52%	ND	6%	1%	ND
S17-02	11-Jul-17	4.5 -5.25 m	4.9	26%	14%	53%	ND	1%	1%	ND
S17-02	11-Jul-17	5.25 - 6 m	5.6	23%	11%	53%	6%	5%	1%	ND
S17-02	11-Jul-17	6 -6.75 m	6.4	21%	11%	58%	7%	1%	2%	ND
S15-03	15-Oct-15	3.5 - 4 m	3.8	27%	13%	44%	ND	15%	1%	ND
S15-03	15-Oct-15	4.5 - 5 m	4.8	22%	10%	52%	9%	5%	2%	ND
S15-03	15-Oct-15	5.5 - 6 m	5.8	26%	11%	56%	ND	6%	1%	ND
S15-03	15-Oct-15	6.5 - 7 m	6.8	26%	11%	56%	ND	6%	1%	ND
S17-03	11-Jul-17	3 - 4.5 m	4.1	27%	12%	55%	5%	1%	1%	ND
S17-03	11-Jul-17	4.5 -5.25 m	4.8	21%	9%	55%	9%	5%	1%	ND
S17-03	11-Jul-17	4.5 -5.25 m	5.1	23%	10%	53%	7%	6%	2%	ND
S17-03	11-Jul-17	5.25 - 6 m	5.6	22%	10%	54%	8%	5%	1%	ND
S17-03	11-Jul-17	6 - 7.5 m	6.5	20%	10%	54%	9%	5%	1%	ND

Table B.1. Continued.

Borehole ID	Sample Date	Core Interval	Depth (mBGL)	Quartz	Albite	Illite	Kaolinite	Dolomite	Calcite	Gypsum
S15-04	15-Oct-15	3.5 - 4 m	3.8	33%	10%	53%	ND	3%	1%	ND
S15-04	15-Oct-15	4.5 - 5 m	4.8	63%	26%	0%	ND	9%	2%	ND
S15-04	15-Oct-15	5.2 - 5.8 m	5.5	22%	13%	58%	ND	5%	1%	ND
S15-04	15-Oct-15	6.5 - 7 m	6.8	28%	12%	54%	ND	6%	ND	ND
S17-04	11-Jul-17	3 - 4.5 m	3.6	25%	9%	55%	ND	1%	5%	6%
S17-04	11-Jul-17	3 - 4.5 m	4.2	28%	11%	58%	ND	1%	1%	ND
S17-04	11-Jul-17	4.5 - 6 m	5.3	21%	10%	54%	8%	5%	2%	ND
S17-04	11-Jul-17	6 -6.75 m	6.4	26%	12%	56%	ND	5%	1%	ND
S15-05	16-Oct-15	3.5 - 4 m	3.8	26%	9%	51%	13%	3%	1%	ND
S15-05	16-Oct-15	4.5 - 5 m	4.8	68%	21%	0%	ND	9%	2%	ND
S15-05	16-Oct-15	5.25 - 5.75 m	5.5	26%	10%	58%	ND	5%	1%	ND
S15-05	16-Oct-15	6.5 - 7 m	6.8	28%	10%	57%	ND	5%	1%	ND
S17-05	12-Jul-17	3 - 4.5 m	3.7	26%	12%	52%	4%	5%	1%	ND
S17-05	12-Jul-17	4.5 - 5.25 m	4.9	25%	11%	53%	6%	4%	1%	ND
S17-05	12-Jul-17	5.25 - 6 m	5.6	23%	10%	55%	6%	4%	1%	ND
S17-05	12-Jul-17	6 -7.5 m	6.4	20%	10%	55%	10%	4%	1%	ND
S15-06	16-Oct-15	3.5 - 4 m	3.8	24%	10%	61%	ND	3%	1%	ND
S15-06	16-Oct-15	4.5 - 5 m	4.8	61%	25%	0%	ND	10%	4%	ND
S15-06	16-Oct-15	5.5 - 6 m	5.8	52%	31%	0%	ND	13%	4%	ND
S15-06	16-Oct-15	6.5 - 7 m	6.8	22%	14%	58%	ND	5%	1%	ND
S17-06	12-Jul-17	3 - 4.5 m	3.8	28%	10%	56%	ND	5%	1%	ND
S17-06	12-Jul-17	4.5 - 6 m	5.1	24%	11%	53%	5%	6%	1%	ND
S17-06	12-Jul-17	4.5 - 6 m	5.6	23%	11%	54%	5%	6%	1%	ND
S17-06	12-Jul-17	6 - 7.5 m	6.8	21%	10%	55%	9%	3%	1%	ND

Table B.2. XRF Results for 2017 sediment samples. ND = not detected.

Borehole ID	Sample Date	Core Interval	Depth (mBGL)	Si	Al	Fe	Ca	Mg	K	Px	Sx	Mn
								(%-mass)				
S17-01	10-Jul-17	3 - 4.5 m	4.2	32.4	9.58	3.24	1.93	1.51	1.26	0.134	0.006	0.013
S17-01	10-Jul-17	4.5 - 6 m	5.3	31.4	8.85	3.52	2.05	1.32	1.40	0.116	ND	0.024
S17-01	10-Jul-17	6 - 6.75 m	6.4	31.2	10.7	4.47	1.77	1.57	1.32	0.118	0.004	0.023
S17-01	10-Jul-17	6.75 -7.5 m	7.1	33.0	8.59	3.54	1.73	1.24	1.30	0.119	0.009	0.017
S17-02	10-Jul-17	3 - 4.5 m	4.1	30.8	8.25	3.16	2.45	1.31	1.41	0.102	0.018	0.027
S17-02	10-Jul-17	4.5 -5.25 m	4.9	32.1	8.77	2.50	2.20	1.23	1.34	0.108	0.052	0.030
S17-02	10-Jul-17	5.25 - 6 m	5.6	32.3	9.87	2.78	1.74	1.46	1.28	0.085	0.013	0.029
S17-02	10-Jul-17	6 -6.75 m	6.4	32.1	11.1	4.04	1.54	1.61	1.33	0.094	0.007	0.025
S17-02	10-Jul-17	6.75 - 7.5 m	7.1	33.1	8.95	3.44	1.68	1.38	1.26	0.124	0.007	0.018
S17-03	11-Jul-17	3 - 4.5 m	4.1	31.4	8.44	2.97	2.23	1.24	1.39	0.094	0.036	0.034
S17-03	11-Jul-17	4.5 -5.25 m	4.8	31.7	11.0	4.22	1.48	1.69	1.32	0.098	0.017	0.029
S17-03	11-Jul-17	4.5 -5.25 m	5.1	31.9	9.64	3.47	2.18	1.56	1.27	0.090	0.017	0.030
S17-03	11-Jul-17	5.25 - 6 m	5.6	30.8	10.1	4.06	1.81	1.49	1.35	0.098	0.043	0.033
S17-03	11-Jul-17	6 - 7.5 m	6.5	31.4	10.7	4.36	1.58	1.59	1.34	0.097	0.017	0.031
S17-03	11-Jul-17	6 - 7.5 m	6.9	30.3	10.8	4.15	1.83	1.63	1.36	0.098	0.210	0.027
S17-04	11-Jul-17	3 - 4.5 m	3.6	27.6	7.07	3.54	2.36	1.12	1.33	0.115	0.121	0.039
S17-04	11-Jul-17	3 - 4.5 m	4.2	28.6	8.03	4.01	2.03	1.35	1.36	0.105	0.095	0.016
S17-04	11-Jul-17	4.5 - 6 m	5.3	31.5	10.6	4.10	1.66	1.61	1.32	0.101	0.013	0.027
S17-04	11-Jul-17	6 -6.75 m	6.4	31.8	8.79	2.72	2.28	1.38	1.29	0.128	0.007	0.056
S17-04	11-Jul-17	6.75 - 7.5 m	7.1	31.4	7.67	3.31	2.05	1.38	1.37	0.106	0.013	0.029
S17-05	12-Jul-17	3 - 4.5 m	3.7	29.4	7.68	3.55	2.69	1.21	1.32	0.084	0.019	0.025
S17-05	12-Jul-17	4.5 - 5.25 m	4.9	29.3	8.69	4.02	2.40	1.36	1.46	0.090	0.029	0.034
S17-05	12-Jul-17	5.25 - 6 m	5.6	29.8	8.20	3.84	2.27	1.23	1.39	0.118	0.083	0.024
S17-05	12-Jul-17	6 -7.5 m	6.4	30.7	10.9	4.20	1.52	1.54	1.38	0.130	0.004	0.030
S17-05	12-Jul-17	6 - 7.5 m	6.9	31.1	10.1	3.89	1.77	1.48	1.33	0.120	0.010	0.041
S17-06	12-Jul-17	3 - 4.5 m	3.8	30.6	8.09	3.37	2.38	1.35	1.37	0.107	0.026	0.041
S17-06	12-Jul-17	4.5 - 6 m	5.1	30.3	8.16	3.72	2.34	1.37	1.41	0.084	0.025	0.031
S17-06	12-Jul-17	4.5 - 6 m	5.6	32.1	9.22	3.06	1.95	1.40	1.29	0.094	0.013	0.028
S17-06	12-Jul-17	6 - 7.5 m	6.8	31.2	10.7	4.55	1.47	1.47	1.32	0.119	0.011	0.370

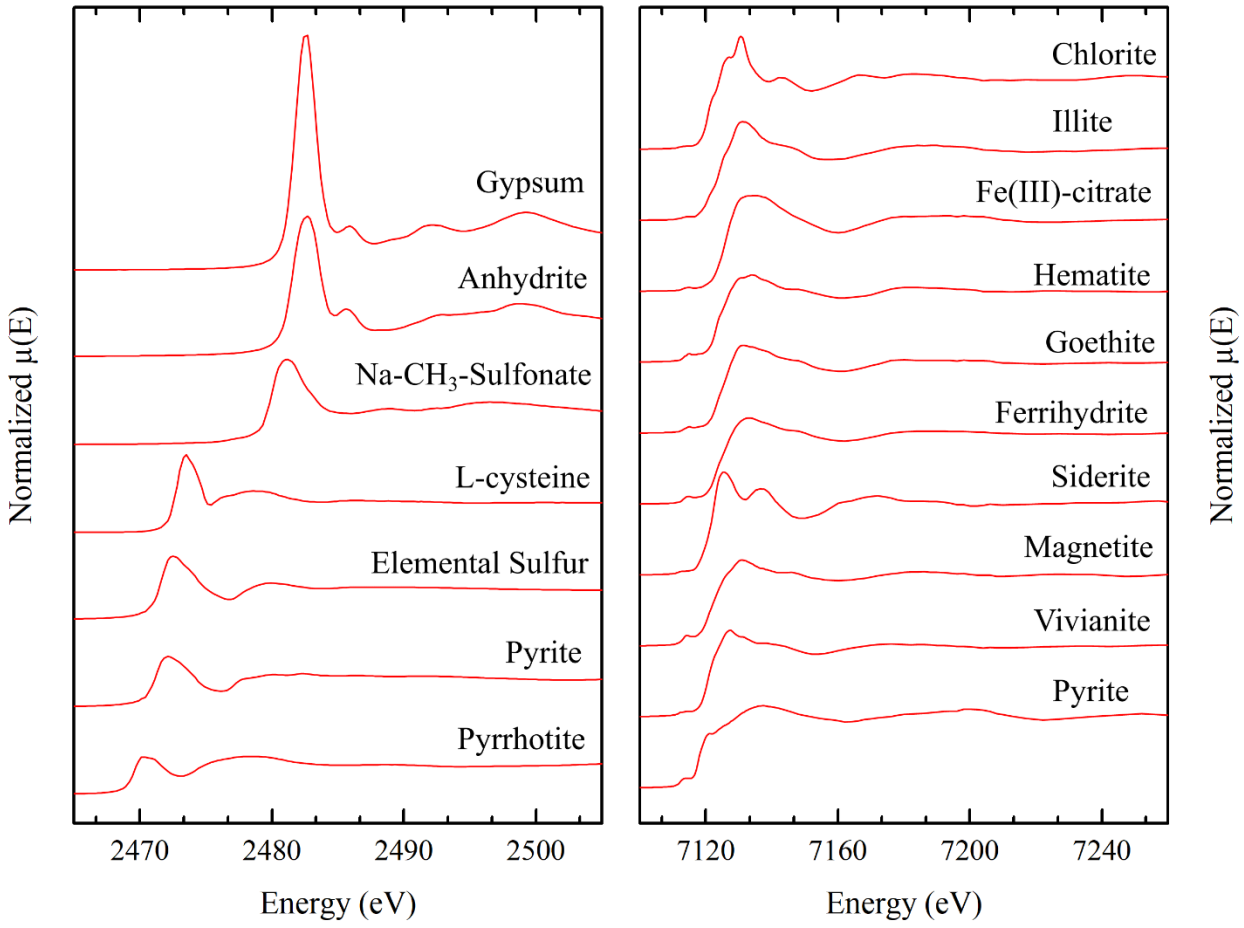

Figure B.1. Reference standards used in LCF combinatorics.

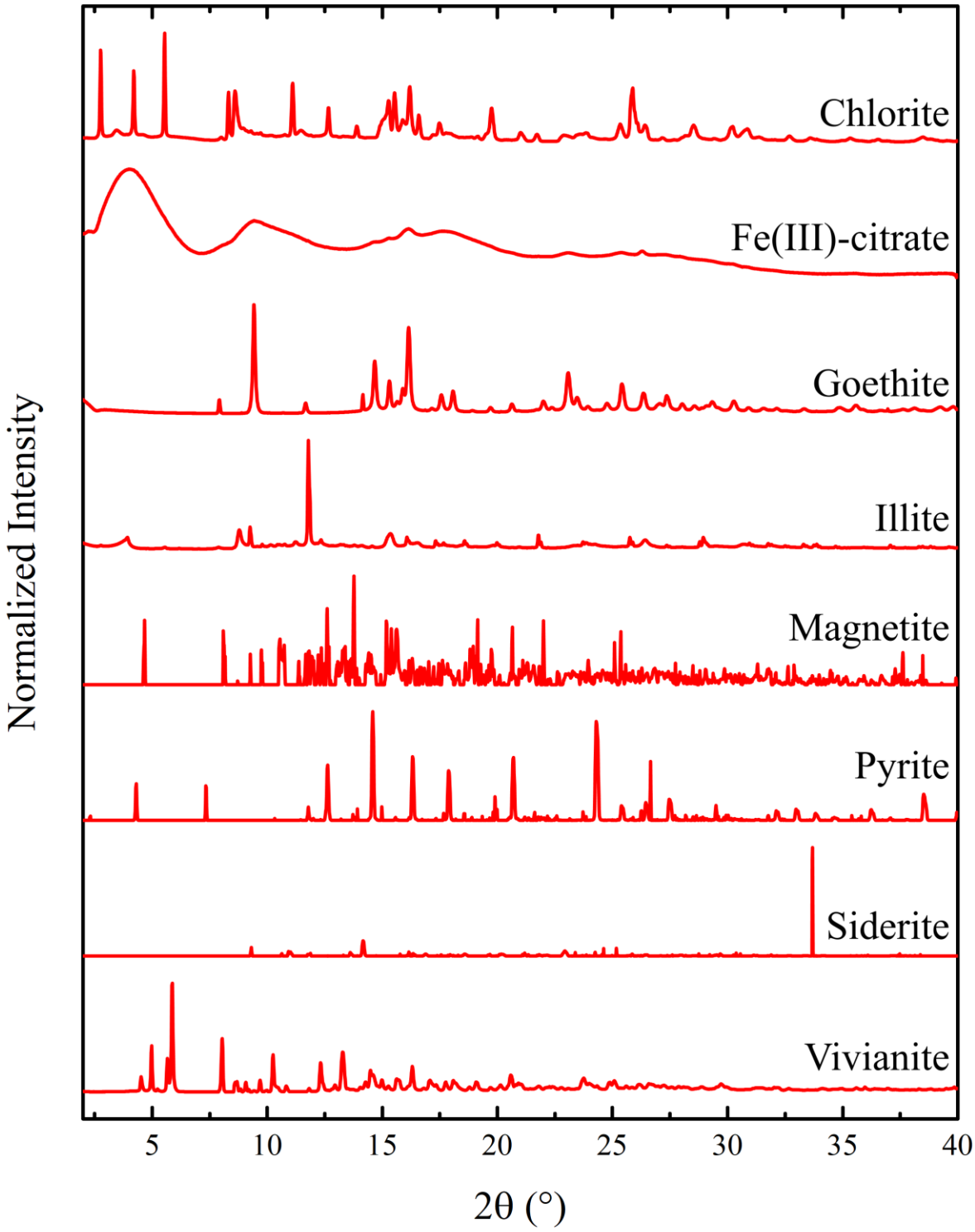

Figure B.2. PXRD spectra of Fe XAS standards

Table B.3. LCF results for Sulfur XAS. ND = not detected.

Borehole ID	Depth (mBGL)	$\chi 2$	Gypsum		Sulfonate		L-cysteine		Sulfur		Pyrite	
S15-01	3.9	1.85	37	± 1%	25	± 1%	ND		39	± 1%	ND	
S15-01	5.8	2.03	35	± 1%	ND		16%	± 2%	49	± 2%	ND	
S17-01	4.2	2.36	41	± 1%	ND		14%	± 2%	45	± 2%	ND	
S17-01	5.3	2.66	46	± 1%	ND		10%	± 2%	44	± 2%	ND	
S15-02	4.8	2.37	23	± 1%	ND		29%	± 2%	48	± 2%	ND	
S15-02	5.8	2.28	13	± 1%	ND		22%	± 2%	66	± 2%	ND	
S17-02	4.9	1.69	10	± 1%	11	± 1%	ND		79	± 1%	ND	
S17-02	5.6	1.52	9.0	±0.4%	ND		15	± 2%	76	± 2%	ND	
S15-03	4.8	3.08	22	± 1%	ND		20	± 2%	58	± 2%	ND	
S15-03	5.8	2.53	35	± 1%	ND		13	± 2%	53	± 2%	ND	
S17-03	5.1	2.62	56	± 1%	ND		6	± 2%	38	± 2%	ND	
S17-03	5.6	1.62	19	± 1%	ND		13	± 2%	68	± 2%	ND	
S15-04	3.8	2.59	64	± 1%	ND		5	± 2%	31	± 2%	ND	
S15-04	5.5	4.29	38	± 1%	ND		17	± 3%	45	± 3%	ND	
S17-04	4.2	2.07	22	± 1%	ND		25	± 2%	53	± 2%	ND	
S17-04	5.3	3.29	22	± 1%	ND		ND		78	± 1%	ND	
S15-05	4.8						no fit					
S15-05	5.5	0.873	15	±0.3%	ND		ND		47	± 3%	38	± 4%
S17-05	4.9	4.54	61	± 1%	ND		ND		39	± 1%	ND	
S17-05	5.6	1.63	5.4	±0.5%	ND		ND		54	± 4%	41	± 5%

Adsorption Length of FeS at the sulfur K-edge

$$\mu = \rho(n_{Fe}\Delta\sigma_{Fe} + n_S\Delta\sigma_S)$$

Given data:

Molecular Weight	87.9 g/mol
Density (ρ)	4.84 g/cm^3
Fe mole fraction (n_{Fe})	0.635
S mole fraction (n_S)	0.365
Fe Mass Adsorption Coefficient ($\Delta\sigma_{Fe}$) 2440 eV to 2480 eV	-40.4 cm^2/g
S Mass Adsorption Coefficient ($\Delta\sigma_S$) 2440 eV to 2480 eV	1942.3 cm^2/g

$$\mu = 4.84\ \frac{g}{cm^3}\left(0.635\ x(-40.4\frac{cm^2}{g}) + 0.365\ x\ 1942.3\frac{cm^2}{g}\right)$$

$$\mu = 2189.6\ cm^{-1}$$

$$\frac{1}{\mu} = 4.6\ \mu m$$

Table B.4. LCF results for Fe XAS. ND = not detected.

Borehole ID	Depth (mBGL)	$\chi 2$	Illite		Organic-Fe(III)		Pyrite		Siderite	
S15-01	3.9	0.036	45	± 1%	55	± 1%	ND		ND	
S15-01	5.8	0.045	39	± 2%	61	± 2%	ND		ND	
S17-01	4.2	0.038	46	± 2%	54	± 2%	ND		ND	
S17-01	5.3	0.071	31	± 2%	69	± 2%	ND		ND	
S15-02	4.8	0.041	48	± 2%	52	± 2%	ND		ND	
S15-02	5.8	0.064	38	± 2%	62	± 2%	ND		ND	
S17-02	4.9	0.037	59	± 2%	27	± 2%	15	± 1%	ND	
S17-02	5.6	0.029	65	± 2%	32	± 1%	3.2	± 0.9%	ND	
S15-03	4.8	0.027	68	± 1%	32	± 1%	ND		ND	
S15-03	5.8	0.046	36	± 2%	64	± 2%	ND		ND	
S17-03	5.1	0.030	55	± 2%	40	± 1%	5.8	± 0.9%	ND	
S17-03	5.6	0.069	31	± 3%	48	± 2%	21	± 2%	ND	
S15-04	3.8	0.015	71	± 1%	29	± 1%	ND		ND	
S15-04	5.5	0.042	45	± 2%	55	± 1%	ND		ND	
S17-04	4.2	0.031	63	± 1%	37	± 1%	ND		ND	
S17-04	5.3	0.025	64	± 1%	36	± 1%	ND		ND	
S15-05	4.8	0.110	83	± 1%	ND		ND		17	± 1%
S15-05	5.5	0.024	58	± 1%	42	± 1%	ND		ND	
S17-05	4.9	0.067	37	± 3%	40	± 2%	23	± 1%	ND	
S17-05	5.6	0.040	54	± 2%	35	± 2%	11	± 1%	ND	

APPENDIX C: Microbiology Results

Table C.1. Extracted DNA samples with concentration and quality.

Well ID	Sample Date	Replicate Vol. (mL)	Replicate	Concentration (ng/µL)	260/280	260/230
11-03	21-Oct-15	200	1	16.4	1.780	0.250
11-03	21-Oct-15	200	2	18.6	1.870	0.082
11-03	21-Oct-15	200	3	14.9	1.827	0.090
11-03	10-Jun-16	300	1	16.1	1.770	0.071
11-03	10-Jun-16	300	2	10.8	1.837	0.096
11-03	10-Jun-16	300	3	10.9	1.799	0.098
11-03	16-Aug-16	300	1	3.98	1.657	0.132
11-03	16-Aug-16	300	2	2.50	1.783	0.069
11-03	16-Aug-16	300	3	6.10	1.818	0.032
11-03	7-Nov-16	150	1	18.0	1.752	0.443
11-03	7-Nov-16	150	2	54.6	1.802	0.511
11-03	7-Nov-16	150	3	29.8	1.762	0.640
11-03	27-Jun-17	300	1	9.38	1.753	0.103
11-03	27-Jun-17	300	2	12.7	1.861	0.284
11-03	27-Jun-17	300	3	11.2	1.661	0.414
11-03	31-Oct-17	300	1	2.78	1.575	0.149
11-03	31-Oct-17	300	2	0.948	0.872	0.027
11-03	31-Oct-17	300	3	1.45	1.895	0.020
S15-01	22-Oct-15	300	1	5.28	1.621	0.069
S15-01	22-Oct-15	300	2	5.58	1.685	0.131
S15-01	22-Oct-15	300	3	8.16	1.752	0.074
S15-01	8-Jun-16	300	1	1.55	1.900	0.019
S15-01	8-Jun-16	300	2	1.15	1.850	0.073
S15-01	8-Jun-16	300	3	5.84	1.628	0.027
S15-01	15-Aug-16	300	1	5.10	1.847	0.053
S15-01	15-Aug-16	300	3	3.86	1.828	0.077
S15-01	25-Oct-16	300	1	1.25	1.667	0.026
S15-01	25-Oct-16	300	2	1.35	1.870	0.017
S15-01	25-Oct-16	300	3	1.04	1.733	0.054
S15-01	28-Jun-17	300	1	0.422	1.613	0.070
S15-01	28-Jun-17	300	2	0.342	1.516	0.082
S15-01	28-Jun-17	300	3	0.398	1.890	0.054
S15-01	1-Nov-17	300	1	3.8	1.527	0.103
S15-01	1-Nov-17	300	2	4.6	1.439	0.036
S15-01	1-Nov-17	300	3	2.9	1.729	0.034
Tech Replicate	15-Aug-16	4100	t	15.6	1.907	0.061

Table C.1. Continued.

Well ID	Sample Date	Replicate Vol. (mL)	Replicate	Concentration (ng/µL)	260/280	260/230
S15-02	22-Oct-15	150	1	4.50	1.585	0.048
S15-02	22-Oct-15	150	2	3.24	1.601	0.040
S15-02	22-Oct-15	150	3	2.92	1.563	0.045
S15-02	8-Jun-16	300	1	25.4	1.830	0.160
S15-02	8-Jun-16	300	2	44.0	1.874	0.126
S15-02	8-Jun-16	300	3	39.4	1.851	0.115
S15-02	16-Aug-16	300	1	68.6	1.859	0.600
S15-02	16-Aug-16	300	2	65.0	1.872	0.277
S15-02	16-Aug-16	300	3	50.2	1.862	0.595
S15-02	27-Jun-17	200	1	33.4	1.806	0.796
S15-02	27-Jun-17	200	2	32.8	1.814	0.620
S15-02	27-Jun-17	200	3	24.6	1.804	0.376
S15-02	1-Nov-17	200	1	7.56	1.767	0.061
S15-02	1-Nov-17	200	2	9.90	1.729	0.061
S15-02	1-Nov-17	200	3	14.2	1.767	0.084
S15-03	8-Jun-16	300	1	14.3	1.864	0.068
S15-03	8-Jun-16	300	2	19.6	1.890	0.045
S15-03	8-Jun-16	300	3	26.0	1.825	0.133
S15-03	16-Aug-16	300	1	15.4	1.808	0.274
S15-03	16-Aug-16	300	2	18.0	1.823	0.301
S15-03	16-Aug-16	300	3	24.0	1.839	0.267
S15-03	1-Nov-16	300	1	20.2	1.820	0.319
S15-03	1-Nov-16	300	2	8.78	1.858	0.113
S15-03	1-Nov-16	300	3	21.6	1.809	0.366
S15-03	28-Jun-17	300	1	24.4	1.881	0.374
S15-03	28-Jun-17	300	2	9.02	1.761	0.147
S15-03	28-Jun-17	300	3	20.2	1.815	0.330
S15-03	31-Oct-17	300	1	1.27	1.406	0.023
S15-03	31-Oct-17	300	2	3.58	1.542	0.066
S15-03	31-Oct-17	300	3	1.91	1.700	0.031

Table C.1. Continued.

Well ID	Sample Date	Replicate Vol. (mL)	Replicate	Concentration (ng/µL)	260/280	260/230
S15-04	22-Oct-15	300	1	36.2	1.701	0.142
S15-04	22-Oct-15	300	2	34.0	1.847	0.207
S15-04	22-Oct-15	300	3	38.0	1.741	0.187
S15-04	8-Jun-16	300	1	30.0	1.594	0.122
S15-04	8-Jun-16	300	2	11.2	1.824	0.047
S15-04	8-Jun-16	300	3	24.4	1.803	0.092
S15-04	16-Aug-16	300	1	78.0	1.848	0.868
S15-04	16-Aug-16	300	2	42.8	1.829	0.366
S15-04	16-Aug-16	300	3	33.6	1.861	0.198
S15-04	1-Nov-16	100	1	17.5	1.848	0.137
S15-04	1-Nov-16	100	2	9.9	1.850	0.178
S15-04	1-Nov-16	150	3	12.3	1.848	0.141
S15-04	27-Jun-17	300	1	21.0	1.755	0.309
S15-04	27-Jun-17	300	2	21.0	1.794	0.370
S15-04	27-Jun-17	300	3	13.1	1.799	0.551
S15-04	1-Nov-17	140	1	33.2	1.774	0.210
S15-04	1-Nov-17	140	2	24.0	1.739	0.178
S15-04	1-Nov-17	140	3	20.2	1.667	0.150
S15-05	8-Jun-16	300	1	7.46	1.771	0.035
S15-05	8-Jun-16	300	2	10.5	1.808	0.049
S15-05	8-Jun-16	300	3	35.8	1.787	0.151
S15-05	16-Aug-16	300	1	31.8	1.851	0.565
S15-05	16-Aug-16	300	2	23.0	1.816	0.181
S15-05	16-Aug-16	300	3	32.6	1.833	0.404
S15-05	25-Oct-16	300	1	79.6	1.853	1.150
S15-05	25-Oct-16	300	2	37.8	1.859	0.668
S15-05	25-Oct-16	300	3	49.6	1.871	0.282
S15-05	27-Jun-17	300	1	15.6	1.787	0.319
S15-05	27-Jun-17	300	2	18.9	1.781	0.196
S15-05	27-Jun-17	300	3	10.4	1.807	0.130
S15-05	1-Nov-17	300	1	3.8	1.527	0.103
S15-05	1-Nov-17	300	2	4.6	1.439	0.036
S15-05	1-Nov-17	300	3	2.9	1.729	0.034
S15-06	22-Oct-15	300	1	4.78	1.809	0.036
S15-06	22-Oct-15	300	2	5.06	1.907	0.025
S15-06	22-Oct-15	300	3	5.90	1.857	0.045
S15-06	10-Jun-16	300	1	1.07	1.581	0.017
S15-06	10-Jun-16	300	2	1.49	1.676	0.022
S15-06	10-Jun-16	300	3	1.07	2.000	0.014

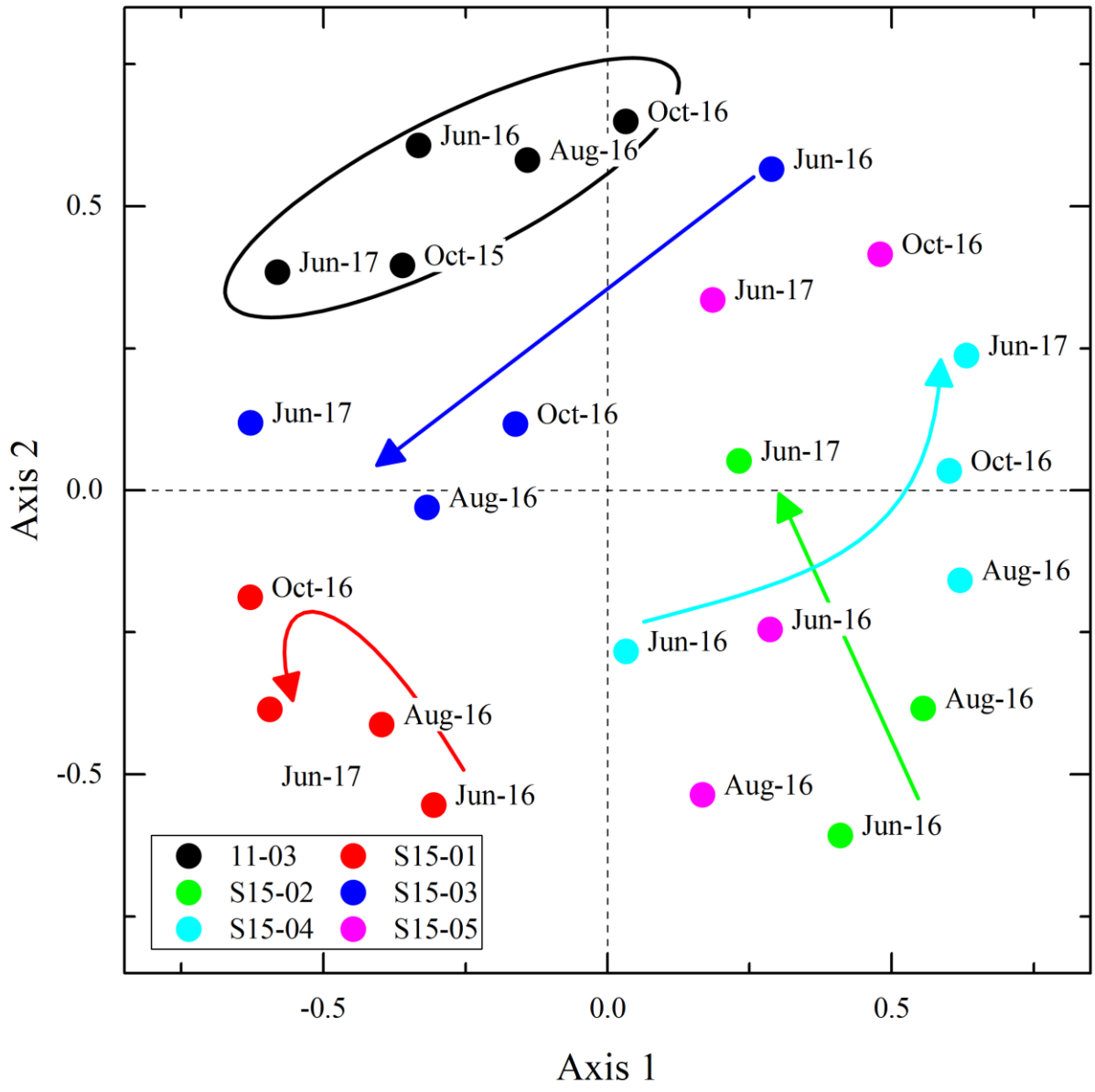

Figure C.1. Jaccard coefficient NMDS plot for microbial communities in groundwater samples. Observed trends and clustering in monitoring wells are noted by arrows and circles (colour corresponds to the monitoring well legend).

Table C.2. Microcosm experiment results.

Treatment	Date	Time (days)	n	[Fe(II)]	Error	[Fe(III)] (mM)	Error	pH (-)
Untreated	21-Feb	0	2	0.002	0.002	0.024	0.009	7.27
	28-Feb	7	3	0.011	0.002	0.009	0.002	7.76
	8-Mar	15	3	0.006	0.001	0.013	0.007	7.68
	14-Mar	21	3	0.017	0.005	0.008	0.005	7.67
	21-Mar	28	3	0.009	0.002	0.015	0.002	7.64
	28-Mar	35	3	0.012	0.006	0.013	0.003	7.59
	4-Apr	42	3	0.013	0.004	0.007	0.003	7.46
Sterile	21-Feb	0	2	0.001	0.001	0.001	0.001	7.30
	28-Feb	7	1	0.003	n.d	0.001	n.d	7.84
	8-Mar	15	3	0.004	0.002	0.003	0.002	7.74
	14-Mar	21	2	0.006	0.001	0.007	0.001	7.81
	21-Mar	28	1	0.002	n.d	0.005	n.d	7.91
	28-Mar	35	0	n.d	n.d	n.d	n.d	7.92
	4-Apr	42	2	0.023	0.005	0.025	0.020	7.78
Refined Biosurfactant	21-Feb	0	2	0.008	0.002	0.005	0.003	7.46
	28-Feb	7	2	0.024	0.000	0.011	0.002	7.46
	8-Mar	15	1	0.008	n.d	0.003	n.d	7.33
	14-Mar	21	3	0.034	0.013	0.035	0.009	7.16
	21-Mar	28	3	0.008	0.005	0.020	0.007	6.98
	28-Mar	35	2	0.011	0.000	0.019	0.000	6.83
	4-Apr	42	2	0.030	0.003	0.035	0.006	6.61
Unrefined Biosurfactant	21-Feb	0	3	0.004	0.001	0.006	0.003	7.58
	28-Feb	7	3	0.008	0.001	0.009	0.002	7.67
	8-Mar	15	2	0.004	0.002	0.004	0.002	7.35
	14-Mar	21	2	0.013	0.008	0.007	0.005	7.11
	21-Mar	28	2	0.050	0.013	0.033	0.000	6.85
	28-Mar	35	2	0.049	0.000	0.023	0.009	6.80
	4-Apr	42	2	0.034	0.010	0.034	0.006	6.64
SDS	21-Feb	0	1	0.009	n.d	0.032	n.d	7.60
	28-Feb	7	3	0.018	0.018	0.032	0.001	7.73
	8-Mar	15	3	0.010	0.005	0.005	0.002	7.40
	14-Mar	21	3	0.099	0.037	0.080	0.016	7.24
	21-Mar	28	2	0.034	0.015	0.011	0.003	7.19
	28-Mar	35	3	0.064	0.014	0.029	0.006	7.08
	4-Apr	42	3	0.050	0.016	0.040	0.013	6.98

Table C.2. Continued.

Treatment	Date	Time (days)	n	[Fe(II)]	Error	[Fe(III)] (mM)	Error	pH -
Malic Acid	21-Feb	0	3	0.008	0.003	0.011	0.008	2.44
	28-Feb	7	3	0.000	0.000	4.756	0.110	4.99
	8-Mar	15	3	0.959	0.407	2.243	0.951	5.94
	14-Mar	21	3	2.263	1.085	1.811	0.403	6.14
	21-Mar	28	3	0.058	0.014	3.448	1.102	6.23
	28-Mar	35	3	0.786	0.393	1.705	0.509	6.07
	4-Apr	42	3	0.678	0.131	3.273	1.083	6.06
Malic Acid + Refined Biosurfactant	21-Feb	0	3	0.010	0.001	0.005	0.001	2.54
	28-Feb	7	3	0.997	0.000	4.512	0.291	5.11
	8-Mar	15	3	0.959	0.000	3.550	0.353	5.86
	14-Mar	21	3	0.115	0.000	4.492	0.427	6.13
	21-Mar	28	3	1.112	0.065	2.962	0.138	6.21
	28-Mar	35	3	0.531	0.201	2.741	0.781	6.24
	4-Apr	42	3	0.959	0.000	7.263	0.626	6.21